



Norwegian University of
Science and Technology

Stability Assessment of Hydropower Tunnel in Swelling and Slaking Rock Mass

Silje-Elin Skrede

Geotechnology

Submission date: June 2017

Supervisor: Krishna Kanta Panthi, IGP

Co-supervisor: Thomas Schonborn, Statkraft

Norwegian University of Science and Technology
Department of Geoscience and Petroleum



Your ref.: MS/N27T40/IGB/SESKKP

Date: 16.01.2017

TGB4930 INGGEOL/BERGMEK - MSc thesis

for

Eng. geo. student Silje-Elin Skrede

**STABILITY ASSESSMENT OF HYDROPOWER TUNNEL IN SWELLING AND SLAKING
ROCK MASS**

Background

Statkraft, and its subsidiaries SN Power and Aqua Imara, have experienced challenging rock behaviour during development of several projects in South America; East Asia and Africa. Many of these challenges were related to a variation of rock properties during construction and operation, compared to the estimated behaviour during planning. Such behaviour included rock mass having low strength and deformability, swelling, disintegration and slaking properties, which is less familiar in the Norwegian hydropower tunnelling environment. This MSc thesis work is a continuation of the ground work that the MSc candidate has carried out in her project work during fall 2016 and the candidate will further investigate in establishing the properties of some volcanic rocks from Chile and use this database to carry out stability assessment of a case from Chile.

MSc thesis task

This MSc thesis is a continuation of the Project work and the candidate will further study the theory related to swelling and slaking potentials of the rocks and further carry out stability analysis using both analytical and numerical approach with following MSc thesis task:

- Theoretical review on the rock engineering principles associated with rock mechanical properties, swelling and slaking potential of rocks and rock masses.
- Review couple of cases with instability problems associated to rock mass quality, swelling, disintegration and slaking effect in water tunnels.
- Further carry out mineralogical study (XRD and thin-section).
- Further carry out test on slaking of rock samples received from Chile.

- Conduct tests on rock mechanical properties such as density, poisson's ratio, and strength and deformation modulus.
- Carry out stability assessment of the case project using empirical and analytical approaches.
- Carry out stability assessment using RS-2D numerical analysis.
- Compare the results from analytical and numerical approaches.
- Discuss the findings and conclude the work.

Relevant computer software packages

Candidate shall use *roc-science package* and other relevant computer software for the master study.

Background information for the study

- Relevant information such as reports, maps, information and data received from Statkraft.
- The information provided by the professor about rock engineering and hydropower.
- Scientific papers, reports and books related to mechanical properties of the rocks
- Scientific papers, reports and books related to swelling and slaking properties of the rocks.
- Scientific papers and books related to international tunnelling and rock engineering cases.
- Literatures in rock engineering, rock support principles, rock mechanics and tunnelling.

Cooperating partner

Statkraft is the co-operating partner. MSc Thomas Shönborn from Statkraft will be contact persons and co-supervisor for this work.

The project work is to start on January 16, 2017 and to be completed by June 19, 2017.

The Norwegian University of Science and Technology (NTNU)
Department of Geology and Mineral Resources Engineering

January 16, 2017



Dr. Krishna K. Panthi

Associate Professor of geological engineering, main supervisor

Acknowledgments

This master thesis has been carried out as part of the Master's Degree Program in Geotechnology at the Department of Geoscience and Petroleum, at the Norwegian University of Science and Technology (NTNU). The co-operating partner has been Statkraft AS, Oslo, Norway.

Associate professor of geological engineering, Krishna K. Panthi has been my main supervisor. His great knowledge and valuable input has meant a lot for the results of the thesis, and a special thanks goes to him. Principal Engineer Geology & Geotechnics Thomas Schönborn, at Statkraft AS, Oslo, has been my co-supervisor. He has provided me with samples for my laboratory work, relevant project information, engineering geological investigation reports and maps. I am grateful for his help and guidance. A special thanks to Statkraft for financial support and Thomas for organizing a field trip to La Confluencia, Chile.

I am grateful for all the help I have gotten with sample preparation and execution of laboratory testing from the employees at the Department of Geoscience and Petroleum. Senior engineer Gunnar Vistnes, Senior Engineer Laurentius Tjihuis, associate professor Kristian Drivenes, PhD Candidate Chhatra Bahadur Basnet, Staff Engineers Arild Monsøy and Kjetil Eriksen and Associate professor Bjørn Eske have all contributed to this work. Quac Nghia Trinh has provided me with valuable advice for the numerical modelling.

I would also like to thank my fellow students for inspiration and interesting discussions throughout the semester. And at last, I am grateful for the never-ending support from my parents. Thank you for always believing in me.

Silje-Elin Skrede

Trondheim, June 2017

Abstract

Chile has a favorable topography for hydropower with the Andes mountain rising along the eastern border of the country. La Confluencia is a 158 MW run of the river plant located in the Tinguiririca Valley approximately 150 km south of Santiago. Parts of the two water tunnels are situated in a rock formation, locally known as Coya Machalí, where problems with expansive rocks have been encountered. Typical problems start out as hairline cracks in the shotcrete which may progress to more serious problems. Deterioration of the rock mass has also been observed. The free flow Portillo tunnel was finished in 2011. After two years of operations, cracks in the shotcrete were discovered in the right wall in a part of the tunnel. The deformation was about 10 cm at the worst, and related to a weakness zone.

A study about swelling and slaking of rocks have been conducted. The main task has been to assess the stability of the section where the described problems occurred. Thin sections have been studied, and point load strength test and slake durability test have been carried out on samples from the Portillo tunnel. In addition data from construction mapping, several reports and maps from the project have been studied. A field visit has also been carried out.

Method and results of XRD, DTA and tests of swelling potential carried out in earlier work are described. The content of smectite has been confirmed through XRD on ethylene glycol treated samples. Thin sections are difficult to interpret due to a fine grained matrix and alteration of the samples. The result from the point load strength test show that the samples have low to medium strength, while slake durability is low for the weakest sample, while it is high for the others.

The focus of the stability analysis is mainly on displacements associated with the weakness zone. This have been conducted through a semi-analytical approach and a numerical analysis in RS^2 . Both show large deformations, but the methods have some weaknesses. In the numerical analysis different material properties have been tested both for the rock mass surrounding the weakness zone, and the zone itself. Special for this type of rock is the time before stability problems occur. The assessment shows that a gradual reduction in rock strength can lead to shotcrete problems. The same displacement can be seen with only weak material in the weakness zone, as when a stronger material combined with swelling pressure is applied. The approach used in the thesis is not suitable to assess the effect of additional support. It is suspected that the material has degraded from the time of excavation, and it is recommended to continue inspections in case of further reduction of rock mass quality.

Samandrag

Langs den austlege grensa til Chile har Andesfjella ei bratt stigning som gjer dette området gunstig for vasskraft. Vasskraftanlegget La Confluencia har ein installert effekt på 158 MW, og er lokalisert i Tinguiririca Valley, omlag 150 km sør for Santiago. Delar av to av vasstunnelane til kraftverket ligg i Coya Machali-formasjonen, der det har oppstått problem grunna svellande bergartar. Radielle riss i sprøytebetongen er typiske indikasjonar på dette, og kan over tid utvikla seg til meir alvorlege problem. Det er òg observert at bergmassekvaliteten kan forverrast med tida. Portillo-tunnelen som høyrer til vasskraftverket vart ferdigstilt i 2011, og etter å ha vore drifta i to år blei det oppdaga ein deformasjon av sprøytebetong på omlag 10 cm i høgre side av tunnelen. Dette området var relatert til ei svakheitssone.

Eit studie av svelling og degradering av berg er gjennomført i denne oppgåva. Særlig stabiliteten i området til svakheitssona har blitt vurdert og undersøkt. Vidare har tynnslipar blitt studert og laboratorietestar som punktlasttest og ”slake-durability” test blitt utført på prøver frå Portillo-tunnelen. I tillegg har data frå kartlegging under driving, rapportar og kart frå prosjektet blitt sett på. Forfattaren av oppgåva har òg besøkt denne tunnelen.

Metode og resultat frå XRD, DTA og test av svellepotensial gjennomført i tidlegare arbeid er beskrive. Gjennom arbeidet har det blitt observert at prøvene inneheld smek-titt, bekrefta gjennom XRD på etylen glycol-behandla prøver. Omdanning samt finkorna matriks vanskeleggjer tolking av tynnslipane. Punktlast-testen viser at prøvene har låg til middels styrke. ”Slake durability” er låg for den svakaste prøva, medan den er høg for dei andre.

Fokus for stabilitetsvurderinga ligg i hovudsak på deformasjonar knytta opp mot svakheitssona. Ei semi-analytisk tilnærming og ei numerisk analyse i RS^2 har blitt brukt. Begge viser store deformasjonar, men metodane har nokre svakheitlar. Forskjellige styrkeegenskaper har blitt testa i den numeriske analysen, både for bergmassen som omgjev svakheitssona og sjølve sona. Spesielt for denne typen bergmasse er tida som går før stabilitetsproblem oppstår. Den numeriske analysen viser at ein gradvis reduksjon i bergstyrken gir deformasjon i sprøytebetongen. Dei same resultatata kan oppnåast med berre svakt materiale i svakheitssona, eller med et sterkare materiale kombinert med svelletrykk. Tilnærminga som brukast er ikkje eigna til å vurdere effekten av sikring som er installert i etterkant. Det er mistanke om at bergmassekvaliteten er redusert i forhold til konstruksjonstidspunktet. Det anbefalast derfor å fortsette med inspeksjonar i tilfelle ein ytterligere reduksjon av bergmassekvaliteten skal skje.

Table of contents

Project Description	i
Acknowledgments	iii
Abstract	v
Samandrag	vii
1 Introduction	1
1.1 Background	1
1.2 Objectives	2
1.3 Limitations	3
2 Characteristics of the Rock Mass	5
2.1 Rock Mechanical Properties	5
2.1.1 Rock strength	5
2.1.2 Elasticity	6
2.2 Geological Settings	7
2.2.1 Discontinuities	7
2.2.2 Groundwater	8
2.2.3 Stress situation	9
2.3 Stability and Failure Modes	11
3 Empirical and Analytical Stability Assessment	15
3.1 Failure Criteria	15
3.1.1 Mohr Coulomb	15
3.1.2 Hoek-Brown	16
3.2 Stress Distribution	18
3.3 Assessing Stability	19
3.4 Rock Mass Classification	24
3.4.1 The geological strength index (GSI)	24
3.4.2 Rock Mass Rating (RMR)	25
3.4.3 The Q-system	25

3.5	Numerical Methods	26
4	Swelling and Slaking	29
4.1	Swelling	29
4.2	Slaking	31
4.3	Support Strategy	33
4.4	Volcanic-sedimentary Rocks and the Chilean Tertiary Rocks	35
4.4.1	Volcanic-sedimentary rocks	35
4.4.2	The Chilean Tertiary rocks	36
5	Case Studies	39
5.1	Svandalsflona	39
5.2	Los Quilos and Chacabuquito Water Tunnels	40
5.3	Numerical Simulation of Weakness Zones	43
5.3.1	Hanekleiva	43
5.3.2	Buon Kuop Hydropower Project	44
6	Portillo Tunnel	47
6.1	Project Background	47
6.2	Geology	47
6.3	Structures and Discontinuities	49
6.4	Laboratory Results	52
6.5	Stress Situation	53
6.5.1	Regional stress	53
6.5.2	Hydraulic fracturing	54
6.5.3	Estimating stress at PK 34+405	55
6.6	Rock Support	56
6.7	Field Observations	57
6.7.1	Portillo Tunnel	57
6.7.2	Outcrop at PK 34+750	58
7	Laboratory Methods	63
7.1	Swelling	63
7.1.1	Free Swelling	63
7.1.2	Swelling Pressure	63
7.2	Mineralogy	65
7.2.1	DTA	65
7.2.2	X-ray Diffraction	66
7.2.3	Thin Sections	68
7.3	Density	68
7.4	Rock Mechanical Properties	69

7.4.1	UCS, Poisson’s ratio and E-modulus	69
7.4.2	Point Load Strength Test	69
7.5	Slake Durability Index	71
8	Results of Laboratory Work	73
8.1	Sample Description	73
8.2	Swelling	74
8.3	Mineralogy	74
8.3.1	DTA	74
8.3.2	X-Ray Diffraction	74
8.3.3	Thin Sections	75
8.4	Density	78
8.5	Rock Mechanical Properties	79
8.5.1	Point Load Strength	79
8.5.2	UCS, E-modulus and Poisson’s ratio	80
8.6	Slake Durability Index	81
8.7	Discussion of Results	82
8.7.1	Mineralogy	82
8.7.2	Swelling	83
8.7.3	Density, UCS, PLI	83
8.7.4	Slake durability	84
9	Estimation of Rock Mass Properties	85
9.1	Rock Mass Properties at PK 34+405	85
9.2	Weakness Zone at PK 34+405	86
10	Stability Assessment	89
10.1	Rock Mass Classification	89
10.1.1	Q-values from mapping	89
10.1.2	GSI	90
10.2	Estimates of Deformation and Support	91
11	Numerical Analysis	93
11.1	Model Set-up	93
11.1.1	Geometry, mesh and displacements	93
11.1.2	Rock stress and loads	94
11.1.3	Rock mass properties	95
11.1.4	Support	96
11.2	Modelling Sequences	96
11.2.1	Defining rock mass properties	97
11.2.2	Weakness zone	97

11.2.3 Support	98
11.3 Results of Numerical Analysis	98
11.3.1 Rock mass properties	98
11.3.2 Weakness zone	99
11.3.3 Support	101
11.4 Discussion of Numerical Analysis	102
11.4.1 Stress situation	102
11.4.2 Input properties	102
11.4.3 Model quality	103
12 Discussion	105
12.1 Estimation of Rock mass Properties	105
12.2 Stability Analysis and Deformations	106
12.3 Modelling Swelling	107
12.4 Rock Support	107
13 Conclusions and Further Work	109
13.1 Conclusions	109
13.2 Further Work	110
Bibliography	112
APPENDICES	119
A Swelling pressure charts	119
B X-ray Diffractograms	124
C DTA Charts	127
D Point Load Test Results	130
E Classifications	132
F PLI and slake durability, PK 40+522 to PK 40+758	134
G Geological map	135
H Strike and dip measurements	137
I The Q-system and modified q-system	138
J Guidelines for the Disturbance factor	141

Chapter 1

Introduction

1.1 Background

Chile is one of the frontrunners in supporting renewable energy technologies in South America. The country is per 2016, number six in installed capacity in the region, with 6622 MW, and it generates 24.57 TWh annually (IHA, 2016). With its 4000 km long coastline the country stretches from north to south on the western coast of the South American mainland. Along the eastern border the Andes mountains are rising to nearly 7000 meters (Pankhurst and Hervé, 2007). These mountains are the seat for several hydropower projects.

La Confluencia is a run-of-the-river plant situated in the Tinguiririca Valley, approximately 150 km south of Santiago. The location is shown in figure 1.1. It is a result of a 50/50 joint venture between Pacific Hydro and SN Power (a subsidiary of Statkraft), formed in 2004 (Pacific Hydro, 2011). The free flow Portillo tunnel and the low-pressure Tinguiririca tunnel are leading water to a vertical pressure shaft, which also functions as a surge shaft. A concrete and steel lined high pressure tunnel leads the water to the power station at the surface (Paul et al., 2012). The commercial operations of La Confluencia started in 2010, and the plant has an installed capacity of 158 MW and a yearly production of 672 GWh (Statkraft, 2011). This thesis is written in cooperation with Statkraft AS and focuses mainly on the Portillo tunnel.

Parts of the tunnel branches are situated in a rock formation of Late Cretaceous-Lower Tertiary age, which from a geological perspective has shown interesting and unexpected behaviour. Longer stretches of rock in this formation have shown expansive behaviour, but identification of such zones have proven difficult since the physical appearance of rocks with different properties are similar. Swellings tests on intact rock have shown that the majority do not swell even though they contain swelling minerals, while some show typical swellings behavior corresponding to the content of swelling minerals. Several projects have experienced troubles which are likely related to expansive minerals. These include La Confluencia and its twin plant La Higuera, as well as the Chacayes, Hornitos, Chacabuquito and Alfalfal hydropower plants (Carter et al., 2010).

The time frame in which stability issues become apparent varies. For example, Carter et al. (2010) describes that problems with shotcrete competence manifested themselves in zones which appeared without any special challenges at the time of excavation. First after a couple of years, to after a decade did the troubles appear. It is therefore necessary to determine how these zones, where long term stability may be reduced, can be identified. The time issue increase the need for periodically inspections, which is both uneconomic because of production loss and can introduce fallouts or similar due to dewatering and dry out of the rock mass. In the Chingaza water supply tunnel project in Colombia, dry-out of the rock mass was partly blamed for the extensive fallouts and slides that happened after the first filling Brattli and Broch (1995). For rehabilitation purposes, a greater understanding of rock mass behaviour can support the decision of rock support in a long time perspective.



Figure 1.1: Location of La Confluencia (Google Earth 6.1.0, 2015)

This master thesis will examine rock mechanical properties of samples from the Portillo tunnel branch of La Confluencia as a result of the experiences above. Together with results on swelling and slaking properties conducted in earlier work, an assessment of the tunnel stability will be made. To achieve this a combination of analytical and numerical analysis will be used. Field observations will contribute to the understanding of the project area.

1.2 Objectives

The main objective of the thesis is to assess stability in a section of the Portillo tunnel, with regard to swelling and slaking rock. As parts of this assessment will be based on

laboratory investigations, the description of test methods, and a critical review of the results are also important parts of the scope. The objectives can be listed as follows:

- Theoretical review on the rock engineering principles associated with rock mechanical properties, swelling and slaking potential of rocks.
- A review of a couple of cases with instability problems associated to rock mass quality, swelling, disintegration and slaking effect in water tunnels.
- Carry out mineralogical study (XRD and thin-section) of rock samples received from Chile.
- Carry out tests on slaking of rock samples received from Chile.
- Conduct tests on rock mechanical properties such as density, Poisson's ratio, strength and deformation modulus.
- Carry out stability assessment of the case project using empirical and analytical approaches.
- Carry out stability assessment using RS-2D numerical analysis.
- Compare the results from analytical and numerical approaches.
- Discuss the findings and conclude the work.

1.3 Limitations

The stability assessment focus only on one part of the Portillo tunnel branch, and will not include any assessment of the pressurized system. Since the analysis is concentrated to a selected part of the tunnel, the results may not be representative for other sections. The number of samples available for laboratory testing is limited, which reduce the reliability of the results. The analysis is focused on deformations. Stress related problems are not focused on, but stress situation has been considered. A field visit have been carried out, however the study has mainly been carried out as a desk study.

Chapter 2

Characteristics of the Rock Mass

A clear understanding of the rock mass and its behaviour both during and after excavation is necessary to determine the appropriate engineering and support measures. Material properties of the rock mass and overall ground conditions with regards to general composition, faults and weakness zones, stress situation and groundwater conditions all have important impact (Palmström and Stille, 2010). This chapter describes the factors which are emphasized later in the thesis.

2.1 Rock Mechanical Properties

Rock strength and elasticity are important properties, in order to understand the behaviour of the rock mass. Intact rock strength, σ_{ci} , is estimated with the uniaxial compressive strength test or from a correlation between point load index and UCS. It is also implemented in classification systems such as the RMR and Q-system, which will be introduced later.

2.1.1 Rock strength

The uniaxial compressive strength, UCS or σ_c , is used to classify the strength of rocks, and to distinguish between rock and soil (ISRM, 1979a). An alternative to UCS is the point load strength, which is also used to estimate UCS. A sample is loaded by two spherically truncated, conical platens; the load is measured and point load strength I_s can be calculated ISRM (1985). σ_c and I_s can be correlated by the factor k (Palmström and Stille, 2010).

$$\sigma_c = k_s \times I_s \quad (2.1)$$

The PLI test has several advantages. The requirements for the samples are not as strict as for UCS and it can be conducted on cores, blocks and irregular lumps, with nearly no preparation. The equipment can be transported to, and used in the field.

The test procedure for both tests is described further in chapter 7. The classification of uniaxial compressive strength and point load strength is provided in appendix E.

The ratio k_s is not a set value, and it varies with strength of the rock. Palmström (1995) suggests to use the correlations in table 2.1 between point load strength and uniaxial compressive strength when no other information is available.

Table 2.1: Suggested values for the factor k_s correlating UCS and PLI, varying with strength (Palmström and Stille, 2010; Palmström, 1995).

Compressive strength σ_c [MPa]	Point load strength: I_{s-50} [MPa]	Suggested value of k_{50}
25*-50	1.8-3.5	14
50-100	3.5-6	16
100-200	6-10	20
>200	>10	25

*Bieniawski (1973) in Palmström and Stille (2010) suggests that point load strength test should not be carried out on rocks having compressive strength less than approximately 25 MPa

Several studies have been conducted to establish correlations between compressive strength and point load index for different rock types. A study conducted by Singh et al. (2012) on Indian rock of various origin, found that the relation depends on mineralogical, textural and deformational factors and recommends that the conversion factor should be used with caution. They suggest, as Palmström (1995), that a division is made based on rock strength. For weak rocks a factor of 14-16 should be applied and for strong rocks a factor of 21-24.

2.1.2 Elasticity

The elastic deformability of a material is specific for each material, and can be expressed by the E-modulus, also called Young's modulus (Myrvang, 2001). A linearly elastic material can be described by Hooke's law as shown in equation 2.2. σ_z is the applied stress in MPa and ε the strain in millistrain. There are different ways of defining the E-modulus, such as the secant and tangent modulus. The tangent modulus is normally calculated at 50 % of the maximum compressive strength, and is used further in the text (ISRM, 1979a).

$$E = \frac{\sigma_z}{\varepsilon_z} \quad (2.2)$$

Poisson's ratio ν is given by the ratio of lateral strain ε_x to axial strain ε_y in equation 2.3 (Nilsen and Palmström, 2000).

$$\nu = -\frac{\varepsilon_x}{\varepsilon_y} \quad (2.3)$$

An elastic linear material follows the same linear curve for loading and unloading. Perfectly elastic material, follows the same curve for loading and unloading, but the stress-

strain curve is not linear (Myrvang, 2001). Rock does not behave as ideal elastic materials, but follows a curve with hysteresis form. A typical loading curve can be divided into different deformation stages, and is shown in figure 2.1. The first stage (O-A) is non-linear,

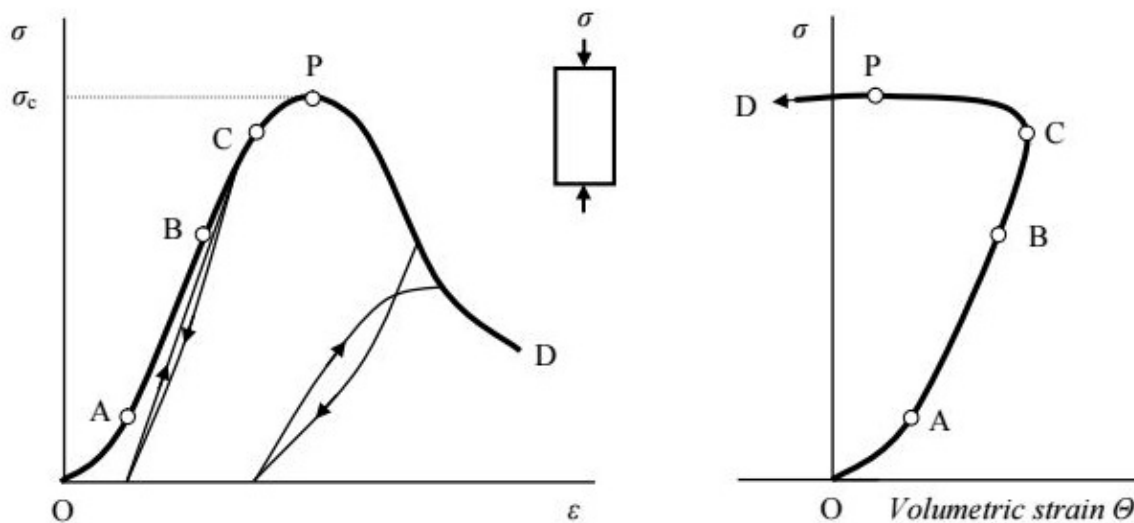


Figure 2.1: The complete stress-strain curve. Left: Axial stress - strain. Right: Stress - Volumetric strain curve. Figure from Li (2017).

and is attributed to closure of cracks and pores in the rock. If unloaded in this stage the deformation is typically reversible. In the second stage (A-B) a linear behaviour is seen. This is where E-modulus and Poisson's ratio is calculated. In the third stage, (B-C) plastic deformation occurs. If unloaded, plastic strain is permanently left in the rock, because of micro-cracking. Near point C, dilatation and unstable fracturing starts. Up until this point the sample has contracted. At stage (C-D) the sample expands, and micro-cracking increases, until the final fracture happens at point P. This is the point where the uniaxial compressive strength is defined (Li, 2017). The equations above apply to isotropic materials. Due to mineral composition, jointing, foliation or bedding planes, this may not always be the case. However, for simplicity, it is usual to assume that the rock mass behaves as an isotropic material (Li, 2017).

2.2 Geological Settings

2.2.1 Discontinuities

To describe ground behaviour, rock mass composition can be divided into general composition, represented between weakness zones and faults, weakness zones and faults and minerals or rock types which have special properties affecting ground behaviour (Palmström and Stille, 2010). In a tunnel, detailed jointing normally dominates. The geological discontinuities may have much greater impact on the overall engineering properties, than the strength of the rock itself. Discontinuities can appear as structures from millimetre

size to several thousand of meter, and their significance for engineering purposes can be very different (Palmström and Stille, 2010). Joints can be defined based on their size and composition or based on their origin. For engineering purposes, the most important characteristics of joints are (Nilsen and Palmström, 2000):

- Roughness, described in terms of large scale waviness and small scale smoothness.
- Condition of joint wall with regards to alteration or coating. E.g. wet minerals like chlorite, talc or graphite can reduce shear strength significantly.
- Possible filling materials. E.g. soft minerals (clay, mica, chlorite e.g.), soluble minerals (calcite, gypsum) and swelling minerals (swelling clays, anhydrite), or loose materials that can reduce friction and shear strength.
- Length and continuity of the joints.

Swelling clay influences stability by reducing friction and/or by exerting a swelling pressure if prevented from swelling. In chapter 4 swelling is thoroughly reviewed. The joints normally appear as sets in different preferred directions and may have different properties depending on how they originated and the type of rock they occur in. The network of joints parts the rock mass into blocks, which size is an important factor to predict rock mass behaviour. (Nilsen and Palmström, 2000).

Faults and weakness zones may have great impact on the excavation process and/or stability of underground openings. Weakness zone refers to a part of the rock mass with significantly lower mechanical properties than the neighbouring rock mass. The two main groups are those formed from tectonic events, or those consisting of weak materials formed by other processes such as weathering or hydrothermal activity (Nilsen and Palmström, 2000).

2.2.2 Groundwater

Groundwater can affect excavation conditions, short and long term stability. Since groundwater is able to move freely through the rock mass for long distances, the regional geology and overall groundwater pattern are important considerations in predicting potential water problems. In general, the hydraulic conductivity of intact rock is small, and groundwater must move through joints and fractures. Some volcanic rocks, may be exceptions to this due to their high porosity (Palmström and Stille, 2010).

The characteristics of the joints are influencing the possibility of water to flow through the rock mass (Nilsen and Palmström, 2000). Due to drainage of joints after excavation, the groundwater pressure close to the opening is normally reduced. However, if impermeable layers exist, water pressure may build up, reducing general stability. Groundwater will reduce strength of the rock material and shear strength of discontinuities. In the case of swelling clay, access to water leads to reduced friction and strength (Palmström and Stille, 2010). The influence of water might be time dependent. Immediately after blasting, water close to the periphery might be displaced due to blasting shock. After a

while the water flows back to the now free surface, but as the water table sinks the flow decreases. In dry tunnels the ventilation dries out the contour, but this is not the case for water tunnels where the rock mass constantly has access to water (Nilsen and Broch, 2012).

2.2.3 Stress situation

Knowledge of the virgin stress situation is important to evaluate magnitude and direction of the stresses around a tunnel after excavation. Both high and low *in situ* stresses can impact the stability, either by exceeding the strength of the rock mass, or by reducing stability in jointed rock mass due to low normal stress on joints respectively (Palmström and Stille, 2010). The type of stability problems that may occur depends on the properties of the rock mass, as well as the tangential stresses (Palmström and Stille, 2010). The initial stress situation before excavation is dependent on gravitational, topographic, tectonic and residual stresses (Nilsen and Palmström, 2000).

Gravitational stress is the stress caused only by gravity. For horizontal surfaces the vertical stress σ_z depends on depth of the excavation beneath the surface, z and the specific gravity of the rock mass γ :

$$\sigma_z = \gamma \times H \quad (2.4)$$

where $\gamma = \rho \times g$. ρ is the density of the rock mass.

In some situations σ_v equals σ_z , but particularly at greater depth the deviation may be considerable (Nilsen and Palmström, 2000). For elastic rock mass with Poisson's ratio of ν , the horizontal stress induced by gravity is:

$$\sigma_x = \sigma_y = \sigma_z \times \frac{\nu}{1 - \nu} \quad (2.5)$$

Typical values for ν is between 0.25-0.33 which gives $\sigma_H = \frac{1}{3}\sigma_v$ or $\sigma_H = \frac{1}{2}\sigma_v$ (Fossen and Gabrielsen, 2005). The gravity induced horizontal stress is normally only a small component of the total horizontal stress, and equation 2.5 does not represent discontinuous rock mass well (Nilsen and Palmström, 2000).

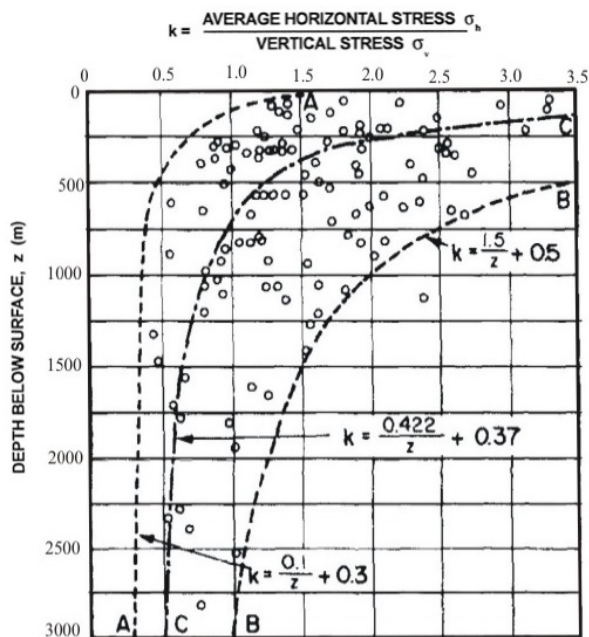


Figure 2.2: Variation of the ratio k between the average horizontal stress and the vertical stress with depth below surface. Hoek and Brown (1980) in Panthi (2006).

Figure 2.2 illustrates variation of the ratio k between average horizontal stress and vertical stress plotted against depth below the surface. At shallow and moderate depths horizontal stress is normally larger than vertical stress.

In steep valley sides the topographical effects of stress is considerable, and might be totally dominating. As illustrated in figure 2.3, σ_1 will be nearly parallel to the valley slope near the surface and σ_3 perpendicular to the the slope.

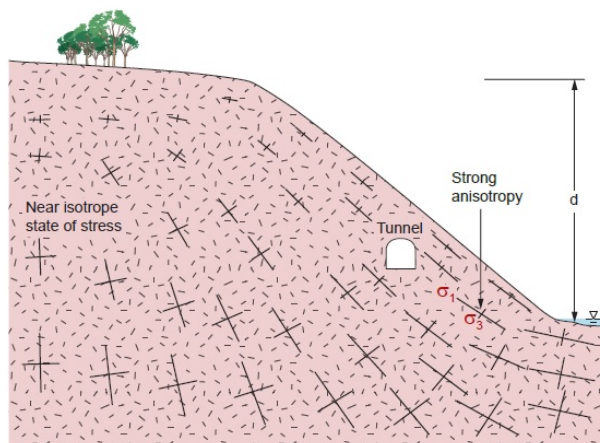


Figure 2.3: Stress anisotropy in valley sides. Figure from NGI (2015).

Tectonic stresses are caused by plate tectonics and are responsible for faulting and folding. In general they cause much higher horizontal stress than those induced by gravity, especially at shallow and moderate depths (Nilsen and Palmström, 2000). The tectonic

or locked in stress can be calculated as follows (Panthi, 2012):

$$\sigma_h = \frac{\nu}{1 - \nu} \times \sigma_v + \sigma_{tec} \quad (2.6)$$

where ν is Poisson's ratio, σ_v is gravity stress.

Residual stresses are locked in stresses caused by happenings in the early geological stages of the rock mass, such as cooling of magma (Nilsen and Palmström, 2000).

2.3 Stability and Failure Modes

Palmström and Stille (2010) have divided failure modes into three main groups; gravity driven, stress induced and water influenced failures. Gravity driven fall outs after excavation occur mostly because of unfavorable orientation of discontinuities. If the stresses in the rock mass exceeds the local strength, failures may happen assisted by gravity. There are two types of stress induced failures; in massive brittle rock it is manifested as buckling, slabbing or rock burst and in massive soft/ductile rock as plastic deformation by creep or squeezing. Squeezing may also occur if highly jointed rock mass containing clay is subjected to overstressing (Palmström and Stille, 2010). Some effect of water is already mentioned, such as the load of the water pressure. Depending on the type of ground, different problems can arise. Flowing ground may appear if materials with low cohesion is subjected to large inflows, or swelling and/or slaking in rocks with particular minerals (Palmström and Stille, 2010).

In relation to swelling and slaking rock mass, time-dependent behaviour must be considered. The stability at the point of excavation may not be representative of the long term stability. Alteration of rock and joint filling/gouge, swelling, softening and weakening along discontinuities are all possible scenarios that can reduce long term stability (Nilsen and Palmström, 2000). Processes such as weathering and alteration can change mechanical properties and behaviour of rock completely. The walls of discontinuities are affected first (Palmström and Stille, 2010). For example Pasamehmetoglu et al. (1981) tested Ankara andesites with different degrees of weathering to assess the changes in rock mechanical properties. It was shown that with a higher degree of weathering, UCS, E-modulus, internal friction angle, cohesion, density and slake durability index decreased. The effective porosity increased. The degree of weathering can be classified according to table 2.2. Grade of weathering effect and strength reduction can be related as figure show 2.4. This figure also show that the variation in strength between sedimentary and crystalline rock is considerable. Also elasticity modulus and shear resistance of discontinuity surfaces can be affected (Panthi, 2006).

Table 2.2: Description of degrees of weathering (ISRM, 1978).

Term	Description	Grade
Fresh	No visible sign of rock material weathering; perhaps slight discoloration on major discontinuity surfaces.	I
Slightly weathered	Discoloration indicates weathering of rock material and discontinuity surfaces. All the rock material may be discoloured by weathering and may be somewhat weaker externally than in its fresh condition.	II
Moderately weathered	Less than half of the rock material is decomposed and/or disintegrated into a to a soil. Fresh or discoloured rock is present either as a continuous framework or as corestones.	III
Highly weathered	More than half of the rock material is decomposed and/or disintegrated into a to a soil. Fresh or discoloured rock is present either as a continuous framework or as corestones.	IV
Completely weathered	All rock material is decomposed and/or disintegrated to a soil. The original mass structure is still largely intact.	V
Residual soil	All rock material is converted to soil. The mass structure and material fabric are destroyed. There is a large change in volume, but the soil has not been significantly transported.	VI

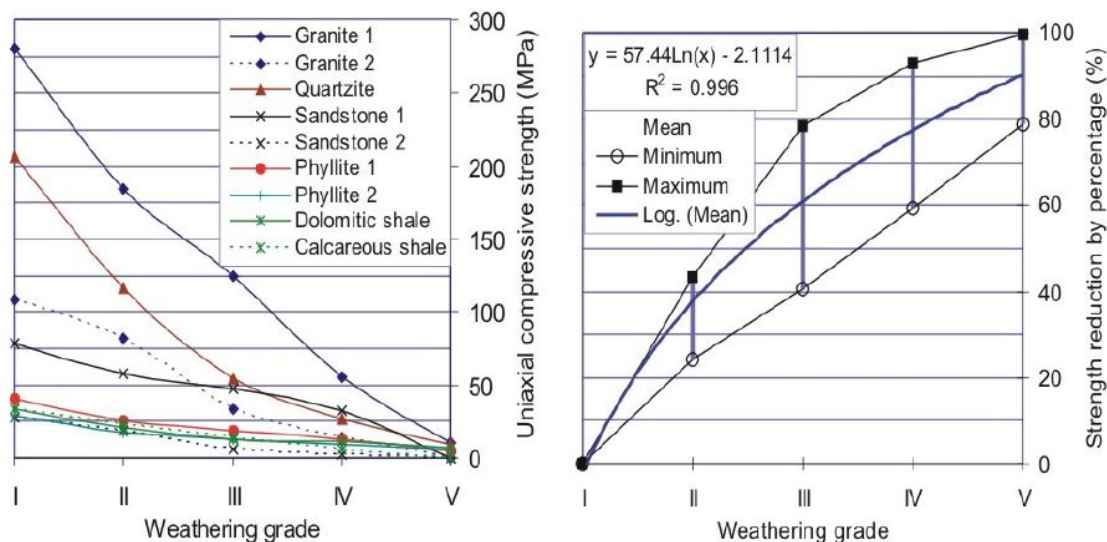


Figure 2.4: Strength reduction of rock related to degree of weathering. Figure from Panthi (2006).

The type of filling/gouge material must be identified to assess expected behaviour. Following associated behaviour of some filling and gouge materials are listed (Brekke and Howard, 1973; Nilsen and Palmström, 2000). Since different materials often occur together, non-swelling materials are also included.

- Swelling clay: swelling, slaking and squeezing; can lead to stability problems such

as rock fall, slides and possibly collapses.

- Inactive clays: squeezing can cause slaking and sloughing.
- Chlorite, talc, graphite, serpentine: Very low shear strength, especially when wet.
- Porous or flaky calcite, gypsum: Can dissolve, and thus reduce stability; can lead to ravelling.
- Quartz, epidote: durable and high strength, can improve stability.
- Crushed rock fragments (gravel size) or sand-like filling: ravelling or running, due to lack of cohesion. Can run or flow into the tunnel right after blasting.

Other factors than the filling material itself can affect the stability of a zone. An example given is a case where a high stress field caused squeezing in a swelling clay zone. This masked the effect of the swelling. In such cases the thickness of the swelling zone is of importance. Another important factor is the loss of stability due to pressure exerted by the swelling material which leads to a loss of strength or loads contributing to failure. According to the same study most problems were accounted for during the excavation time, but also some after longer time periods. The long term troubles were associated with poor support solutions (Brekke and Howard, 1973).

Chapter 3

Empirical and Analytical Stability Assessment

A number of factors should be evaluated to assess the stability of an excavation. The most difficult input parameters to quantify are in general magnitudes and directions of virgin stresses, and properties of the in situ rock mass (Nilsen and Palmström, 2000). This chapter gives an introduction to analytical and empirical methods for evaluation of stability. Numerical analysis is a sub-group of analytical methods (Nilsen and Palmström, 2000). The classification systems that discussed are the RMR-system, the Q-system and the Geological Strength Index.

3.1 Failure Criteria

3.1.1 Mohr Coulomb

The much applied Mohr Coulomb failure criterion assume that failure initiation along a plane is dependent on the cohesion c of the material and the friction coefficient μ multiplied with the normal stress on the plane, as described by equation 3.1. The friction coefficient is given by $\mu = \tan \phi$, where ϕ is the internal friction of the material (Nilsen and Broch, 2012).

$$\tau = c + \mu \times \sigma_n \quad (3.1)$$

The onset of plastic failure can be defined by the Mohr-Coulomb criterion expressed in terms of effective confining stress and uniaxial compressive strength of the rock mass (Hoek, 2007a):

$$\sigma'_1 = \sigma_{cm} + k \times \sigma'_3 \quad (3.2)$$

where,

$$\sigma_{cm} = \frac{2c' \cos(\phi)'}{1 - \sin(\phi)'} \quad (3.3)$$

and

$$k = \frac{1 + \sin(\phi)'}{1 - \sin(\phi)'} \quad (3.4)$$

where

σ_1' = axial stress when failure occurs

σ_3' = confining stress

c' = cohesive strength

ϕ = friction angle of the rock mass

3.1.2 Hoek-Brown

The empirical Hoek-Brown criterion, describes the relation between minor and major principle stresses and failure of the rock. It has been widely accepted and applied in many projects around the world. The first version of the criterion was published in 1980, and has since that been continuously developed. The original criteria is presented in equation 3.5 (Hoek et al., 2002).

$$\sigma_1' = \sigma_3' + \sigma_{ci} \left(m_i \times \left(\frac{\sigma_3'}{\sigma_{ci}} \right) + s \right)^{0.5} \quad (3.5)$$

where

σ_1' and σ_3' are the major and minor principle stresses at failure

σ_{ci} is the uniaxial compressive strength of the intact rock material

m_i and s are material constants, for intact rock $s=1$.

(Hoek et al., 2002).

The constant m_i is dependent on frictional characteristics of the minerals the sample consist of, and has large impact on the strength properties of the rock (Hoek and Marinos, 2000). The values depend on granularity and interlocking of the crystal structure. A higher value is associated with samples which are firmly interlocked and have more frictional characteristics (Marinos and Hoek, 2000). The original criterion had weaknesses regarding the description of very poor quality rock mass, thus the generalized Hoek-Brown criterion was introduced in 1994. The equation and input parameters are presented in equation 3.6 to 3.9 (Hoek et al., 2002; Hoek and Marinos, 2007). At the same time the Geological Strength Index (GSI) was presented, which is described later in this chapter.

$$\sigma_1' = \sigma_3' + \sigma_{ci} \left(m_b \times \left(\frac{\sigma_3'}{\sigma_{ci}} \right) + s \right)^a \quad (3.6)$$

where m_b is a reduced value of m_i

$$m_b = m_i \exp\left(\frac{GSI - 100}{28 - 14D}\right) \quad (3.7)$$

s and a are material constants given by

$$s = \exp\left(\frac{GSI - 100}{9 - 3D}\right) \quad (3.8)$$

$$a = \frac{1}{2} + \frac{1}{6}(\exp\frac{-GSI}{15} + \exp\frac{-20}{3}) \quad (3.9)$$

(Hoek et al., 2002).

The GSI value is obtained from assessment of the rock mass. The other parameters are the same as in equation 3.5. The disturbance factor D is used to account for the disturbance the rock mass is subjected to from blasting and stress relaxation, and applies to a limited zone around the excavation (Hoek et al., 2002).

After failure rock normally exhibit strain softening behaviour, which means that the rock has some post-peak strength (Cai et al., 2007). For modelling of rock mass behaviour it is important to estimate this. The following parameters are suggested for estimating the residual strength parameters, using the GSI system.

$$GSI_r = GSI^{-0.0134GSI} \quad (3.10)$$

$$m_r = m_i \exp\left(\frac{GSI_r - 100}{28}\right) \quad (3.11)$$

$$s = \exp\left(\frac{GSI_r - 100}{9}\right) \quad (3.12)$$

$$a_r = \frac{1}{2} + \frac{1}{6}(e\frac{-GSI_r}{15} + e\frac{-20}{3}) \quad (3.13)$$

The parameter GSI_r in equation 3.10 is based on an empirical relationship found. If the rock mass is of poor quality, residual GSI is close to equal to peak GSI, illustrated in figure 3.1. If possible residual GSI-values should be estimated from the GSI chart or from the relationship between joint condition factor and block volume as described in Cai et al. (2007).

Hoek et al. (2002) presents two different equations for the rock mass modulus of deformation. The equation valid for $\sigma_{ci} \leq 100MPa$ is presented in equation 3.14.

$$E_m[GPa] = \left(1 - \frac{D}{2}\right) \sqrt{\frac{\sigma_{ci}}{100}} \times 10^{\left(\frac{GSI-10}{40}\right)} \quad (3.14)$$

For rock mass with $\sigma_{ci} > 100MPa$ equation 3.15 is applicable.

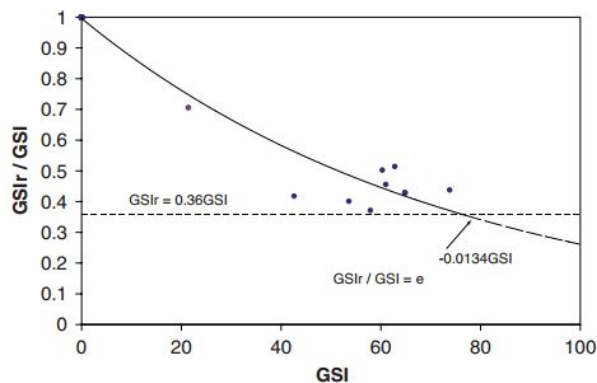


Figure 3.1: Relation between GSI and residual GSI values (Cai et al., 2007).

$$E_m[\text{GPa}] = \left(1 - \frac{D}{2}\right) \times 10^{\left(\frac{GSI-10}{40}\right)} \quad (3.15)$$

3.2 Stress Distribution

Stress distribution around a tunnel can be described by different equations depending on the in situ stress situation and the geometry of the opening. If the stress situation is anisotropic, *Kirch's equations* are used to describe the maximum and minimum tangential stresses $\sigma_{\theta(max)}$ and $\sigma_{\theta(min)}$ (Nilsen and Palmström, 2000).

$$\sigma_{\theta(max)} = 3\sigma_1 - \sigma_3 \quad (3.16)$$

$$\sigma_{\theta(min)} = 3\sigma_3 - \sigma_1 \quad (3.17)$$

These equations describe the four points with maximum and minimum tangential stresses. If the symmetry varies from this, and especially if the excavation has sharp corners, the stress distribution is strongly affected. The magnitude of the tangential stress will increase as the radius of curvature decreases. The size of the opening does not affect the magnitude of σ_{θ} in theory, but the zone of influence around the opening will increase with larger openings. A normal assumption based on in situ stress measurements is that the stresses are stabilized at a distance outside of the contour equal to half the tunnel width. Due to drill and blast excavation most tunnels behave like this (Nilsen and Palmström, 2000). The character of the rock mass is important for the stress distribution. For soft or fractured rock the peak stress is found some distance away from the tunnel contour, as illustrated in figure 3.2. Plastic deformation involves a redistribution of stress after excavation, where the highest tangential stress is found outside the transition between the plastic and elastic zone. The problem can be assessed empirical, analytical, numerical and probabilistic (Panthi, 2017).

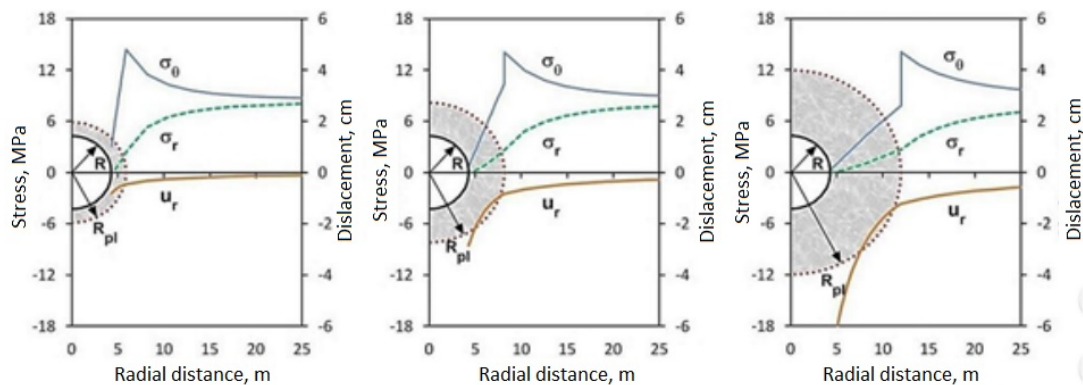


Figure 3.2: Left: Elastic – brittle failure, in hard rock mass. Middle: Strain softening failure in average quality rock mass. Right: Elastic perfectly plastic failure in very poor rock mass (Panthi, 2017).

Other important considerations regarding stress and rock mass, is the direction of the stress with regards to major weakness zones and dominating structural features in the rock mass. The stress situation may be affected by large weakness zones since their ability to transfer stress may be reduced. This can lead to a build up of high stresses on one side and reduced stress on the other side (Palmström and Stille, 2010).

3.3 Assessing Stability

The rock mass can fail in different manners according to the rock mass properties and stress situation. In hard rock mass elastic brittle failure is usual. Average quality rock mass can experience strain softening failure, and in very poor quality rock mass elastic perfectly plastic failure occurs. When a tunnel is excavated in highly fractured rock with high in situ stress ($\frac{\sigma_1}{\sigma_c} > 0.4$), an elastic/plastic continuum develops, and squeezing and swelling can occur (Hoek et al., 1995) in Martin et al. (1999).

In hard rock, the intact rock strength and fracture network in addition to in situ stress are the deciding factors. Depending on the depth of excavation, the failure process ranges from structurally controlled failures to stress induced failures. In moderately fractured rock ($50 < \text{RMR} < 75$) and at intermediate in situ stress ($0.15 > \frac{\sigma_1}{\sigma_c} < 0.4$) localized brittle failure of intact rock and movement of blocks can be expected. In highly fractured ($\text{RMR} < 50$) rock and intermediate in situ stress, unravelling along discontinuities can occur in addition to brittle failure. The assessment of stability problems in weak rock or weakness zones is complicated.

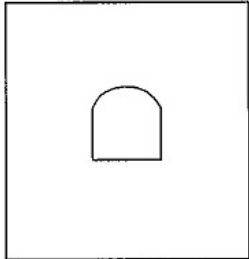
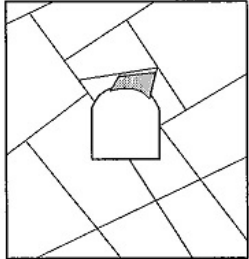
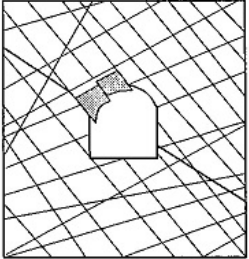
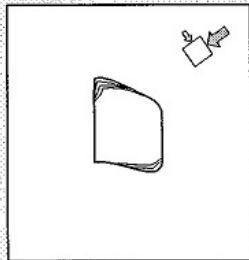
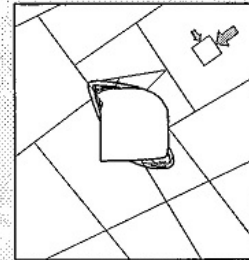
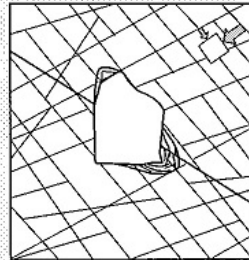
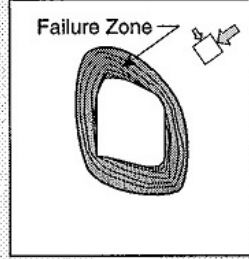
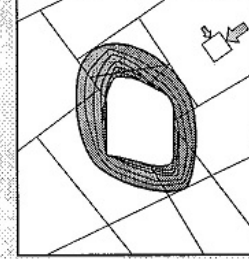
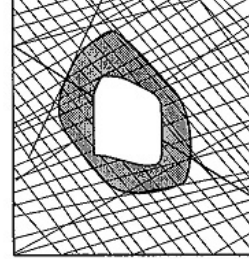
	Massive ($RMR > 75$)	Moderately Fractured ($50 > RMR < 75$)	Highly Fractured ($RMR < 50$)
Low In-Situ Stress ($\sigma_1 / \sigma_c < 0.15$)	 <p>Linear elastic response.</p>	 <p>Falling or sliding of blocks and wedges.</p>	 <p>Unravelling of blocks from the excavation surface.</p>
Intermediate In-Situ Stress ($0.15 > \sigma_1 / \sigma_c < 0.4$)	 <p>Brittle failure adjacent to excavation boundary.</p>	 <p>Localized brittle failure of intact rock and movement of blocks.</p>	 <p>Localized brittle failure of intact rock and unravelling along discontinuities.</p>
High In-Situ Stress ($\sigma_1 / \sigma_c > 0.4$)	 <p>Failure Zone Brittle failure around the excavation.</p>	 <p>Brittle failure of intact rock around the excavation and movement of blocks.</p>	 <p>Squeezing and swelling rocks. Elastic/plastic continuum.</p>

Figure 3.3: Failure prediction according to rock mass rating and ratio between maximum far field stress and compressive strength. The highlighted squares are related to brittle failure (Hoek et al., 1995) in Martin et al. (1999).

To assess stability and design support systems, magnitude and distribution of deformations and the effect of the support in terms of induced support pressure should be evaluated (Hoek, 2007b). For analysis of rock mass with plastic behaviour several methods exists. An analytical and semi-analytical approach described in Hoek (2007a) and Hoek and Marinos (2000) are presented. These methods describes the immediate deformation process after excavation, and not time dependent deformations (Hoek, 2007a). A simple assessment of tunnel deformation can be done based on the Mohr Coulomb criterion.

Failure of the rock mass surrounding a tunnel occurs when the internal support pressure p_i is less than the critical support pressure p_{cr} (Hoek, 2007a). This can be expressed by equation 3.18. k is the slope of the σ'_1 versus σ'_3 line in the Mohr Coloumb criteria and introduced in section 3.1.1. The plastic zone and input parameters for this method are illustrated in figure 3.4.

$$p_{cr} = \frac{2p_0 - \sigma_{cm}}{1 + k} \quad (3.18)$$

Failure will not occur if the internal support pressure is larger than the critical support pressure. In this case the rock mass behaves elastic and the radial displacement is given by equation 3.19 where E_m is the Young's modulus and ν is the Poisson's ratio.

$$u_{ie} = \frac{r_0(1 + \nu)}{E_m}(p_0 - p_i) \quad (3.19)$$

If this is not the case, and the internal support pressure is less than the critical support pressure, plastic failure occurs and the radius of the plastic zone r_p is given by equation 3.20:

$$r_p = r_0 \left[r_0 \frac{2(p_0(k - 1) + \sigma_{cm})}{(1 + k)((k - 1)p_i + \sigma_{cm})} \right]^{(1/(k-1))} \quad (3.20)$$

The total radial displacement of the tunnel walls u_{ip} are given by equation 3.21:

$$u_{ip} = \frac{r_0(1 + \nu)}{E} \left[2(1 - \nu)(p_0 - p_{cr}) \frac{r_p^2}{r_0} - (1 - 2\nu)(p_0 - p_i) \right]^{1/(k-1)} \quad (3.21)$$

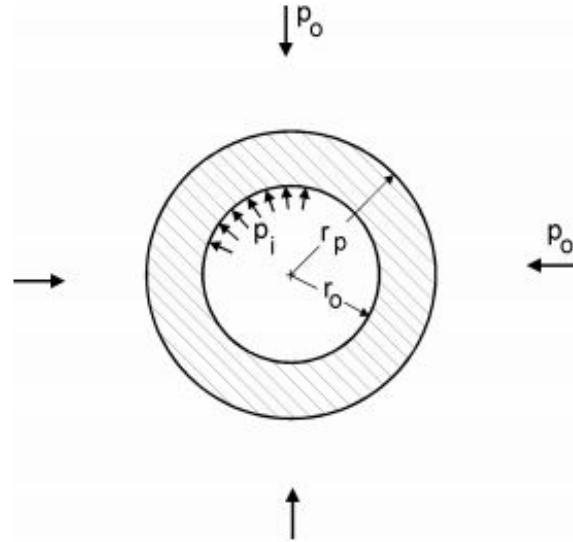


Figure 3.4: Plastic zone around a circular tunnel (Hoek, 2007a).

This approach, as most approaches is based on a circular tunnel subjected to hydrostatic

stress, with an uniform internal support pressure. The rock mass behaves as an elastic-perfectly plastic material (Hoek, 2007a).

Hoek (2007a) presents a method for estimating the potential of tunnel squeezing rock mass. The method requires input in the form of the uniaxial compressive strength of intact rock σ_{ci} , the material constant m_i and GSI. The uniaxial compressive strength of the rock mass σ_{cm} is estimated with equation 3.22.

$$\sigma_{cm}(MPa) = 2c' \times \frac{\cos(\phi)}{1 - \sin(\phi)} \quad (3.22)$$

The method is based on the relationship between σ_{cm} and in situ stress p_0 , which can be related to percentage strain in the tunnel. A curve fitting process after Monte Carlo analysis of a variation of input parameters resulted in two equations which define, 1) the size of the plastic zone (equation 3.23) and 2) tunnel deformation in squeezing ground, (equation 3.24). In these equations, an internal pressure which represent the effect of support is included (Hoek, 2007a).

$$\frac{r_p}{r_o} = \left(1.25 - 0.625 \frac{p_i}{p_o} \right) \times \frac{\sigma_{cm} \left(\frac{p_i}{p_o} - 0.57 \right)}{p_o} \quad (3.23)$$

$$\frac{\delta_i}{r_o} = \left(0.2 - 0.25 \frac{p_i}{p_o} \right) \times \frac{\sigma_{cm} \left(2.4 \frac{p_i}{p_o} - 2 \right)}{p_o} \quad (3.24)$$

where

r_p = radius of plastic zone

r_o = original radius of tunnel (m)

δ_i = deformation on tunnel sidewalls

p_i = internal support pressure

p_0 = in situ stress ($\rho \times g \times h$)

σ_{cm} = rock mass strength

(Hoek, 2007a).

When applying this method as part of preliminary studies it is recommended to give estimates of the input values within a range of values, to assess worst and best case conditions (Hoek and Marinos, 2000). Limitations of this method is that it only considers circular shape, isostatic stress conditions and vertical stress. Only the final tunnel strain is estimated (Panthi, 2017).

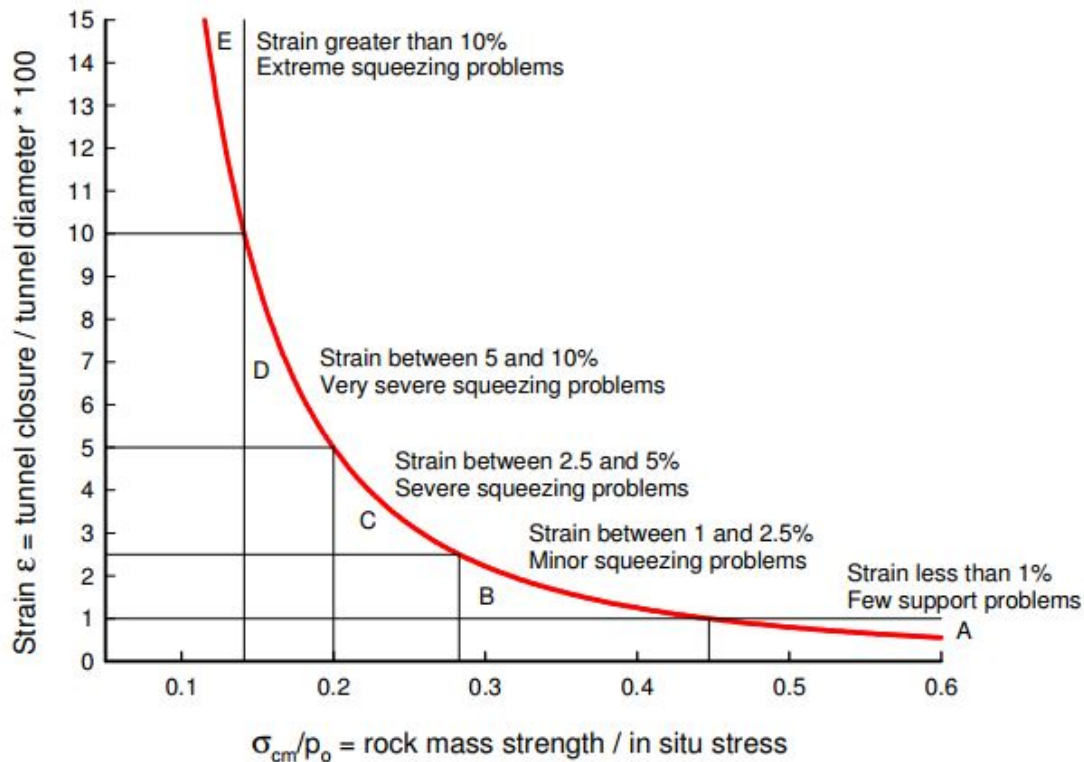


Figure 3.5: Tunnel strain versus rock mass strength/in situ stress and expected geotechnical issues (Hoek and Marinos, 2000).

When rock mass strength is less than 20 % of in situ stress level it is seen that tunnel collapse is likely because of a substantial increase in deformations. It is proposed that a tunnel strain of 1 % and larger is associated with tunnel stability. However it has been seen tunnels with strain up to 5 % without stability problems. In figure 3.5, the rock mass strength/in situ stress ratio is plotted against strain, and expected stability problems (Hoek, 2007a).

The rock mass strength can also be assessed with a number of empirical equations. Panthi (2006) presents equation 3.25, which is based on assessment of several empirical methods.

$$\sigma_{cm} = \frac{\sigma_{ci}^{1.50}}{60} \quad (3.25)$$

This equation applies to rocks that are highly schistose, foliated, thinly bedded and anisotropic and of metamorphic and sedimentary origin with low compressive strength (Panthi, 2006).

The support pressure provided by shotcrete is difficult to estimate. Table 3.1 gives some equations that can be used to calculate maximum support pressure for shotcrete.

Table 3.1: Maximum support pressure $p_{i,max}$ of a concrete or shotcrete lining in a tunnel with diameter D in meter, table modified after (Hoek, 2007a).

Thickness [cm]	Age [days]	UCS [MPa]	$p_{i,max}$ [MPa]
30 cm	28	35	$19.1 \times D^{-0.92}$
15 cm	28	35	$10.6 \times D^{-0.97}$
10 cm	28	35	$7.3 \times D^{-0.98}$
5 cm	28	35	$3.8 \times D^{-0.99}$
5 cm	3	11	$1.1 \times D^{-0.97}$
5 cm	0.5	6	$0.6 \times D^{-1.0}$

These equations assume that the support is installed as a closed ring in a circular tunnel, under hydrostatic loading and gives therefore an optimistic estimate. Bending moments will form due to asymmetric loading on irregular surfaces, causing a lower support capacity than estimated. The stiffness and capacity will also be reduced if the support is not installed in a closed ring, as is most often the case (Hoek, 2007a).

3.4 Rock Mass Classification

In mapping of the tunnel of the Portillo tunnel, both RMR- and Q-values have been estimated. Therefore these systems are further described, as well as GSI due to its importance as an input parameter for the Hoek Brown failure criterion. These are also the most widely used empirical classification systems (Palmström and Stille, 2010). The Q and RMR-classification systems are used for both for simple classification of rock mass quality and for the decision of rock support (Nilsen and Broch, 2012). According to Palmström and Stille (2010) swelling, squeezing or ravelling ground are not covered well in neither the RMR or the Q-system.

3.4.1 The geological strength index (GSI)

GSI was developed to better suit the application of the Hoek Brown criterion to weak rock (Marinos and Hoek, 2000; Hoek and Marinos, 2007). The rock mass is described visually based on the blockiness of the rock mass and the surface conditions with regards to joint roughness and alteration of discontinuities (Palmström and Stille, 2010). In chapter 9 a GSI chart is given together with estimation of GSI value in a section of the Portillo tunnel. This value is used as input in equation 3.7, 3.8 and 3.9, reducing σ_{ci} and m_i to appropriate values for the rock mass. Ideally laboratory values together with GSI are used as input, but as this often is not possible, values for σ_{ci} and m_i must be estimated. Marinos and Hoek (2000) present tables for estimation of these parameters, which are discussed later in the thesis. The applicability of the Hoek and Brown criterion assumes isotropic behaviour of the rock mass. It must therefore be used with care in heterogeneous rock mass. For example will failures in a strong and blocky rock with clay coated bedding

planes, be structurally controlled. If the rock mass is heavily fractured on the other hand, it may act as an isotropic mass (Marinos and Hoek, 2000).

3.4.2 Rock Mass Rating (RMR)

The RMR system takes strength of intact rock (PLI or UCS), RQD-index, discontinuity spacing, discontinuity character and groundwater conditions into account. Each parameter is given a rating, and the total value is adjusted due to orientation of discontinuities. Finally the rock mass is assigned a class, ranging from very poor rock to very good rock. Associated with each class is the unsupported stand up time for different spans, and the recommended excavation method and rock support (Nilsen and Broch, 2012). RMR can be used to assess GSI by the correlation $GSI=RMR-5$. This is applicable for rock mass where the quality is such that GSI is higher than 25 (Hoek and Brown, 1997).

3.4.3 The Q-system

The tunneling Quality index was introduced by NGI in 1974 (NGI, 2015). It is an empirical method based on a large number of tunnel mappings and analyses. Six parameters each given a rating after their impact on stability are used to calculate the Q-value, as equation 3.26 show. (Nilsen and Broch, 2012).

$$Q = \frac{RQD}{J_n} \times \frac{J_r}{J_a} \times \frac{J_w}{SRF} \quad (3.26)$$

where

RQD is the Rock Quality Designation

J_n is the joint set number

J_r is the joint roughness number

J_a is the joint alteration number

J_w is the joint water reduction factor

SRF is the stress reduction factor

The first quotient represent the degree of jointing the rock mass, the second the shear strength of the rock mass, and the third the stress situation. The Q-value ranges from 0.001 which is exceptionally poor, to 1000, which is exceptionally good. To assess support the equivalent dimension (D_e) must be defined. It is dependent on two factors in addition to the rock mass quality. The excavation support (ESR) ratio is given a value based on the degree of safety that is required for the construction. Water tunnels for hydro power (excluding high pressure penstocks) have an ESR value of 1.6 (NGI, 2015). The required support will also in general increase with tunnel span or height. D_e is defined as the excavation span or height divided by ESR. The Q-value and D_e is plotted against each other in a support chart to find the proposed rock support (NGI, 2015). The support

chart and guidelines for estimation of the input parameters are provided in appendix I.

Palmstrom and Broch (2006) have discussed several limitations with the Q-system, and here factors relating specially to the case of water tunnels with swelling rock mass are mentioned. The swelling pressure of montmorillonite is a factor that could possibly be included in the the second quotient J_r/J_a . The occurrence of swelling minerals is included in the table for J_a . Another measure that maybe should be assigned to J_a is the location of the excavation with regards to the ground water table. This is important due to possible softening of clay with water. When it comes to SRF, values are included for swelling rock with mild or heavy swelling pressure, but no limit between these categories is indicated. Neither is there given any recommendations for when swelling rock should be used in the case of weakness zones containing swelling clay. Due to the complexity of swelling, Palmstrom and Broch (2006) find the characterization of such rock mass too intricate. Comparing roof support in road and water tunnels, it is shown that for poor quality rock mass the difference is small, rising the question if the effect of the ESR factor is too small. However, due to different safety requirements in different countries the value of ESR may vary. Caution must be taken when estimating Q-values. According to (Mao et al., 2015) the complexity of weakness zones containing swelling clay cannot be fully accounted for in the common rock classification systems.

3.5 Numerical Methods

Numerical modelling is a very useful tool to evaluate design of underground excavations, carry out stability assessments or to do back analysis based on measurements during/after the excavation process. There are two main groups of numerical models, continuous and discontinuous models. The continuous methods treat the rock mass as a continuous medium, which mean that only a limited number of discontinuities can be modelled. Discontinuous models treat the rock mass as a system of individual blocks which interact along their boundaries. This type of method is referred to as *Distinct Element Methods (DEM)*. Continuous models are the most common type of models. These are represented by the *Finite Element Method (FEM)*, the *Finite Difference Method (FDM)* and *integral methods* (Nilsen and Palmström, 2000). The difference between the two first can be attributed to the mathematics behind the equations (Myrvang, 2001). RS^2 , which is used in this thesis, is a finite element method, and can be used to model a variety of situation and is much preferred due to its simplicity (Rocscience, 2017a).

The result of a numerical analyse is always a result of the quality of the input parameters. The most important input parameters are in situ rock stress, deformation properties, strength properties and the degree of jointing (Myrvang, 2001). For complex situations including weakness zones three-dimensional programs are normally preferred according to Mao (2012), but 2D models have also been used successfully (Trinh et al., 2009). An example of a 3D program is FLAC3D which is a numerical modelling software which

can be used for geotechnical analyses of soil, rock, groundwater, constructs, and ground support (Itasca, 2017). The effect of swelling pressure can be modelled as an uniformly distributed load (Mao et al., 2011b), both in 2D and 3D. In the case histories in section 5.3 some examples of modelling of weakness zones both in 2D and 3D are given.

Chapter 4

Swelling and Slaking

The properties within a certain rock group can vary a lot due to arrangement of minerals, their shape, size and the bonding between them. Minerals such as micas or swelling minerals can affect the properties of the rock, making it important to understand the mineralogy (Nilsen and Broch, 2012). The aim of this chapter is to give an introduction to the concept of swelling and slaking, and to explore the occurrence of swelling minerals. Finally some experiences from the Chilean Tertiary rock mass is described, together with an introduction to volcanic-sedimentary rocks.

4.1 Swelling

To begin with, some definitions must be stated. Nilsen and Palmström (2000) defines swelling ground as advancement of ground into a tunnel, due to expansion caused by water adsorption. This ability is limited to rocks containing clay minerals such as montmorillonite and to rocks with anhydrite. A cause of deformation of tunnel periphery that can be confused with swelling, is squeezing. Whittaker and Frith (1990), in Carter et al. (2010), describes the difference between swelling and squeezing like this: *"Squeezing ground commonly refers to weak, plastic rock materials which displace into the tunnel excavation under the action of gravity and from the effect of stress gradients around the tunnel opening. Swelling ground displaces into the tunnel opening as a result of volume change due to water adsorption and absorption effects"*. Squeezing will take place immediately after excavation while deformation caused by swelling may take longer time periods before visible.

In Norway one of the most common reasons for stability problems is crushed zones with gouge filled joints. Gouge consisting of minerals with swelling capacity normally cause the greatest problems (Nilsen and Broch, 2012). Swelling clays are mainly associated with weakness zones either as filling material in joints, veins, fractures or faults, or as a rock forming mineral in altered rock. The latter is less usual (Nilsen and Palmström, 2000). In addition to the characteristics of the gouge and swelling minerals, width and orientation of the weakness zone, access to water, frequency of occurrences, competence of side rock

and dimension of the tunnel (Mao et al., 2011b) affects the stability. According to Nilsen and Broch (2012), the most usual materials found in weakness zones are:

- Inactive minerals such as kaolinite, illite, limonite, zeolite etc. In Norway, this is the most common group.
- Minerals with low friction, such as chlorite, talc, graphite etc. The friction is particularly reduced when water is present.
- Solvable minerals such as carbonates
- Minerals with swelling properties, such as smectite.

Zeolites are listed as inactive in this table but the literature mention cases where they have been related to swelling together with smectites (Bell and Haskins, 1997)). It is usual to find zeolites as well developed crystals in amygdules and fissures in basic volcanic rock, or as a product of hydrothermal activity and burial metamorphism (Deer et al., 1992). Laumontite is considered to be one of the most abundant naturally occurring zeolites (Deer et al., 1992), and can change its volume upon hydration or dehydration (Bell and Haskins, 1997). It changes to secondary leonhardite when dried, and back to laumontite when wetted (Bell and Haskins, 1997).

Kaolinite, illite, smectite and vermiculite are the most important groups of layered clay minerals. They are sheet silicates, normally occurring as fine grained platy aggregates. When mixed with water they show varying degrees of plasticity (Deer et al., 1992). Swelling is mainly related to smectites, vermiculites and mixed-layer minerals, which are all secondary minerals caused by alteration (Selmer and Palmstrom, 1989). The smectite group consists of several subclasses, including montmorillonite, beidellite, nontronite, hectorite, saponite and sauconite. The swelling properties come from the ability these minerals have to take up water between their structural layers, as shown in figure 4.1. The structural formula of di-octahedral smectite is $(\frac{1}{2}Ca, Na)_{0.7}(Al, Mg, Fe)_4[(Si, Al)_8O_{20}](OH)_4 \times nH_2O$. The cations are exchangeable and sodium (Na) and calcium (Ca) are the most common. Na-smectites are associated with the greatest water adsorption (Deer et al., 1992).

The swelling process can be divided into two stadiums, hydration and osmotic swelling. The mineral is hydrated by surface adsorption of water between the Si-layers, and this can lead to up to 100 % volume increase of dry material. The osmotic effect is the result of a higher concentration of ions between the Si-layers, than in the interstitial water outside. To reach equilibrium water will stream against the highest concentration. Swelling and swelling pressure are mainly caused by these two effects. The amount of water that can be adsorbed depends on the type of smectite, which cation is present and the physical conditions (Nilsen and Broch, 2012). The clay minerals are created either through transformation of crushed material and country rock, or by hydrothermal alteration and deposition. Feldspar is transformed to either smectite or illite in Scandinavian climate, but under more warm and humid climate kaolinite is created. The composition of feldspar

is deciding which kind of clay mineral it is transformed to. For the formation of montmorillonite, plagioclase-feldspar is the country rock, while illite and kaolinite is created from alkali-feldspar (Nilsen and Broch, 2012). Several laboratory methods are used to determine the properties of gouge material and swelling clays. Mineralogical analysis includes X-ray diffraction (XRD), differential thermal analysis (DTA) and color testing. Ethylene glycol treatment is useful to identify smectites, due to the ability to occupy and expand the inter-layer spacing of the mineral, and keep them from retracting when drying (Nesse, 2000). Free swelling and different forms of swelling pressure measures more directly the swelling properties of the material (Nilsen and Broch, 2012). The results from the laboratory indicates the potential ability of swelling, but the physical conditions are as important for the actual in situ stability. The most important physical conditions are degree of consolidation, access to water and bonding between particles Nilsen and Broch (2012).

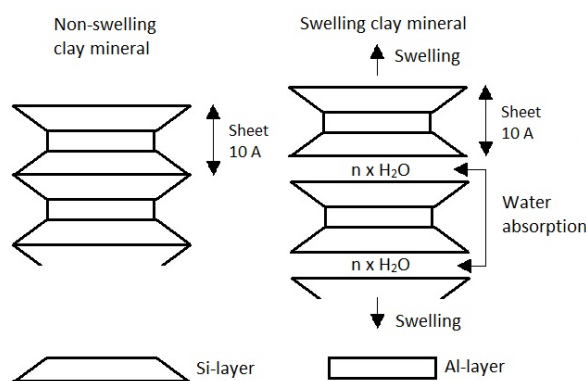


Figure 4.1: Structural difference between swelling and non-swelling clay minerals. The length is given in Angstrom, $1\text{A} = 10^{-7}\text{mm}$. Redrawing after Selmer and Palmstrom (1989)

4.2 Slaking

According to Goodman (1993) slaking is the deterioration and breakdown of rocks after it is exposed to air and water, and it is dependent on, and intensified when subjected to cycles of drying and wetting. Shales and mudstones that are not yet cemented, clayey friable sandstones and conglomerates are known to have this behaviour. Shales will break up along their fissility, while in mudstones new cracks will develop, which at some point will intersect and the rock starts to disintegrate. Clay bearing weathered igneous rock are also susceptible to slake deterioration (Franklin and Chandra, 1972). Slaking is most common when the rocks contain swelling minerals, but can also happen due to more complex mechanisms in non-expansive shales and mudstones. In several cases slaking of rock mass have been seen together with swelling (Brattli and Broch, 1995; Bell, 2007; Tu et al., 2005). Following the three controlling factors for slake-durability according to Franklin and Chandra (1972) are listed:

1. Permeability and porosity decides the possibility for fluids to enter the rock, and their mobility within the rock mass.
2. Fluid behaviour in the rock mass; adsorption, solution of cement or breaking of bonds or generation of pore-pressure changes.
3. Extent of weakening, swelling or disintegration is decided by the rocks ability to resist disruptive forces.

The mechanisms that Franklin and Chandra (1972) describe as responsible for slaking of rocks are ion exchange, capillary effects and stress relief. Ion exchange is considered the dominant mechanism. Capillary effects originate when water enters the rock, and increase the radius of curvature of the water meniscuses, leading to reduced capillary tension between grains. The rock can also be disrupted when capillary forces draw water into the rock and compress air on its way. Rocks containing clay may store elastic strain due to over-consolidation and weakening of the intergranular bonds can then lead to stress relief.

The effect of slaking is shown in figure 4.2. Repeated cycles of wetting and drying leads to a loss of mass, suggesting that long term drying and wetting of rock mass, can lead to weakening of mechanical properties (Panthi, 2006). In tunnels where slaking is a problem, the installment of rock support can be troublesome. Rock bolts may lose contact with the rock mass and/or be hard to anchor, while shotcrete might not adhere properly to the walls. Because of this, the tunnel should be lined immediately after excavation (Goodman, 1993). Index tests such as swelling and slake durability tests are used to predict this behaviour (ISRM, 1979b).

Under site investigation for the Heimifeng Pumped Storage Power Station in China highly altered granite bands with swelling properties were found (Tu et al., 2005). Slaking and disintegration of rock blocks were also seen in connection with these alteration zones. It was inferred that intrusion of magma had led to hydrothermal alteration. The alteration process caused formation of montmorillonite in the rock mass, in addition to chlorite and kaolinite. The altered granite has weak geomechanical properties, associated with the degree of alteration, which again was connected to increasing montmorillonite content. With increasing absorption of water the mechanical properties are decaying further and the rock mass swells and eventually disintegrates (Tu et al., 2005).

Dhakal et al. (2002) did tests on argillaceous clastic rocks from Japan and found that mineral composition, textural features and the degree of rock alteration affected the slake durability. In the Lesotho Highlands Water Project slaking of basalts were experienced. The slaking was explained by the presence of secondary minerals belonging to the smectite family in addition to zeolites (Bell and Haskins, 1997). The basalts were subjected to a number of tests to assess their durability for construction material purposes. Ethylene glycol testing proved to distinguish slaking basalts from non-slaking.

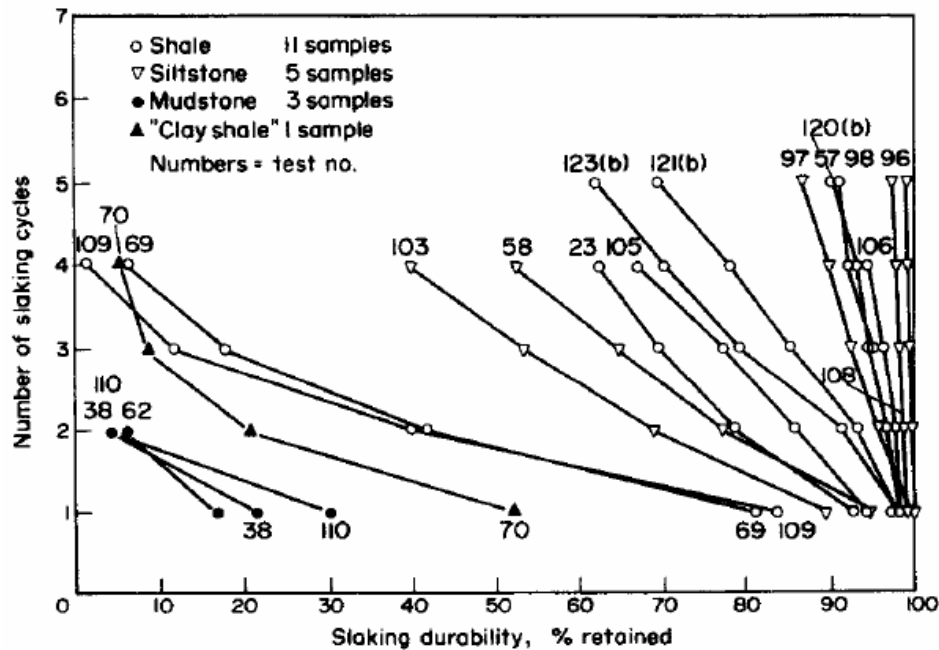


Figure 4.2: Effect of several numbers of slaking cycles on slake-durability (ISRM, 1979b)

4.3 Support Strategy

In Norway most of the hydropower tunnels have from 2-4 % concrete or shotcrete lining, except for a few cases where the use has increased to 40-60 %. Even though the tunneling conditions often are favourable, this is also due to a support philosophy where a certain degree of rock fall is accepted (Broch, 2013). In this section both support of weakness zones with swelling clay and support of swelling rock mass will be described.

The philosophy for support in weakness zones containing swelling clay is based on the fact that if the material is given the opportunity to expand only a little bit, the swelling pressure can be reduced strongly. In figure 4.3 the reduction of swelling pressure is shown for some Norwegian clays, in addition to a proposed method for support of small weakness zones. Shotcrete is usually not recommended as support in swelling clay zones since it does not have room for expansion, however if installed as in the figure good results have been achieved for narrow zones. For larger zones full concrete lining is recommended (Nilsen and Broch, 2012).

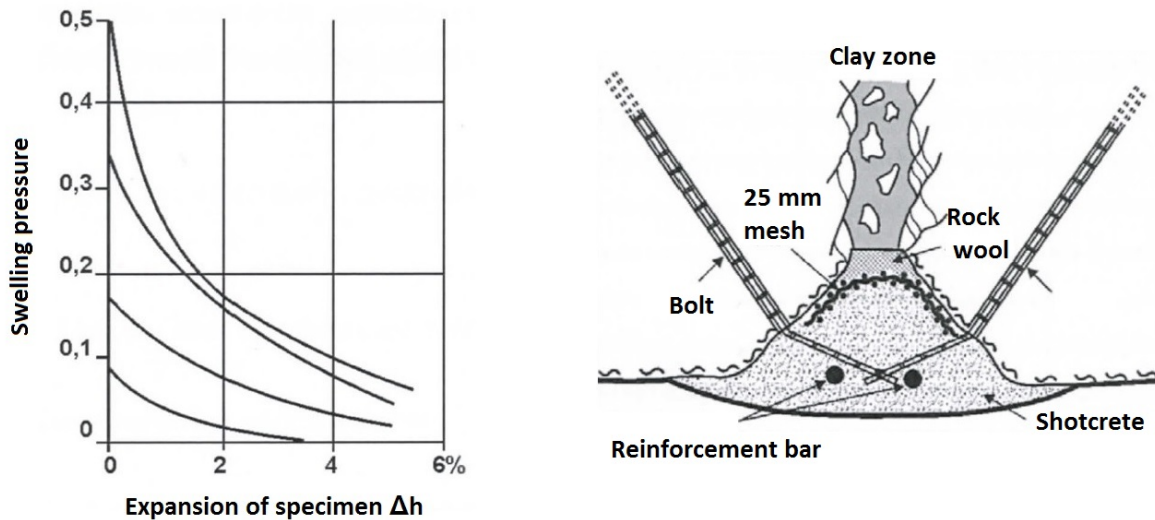


Figure 4.3: Left: Reduction of swelling pressure after volume expansion of the specimen is allowed (for Norwegian swelling clays). Right: Proposal of support of small weakness zones containing swelling minerals. Modified from Nilsen and Broch (2012).

The principle that increasing deformation of the rock leads to reduced swelling pressure also applies for swelling rock mass. Support can be designed in such a way that it allows for both deformation of the rock mass, as well as applying a supporting pressure (Kovári, 2009). The two problems directly associated with swelling rock is failing of the invert arch due to the swelling pressure, or heave of the tunnel under low overburdens. The latter may leave the tunnel nearly undamaged, however it may limit the serviceability of the tunnel.

Ordinary shotcrete has low deformation capacity and is as mentioned not recommended as support of swelling rock alone. A solution for this, is to implement yielding elements in the shotcrete, which allows for contraction of the profile in addition to resistance against deformation. Another solution is to insert highly compressible concrete elements, composed of a mix of cement, sand, hollow glass particles, steel fibres and additives, in the shotcrete lining. Depending on the yielding stress, such elements can be compressed up to 40-50 % (Kovári, 2009).

The support solutions mentioned above are used for railway and road tunnels, and the kind of solution that is chosen, should be in accordance for the kind of safety level that is required in a water tunnel. The installment of effective support against swelling rocks is expensive, and it is therefore of great importance to identify the zones where this is necessary. According to Kovári (2009), the squeezing and swelling potential along a tunnel might not be uniform, and may vary with time. This means it is important to install support which can withstand future deformations as well as deformations at the time of excavation. According to Mao et al. (2011b), the support of weakness zones containing swelling clay may often be overestimated, due to a tendency that only cases where actual failure have happened are focused on. The value of swelling pressure determined from

laboratory tests must be evaluated.

The swelling pressure measured in the laboratory can not be directly compared to in situ pressure as it also depend on factors such as the consolidation degree (Mao et al., 2011b; Nilsen and Broch, 2012). At NTNU research has shown that the in situ swelling pressure normally is lower than the laboratory value, and can be as low as 50 % (Tyssekvam, 1996) in (Mao et al., 2011b). Numerical analysis can be used to quantify the swelling pressure by applying different loads, and comparing it to actual load if such measurements have been carried out in the tunnel.

Under dry tunneling conditions, differentiation between non-swelling and swelling materials may be impossible, unless special testing is undertaken. Under wet tunneling conditions, swelling can squeeze rock material out of the walls, especially in the lower parts of the walls as the clay can absorb water from ditches (Nilsen and Palmström, 2000).

4.4 Volcanic-sedimentary Rocks and the Chilean Tertiary Rocks

4.4.1 Volcanic-sedimentary rocks

The tunnels of La Confluencia is constructed in the Coya-Machalí Formation, one of the Cretaceous Tertiary rock units where swelling and disintegration of the rock mass has been experienced (Carter et al., 2010). According to Carter et al. (2010)(p.216) the most swell prone units in this formation are present as *relatively thin intercalations of detrital volcanoclastic rocks, principally finely bedded reddish brown and dark brown haematized siltstones, shales, sandy siltstones, lapilli tuffs and/or fine grained sandstones and/or breccia/conglomerates.*

In the following an introduction to volcanic-sedimentary rocks are given with emphasize on those present in this formation. Pyroclastic rock is made up off consolidated pyroclastic sediments from active volcanism, tuff, volcanic breccia/conglomerates and ignimbrites are all subgroups (Goodman, 1993).

- Tuff is a consolidated pyroclastic sediment of ash and lapilli size. Lapilli refers to pyroclastic debris between 2 and 64 mm which consist of rock fragments from the same eruption or from other nearby volcanic rock types. Volcanic ash is normally silt sized and consists of volcanic glass which has solidified too rapidly for a crystal lattice to form. Tuff can be welded and non-welded, and both types may exist in the same deposit. Devitrification, a process where glass grows in to a lattice, commonly alters volcanic ash to montmorillonite, and it is common that tuff has layers of bentonite. Tuff can also be cemented by carbonate or opal (Goodman, 1993).

- Volcanic breccia is coarse grained and consists mainly of blocks of pre-existing rock fragments larger than 64 mm (Goodman, 1993).
- Ignimbrite is formed by glowing avalanches, and is poorly sorted and welded pyroclastic rock. The rocks become welded at temperatures above 535°C, and is also called welded tuff. Upon cooling they typically show columnar jointing (Goodman, 1993).
- Andesite is a product of subduction volcanism. The plutonic rock is diorite or granodiorite. It is typical that these rocks are highly porous near their margins due to the content of gas bubbles before cooling. A rock with a high content of vesicles are called scoriaceous. These vesicles can later be turned into amygdules which are filled with secondary minerals (Goodman, 1993).

The content of coarse rock crystals or rock fragments in a fine grained ash matrix is called a porphyritic texture. If the matrix is so fine-grained that the individual crystals can not be seen it is called aphanitic. This is characteristic for volcanic rocks and tuff. It is typical that different volcanic sediments and rocks are found together in non-homogeneous formations, often with sediments of non-volcanic origin interbedding the volcanic material (Goodman, 1993).

4.4.2 The Chilean Tertiary rocks

According to (Carter et al., 2010) one of the issues in these rocks is to identify the zones in which extra support is required since they typically appear as rock mass of good quality in the construction period. The projects listed in the introduction typically was excavated without special problems, except for the crossing of faults or fractured ground. The support has mainly been installed according to the Q- and RMR system. The zones where red beds have been observed are shotcrete lined to limit degradation due to erosion or slake-durability. This limits therefore the possibility of geological observations.

The degradation process is slow going and it may take from years to decades for stability problems to appear. These are typically related to shotcrete competence, which may first appear as hairline spiderweb cracks that later progress to larger cracks and eventually fall-outs. The zones where the cracks were first observed are inferred to have a mineralogical or structural variation from surrounding rock that highlights the swelling and degradation process and initiates cracks in the lining. The original rock mass in the worst damage zones is decomposed into a clayey sand matrix with fragments from the original rock.

Results from the extensive laboratory testing have resulted in three main observations. Hematite on the swelling clay surfaces and/or in the crystal lattice seems to affect the swelling potential. The chemistry of the pore water versus the water in the tunnel can affect the swelling by reducing hematite, which may lead to a loss of cementation in the rock mass. The time rate of the swelling process is likely affected by the type of swelling

clay. Identification of the problematic zones, and establishment of correct design pressures are important for a time and cost effective approach.

One of the steps that may be used to evaluate appropriate support design is to model the interaction between rock and liner by using input parameters from the testing program. By establishing the degree of swelling severity together with a relationship between strain rate and pressure to suppress swelling, long term deformations can be modelled, if also the stress conditions and tunnel geometry are known. The swelling process can be modelled in 2D by applying different sections from disturbed to undisturbed rock mass around the tunnel lining and water filled tunnel. The degradation/swelling process is assumed to be water driven and each section is assigned a hydraulic conductivity and diffusion coefficient. By modelling diffusion into the rock mass, the long term behaviour and swelling strain relationship can be decided. The input parameters in such a model is complicated to obtain and it is recommended to supply the data with monitoring in the relevant tunnel sections (Carter et al., 2010).

Chapter 5

Case Studies

According to Panthi (2014), collapses in headrace tunnels and shafts under operation, can be attributed to compromises regarding support system at the time of construction or misjudging of the geological and stability conditions. Compromises on safety done under construction, may later lead to economic loss, and it is therefore crucial to install proper safety measures also with long term stability in mind. Two case histories are chosen to highlight the importance of long time stability and adequate support measures in hydropower tunnels. As for the case from Svandalsflona, swelling clay is not mentioned, but the case is still seen as important as it illustrates that stability issues can happen long after excavation is finished. The case from the Chacabuquito Hydropower plant in Chile, describes the measures that were taken to support zones where expansive behaviour was encountered. Finally some examples of numerical simulation of swelling behaviour around tunnels and modelling of weakness zones are provided.

5.1 Svandalsflona

This case is based on the assessment made by Panthi (2014), on analysing the burst debris flood that happened after a major rockslide in one of the tunnels at Svandalsflona hydropower project. Svandalsflona is part of the Røldal/Suldal development scheme in Southern Norway, and has an installed capacity of 20 MW, and a yearly production of 36 GWh. Three lakes are contributing to the production. One of these is lake Stutakvelven, which also functions as a surge shaft. It is connected to the headrace tunnel by a 45° inclined shaft. The project came in operation in 1978, and in 2008, after nearly 30 years of operation a major rockslide took place in this shaft. As a result a sinkhole appeared all the way to the surface topography.

The geology in the area is represented by a Precambrian basement consisting of greenstone and greenschist, a Cambro-Silurian basement with schistose phyllite and quartzite, which is overthrust by nappes from the Caledonian orogeny. The overthrust nappes consist of quartzitic gneiss. The boundary between phyllite and quartzite is represented by a weakness/fracture zone, which also crosses Stutakvelven shaft. The geology and

waterway system is shown together with the location of the shaft in figure 5.1.

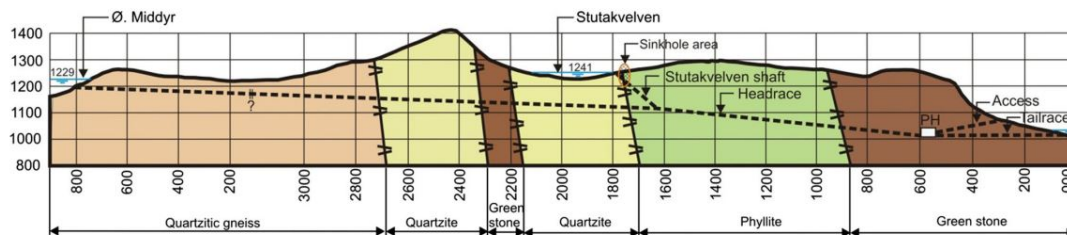


Figure 5.1: Geological profile from Svandalsfjona hydropower project showing geology in the area and the Stutakvelven inclined shaft and weakness zone, together with the waterway system. Figure from Panthi (2014).

At the time of construction, it appears that there was no substantial need for special rock stabilisation measures. The tunnel systems are for the most part unlined, except for some major weakness zones which were fully concrete lined. The rock support elsewhere consists of scattered bolting, in addition to unreinforced and mesh reinforced shotcrete where necessary. In 2009, it was found that the tunnel crosses several clay-filled and crushed zones, of thickness less than 1 m. At a few locations it was observed rock falls, mainly located in the Cambro-Silurian basement. Two concrete lined zones, coincide with the weakness zone which also crosses Stutakvelven shaft. The zone consisted of highly fractured rock material, mixed with clay, silt and sand. The rock mass had low cohesion and frictional properties, in addition to being very permeable (Panthi, 2014). The excavation of this zone was challenging, as the initial bottom up excavation by Alimak raise climber, had to be exchanged with top to bottom excavation. At the point of excavation the weakness zone was secured with concrete lining, which it is inferred may not have been of top quality due to the technology at that time.

The rock slide was discovered after observations of unusual water level at lake Stutakvelven, which meant that there was a blockage somewhere in the waterway system. During clean up of the slide mass a burst flood happened, which lead to the loss of two workers life. The events of this is not further explored since it is the long term rock stability that is of interest. The slide happened as mentioned after nearly 30 years of production, showing the importance of long term stability. A constant supply of water, lead to saturation of the rock mass behind the concrete lining, and weakening of frictional properties and cohesion.

5.2 Los Quilos and Chacabuquito Water Tunnels

This case will focus on the reinforcement of zones with swelling behaviour encountered during construction of the tunnel system for The Chacabuquito Hydropower Plant. The Plant is located in the Andes Mountains, 65 km north-northeast of Santiago, Chile, and can generate approximately 25 MW. The water conduction system consists mainly of

an open channel and two horse shoe section tunnels: Los Quilos, 788 m long, and Chacabuquito, 2171 m long. The case is based on the description of the tunnels by Castro et al. (2010).

The tunnels were excavated in the Los Pelampres Formation of Cretaceous age, which are built up of stratified porphyric and aphanitic andesite, aphanitic basaltic andesite and basalt, in addition to local layers of fine grained sandstone and/or andesitic tuff and limolites. During construction of the two tunnels expansive rock behaviour was encountered. The most serious problems were related to three different geological features.

- Both tunnels crosses north south trending faults with strongly fractured rock and clayey filling. The clay filling is montmorillonitic and kaolinitic.
- At the eastern front of the Chacabuquito tunnel, zones with thin veins of zeolite, calcite, montmorillonite, kaolinite and illite were encountered.
- At the eastern front of the Los Quilos tunnel, the andesitic rock mass had been hydrothermally altered, which have lead to the presence of montmorillonite, sericite and minor kaolinite.

In the Chacabuquito tunnel, the most critical situation was related to the north south trending faults. Here, the rock mass was of very poor geotechnical quality, soft and decomposed with hematite and montmorillonite. Expansion pressure was measured of 0.03-0.14 MPa in the laboratory. In three other fault zones, some fall-outs were experienced during excavation, requiring heavy support. The tunnel floor was unsupported, and very little deformation was observed, as opposed to the other tunnel.

The hydrothermally altered rock mass of The Los Quilos tunnel was very fractured and oxidized, consisting of softer rocks mixed with relatively stronger rocks. During excavation the stability was relatively good, except for some fault crossings with highly plastic and expansive clay. When the hydrothermal altered rocks were exposed to water or natural humidity, they had a tendency to disintegrate. Expansion pressure of 0.03-0.33 MPa was measured along this zone, in general less than 0.2 MPa (laboratory values). The highest pressure of 0.33 was from clay in a fault core zone, and therefore not considered as representative for the support design. The invert of the tunnel had to be repaired in the areas with clayey rock, due to sinking of the floor, because the clayey rocks softened due to a combination of saturation and heavy vehicles. Some minor rockfalls were also experienced.

Throughout the construction process rock samples were collected to conduct classification tests, free swelling, swelling pressure and slake durability tests. Grain size distribution analysis was carried out on decomposed rock, as it behaved more like soil. Slake durability tests did in general show medium high to high slake durability index, with the lowest value of 66 % which classifies as medium according to (ISRM, 1979b).

Swelling of the clay minerals are suggested as a possible reason for the sinking of the tunnel floor. Geomechanical analysis was used to design flexible rock support that allowed for expansion of the rock mass. A reaction curve was made based on calculations of the

reduction of expansion pressure at the tunnel floor, as a function of support displacement, shown in figure 5.2.

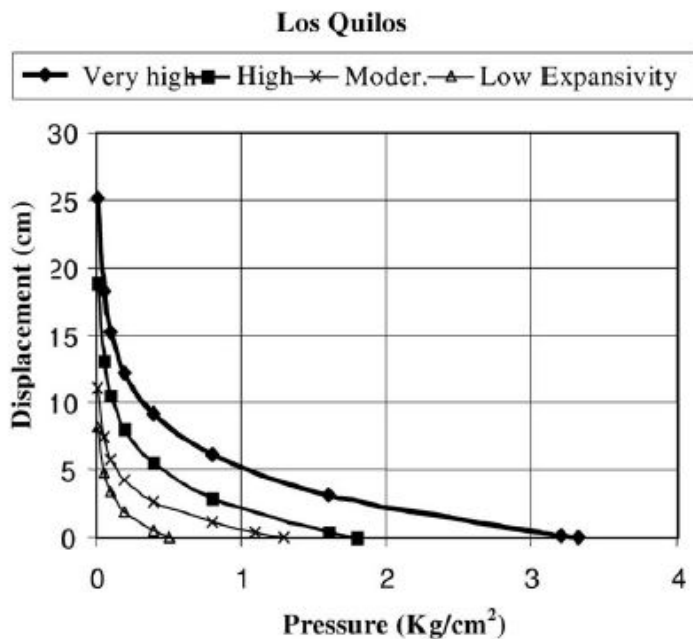


Figure 5.2: The reaction curve of Los Quilos Tunnel. Displacement of support in cm is plotted against swelling pressure in kg/cm³ (Castro et al., 2010).

In addition a ballast coefficient was established, and the load of loose rock blocks were calculated, to model the full load on the support. A load factor of 1.4 was applied to both expansion pressure and vertical load. In this way both swelling pressure of the rock mass and pressure of loose rock blocks were accounted for, and the support system finally consisted of different variations with systematic rock bolts and reinforced shotcrete combined with lattice girders, and a reinforced concrete invert. The final support in the Los Quilos Tunnel are illustrated in figure 5.3.

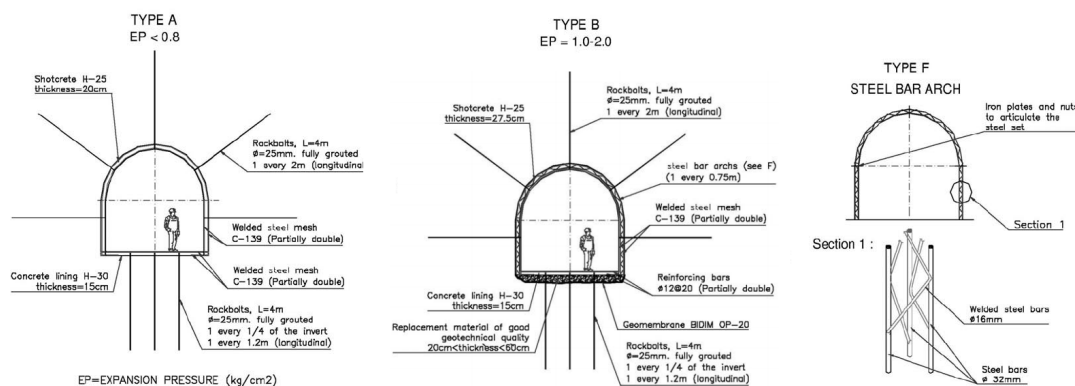


Figure 5.3: Example of rock support in the expansive zones in the eastern Los Quilos Tunnel, where sinking of the floor was experienced (Castro et al., 2010).

With the load factor of 1.4 some damage of the support is accepted, such as local

cracks in the shotcrete as well as deterioration of the rock mass behind. In the areas of softened invert, the soft rock was removed and a geomembrane put in place, and the material replaced with muck. After one year of operation there were not detected any problems. (Castro et al., 2010).

5.3 Numerical Simulation of Weakness Zones

5.3.1 Hanekleiva

Mao et al. (2015) simulated the rockfall at the Hanekleiva road tunnel, in Norway. This incident happened in a fault zone with swelling clay, ten years after the tunnel was completed. In addition to the swelling process, low internal friction contributed to gravitational collapse. The fault zone is localized in Permian syenite, and was discovered during excavation. It was then supported by 15 cm of reinforced shotcrete. Still, cracks in the shotcrete was discovered as the excavation progressed, and the affected area was covered with 10 cm additional shotcrete. 10 years after the tunnel was completed the rock fall happened. Table 5.1 list the input parameters of the side rock, and the fault zone, both in its original version and after strength reduction has occurred. They are estimated based on engineering experience. The material in the cave in was a mixture of small blocks, gravel and altered fragments of syenite, in addition to one large block of syenite. A Q -value of 0.01-0.02 was assigned to the zone, which is extremely poor. Strength reduction of the material happened as water was absorbed during the swelling process.

Table 5.1: Relevant input properties of fault zone and side rock at case Hanekleiva, modified after Mao et al. (2015).

Properties	Original fault zone	Weakened fault zone	Siderock
Density [g/cm^3]	2.7	2.7	2.7
E-modulus [GPa]	3.1	2.0	45
Poisson's ratio	0.3	0.3	0.22
Cohesion [MPa]	0.45	0.2	6
Friction	30 °	15 °	50 °
Dilatation	-	-	15 °
Tensile strength [MPa]	-	-	1

FLAC3D was used to assess the events using the Mohr-Coulomb model and elasto-perfectly plastic stress-strain law. The effect of ground water was not considered. A conservative approach is applied for the properties of the weakness zone. Strength reduction mainly occurred in the zone close to the tunnel periphery, but the same weak material was assigned to the whole zone. The simulation focused on three stages. Initially the shotcrete cracks at the time of excavation were verified. Later the swelling pressure of 0.18 MPa found from laboratory tests, was applied between the weakened zone and the shotcrete, and the results showed that the effect on shotcrete loading was

limited. The effect of swelling pressure on the rock support was simulated as a uniformly distributed load. Finally, the strength reduced material was applied to the zone where the slide happened, and collapse of the zone was verified (Mao et al., 2015).

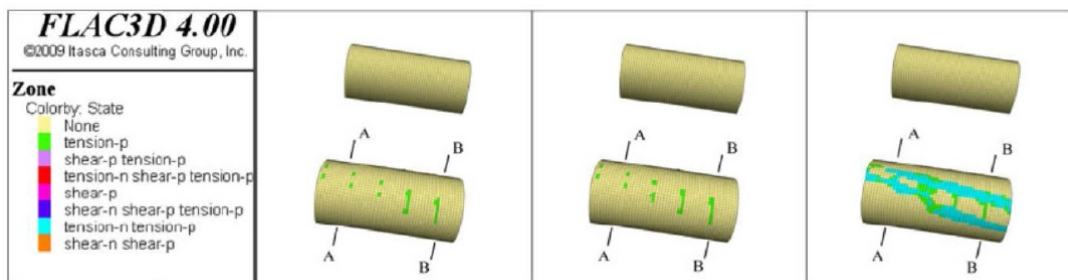


Figure 5.4: The three stages of the numerical simulation at Hanekleiva. The left image show yielded zones after excavation, the middle, yielding due to swelling pressure, and right yielding due to strength reduction of material (Mao et al., 2015).

5.3.2 Buon Kuop Hydropower Project

A cave in happened in the headrace tunnel of Buon Kuop hydropower project in Vietnam. When cutting the 15-20 m wide weakness zone, material collapsed in to the tunnel together with water and created a sinkhole up to the surface. The weathered, sedimentary rock material had been sheared and consisted mainly of clay (Trinh et al., 2009). The convergence-confinement method and 2D analysis in Phase 2 were used for a parametric study and to assess if the applied failure criterion was suitable (Trinh and Broch, 2008). Data from the pre-investigation and from observations during construction was studied. Three options of rock mass properties was considered and the CC-method was used to determine which was more realistic. Two of the methods was based on curve fitting of in situ test results from the construction design phase. Curve fitting was done by the Mohr Coloumb and Hoek Brown criteria. The third method estimated rock mass properties based on observations at the location of the failure and the program RocLab was used to estimate the rock mass properties. The last method gave the most realistic results and was used as input in the Hoek Brown criterion for the 2D model. The weakness zone was modelled with a UCS of 12 MPa, a GSI of 25, and a Hoek Brown parameter m_i of 7, the surrounding rock mass with a GSI of 58 and a UCS of 25 MPa.

For the same case, Trinh et al. (2009) compared 2D modelling in Phase 2 (now RS^2) and 3D modelling in Flac3D. Since the material is inferred to be soft, the behavior is ductile and analysis of displacements can be used to indicate stability. Three situations were modelled; first the models were verified by simulating the situation as it happened, then the model was simulated as a half face excavation with support to check if it was appropriate. Finally, the stability with full face excavation and support was assessed. The 2D model is here a longitudinal section, not a cross section, as the model setup in figure 5.5 show.

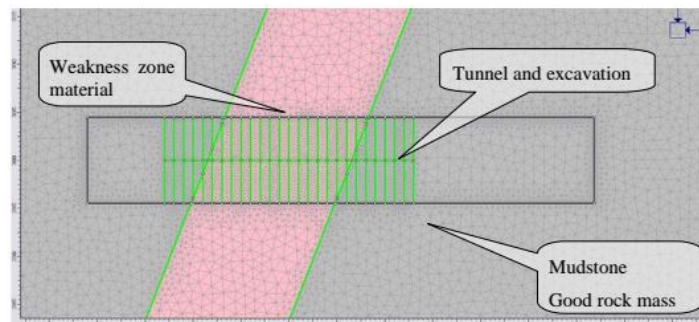


Figure 5.5: Model set up of weakness zone, Buon Kuop. The tunnel is seen in the longitudinal direction and deformation during excavation is simulated (Trinh and Broch, 2008).

For the case of unsupported full face excavation, the displacements in the 2D model was larger than in the 3D model. A possible cause for this is that in 2D, the model is not bounded in the out of plane direction, which means the material is infinite. Groundwater clearly affected the displacements. When simulating the tunnel in a longitudinal section in 2D, the usual application of liner elements is not suitable. For this reason an internal pressure equivalent to the support pressure was applied. In FLAC3D, both spiling bolts, shotcrete and steel ribs can be modelled, and forces acting on the support can be analyzed. In this stage both tunnels had reasonable deformation in the roof, but for this case smaller in the 2D model, possibly due to overestimation of support pressure. The 3D model, however, had large displacements at the face and in the floor. This was not experienced during construction, and may be related to geometry of the model. The displacement dropped quickly to realistic values after the one meter thick high displacement zone. It is therefore suggested to ignore these displacements, with emphasis on using judgment by experienced engineers. The 2D model is used successfully to assess a complicated issue, but has some weaknesses regarding simulating support such as spiling bolts. The more complicated 3D model is very useful for this purpose and can give input for structural design of support (Trinh et al., 2009).

Chapter 6

Portillo Tunnel

The samples that are tested in the laboratory program are taken from the Portillo tunnel. A general overview of geology and structures along the tunnel alignment is presented in this chapter, based on the report from the pre-investigations from Golder Associates (2016). Further it is focused on a section between PK 34+390 and PK 34+405, where a weak zone was encountered. This zone is modelled in the numerical analysis. Information from construction mapping, in addition to a field visit conducted on March 28.-29. is used to describe this area.

6.1 Project Background

La Confluencia is as mentioned in the introduction located in the Tinguiririca Valley, approximately 150 km south of Santiago (Statkraft, 2011). Water is collected from the Portillo and Tinguiririca valleys. Each valley has a main intake, and 3 and 2 secondary intakes respectively. The highest intake is at 1520 m.a.s.l., and the powerhouse is located at 1100 m.a.s.l. The plant is comprised of the 9.5 km long Tinguiririca pressure tunnel, and the 12 km long, unlined free flow Portillo tunnel, which meets in a junction. Construction of the Tinguiririca branch started in December 2008, and was finished in April 2010. The Portillo branch started in November 2008 and ended September 2011 and was constructed in lesser quality rock mass than Tinguiririca (Paul et al., 2012).

6.2 Geology

Four different rock units have been registered in the project area, among them the earlier mentioned Coya Machalí formation. The tunnel alignment can be seen in the geological map and profile provided in appendix G. The rock units are described from oldest to youngest based on the geological and geotechnical report and maps by Golder Associates (2006, 2016). Only the rocks seen along the Portillo-Azufre tunnel are presented. The Farellones Formation is left out of the description as it affects neither of the tunnels.

Coya Machalí Formation (KCM)

KCM is of Middle to Upper Cretaceous age and consists of three different subunits, presented from oldest to youngest. All of the units have intercalations of reddish sandstones with extensive weathering and fracturing, reducing the geotechnical quality in varying degree according to thickness and amount.

- *KCM-a: Andesites, andesitic tuffs, volcanic breccias.* The weathering degree is moderate to weak in the surface, with strong and dense rock mass and a moderate fracture degree. The geotechnical quality is regular to good. They cover the final part of the Portillo-Azufre tunnel branch.
- *KCM-t: Andesitic lava flows, andesitic tuffs, reddish/greenish breccias and/or conglomerates, and intercalations of reddish shales and fine sandstones.* Stratified in more than 1 m thick strata except for the shale and sandstone which are from centimeter to decimeter scale. Moderate surface weathering and fracturing, regular to locally good geotechnical quality. The thin layers of fine sandstones and shales are soft, strongly fractured, with planar and smooth fracture surfaces and show a friable and/or expansive behaviour. The geotechnical quality is poor to very poor in these layers. Observed upstream of adit 1 in the Portillo-Azufre tunnel branch.
- *KCM-s: Sandstones, shales and cineritic tuffs with isolated intercalations of conglomerates.* Stratified in centimeter to decimeter scale stratas. Soft rocks, intensively weathered and fractured with planar smooth to moderately smooth fractures. Fracture coating of iron oxide, some clay and calcite are observed. The geotechnical quality is poor to very poor. Observed around Adit 1 in the Portillo-Azufre tunnel branch.

Intrusive Granodioritic Complex (Tg)

Intrusive complex of Middle Tertiary age, composed mainly of light grayish granodiorites, generally sound, very strong and dense rocks. Moderate to weakly fractured with sinuous or irregular and very rough surfaces, weathering degree is in general weak to moderate, except for a decomposed/highly weathered part affected by an old slide. The geotechnical quality is good to very good. Observed in the initial parts of the Portillo-Azufre tunnel branch.

Tinguiririca Volcanic complex (Qt)

Volcanic complex of Tertiary age affecting only the Portillo-Azufre tunnel branch. It is composed of both semi-consolidated soil deposits and rock units, and can be divided in two:

- *Tuff Ignimbrite Deposit (Qt)*. Resulting from eruptions of the Tinguiririca volcano, and consists of consolidated to partly consolidated layers of tuff. The geotechnical quality is varying from moderate to poor depending on the consolidation degree.
- *Basaltic lava flows (Qb)*. Sound, dense and moderate to strongly fractured rocks, with relatively planar and moderately rough fracture planes. In general representing a regular to locally good geotechnical quality. It is interpreted that this unit is covering the older rocks (KCM and Tg), however the thickness is not known.

The geotechnical categorization are given based on the modified Q-index method (Golder Associates, 2016). The classification is provided in appendix I. The soil units are not considered as their thickness is estimated to be maximum 3 m in the upper parts of the hillsides. It is therefore assumed that the contribution to the overburden in the modelled area is negligible. A simplified cross section between PK 33+500 and PK 34+900 is presented in figure 6.1.

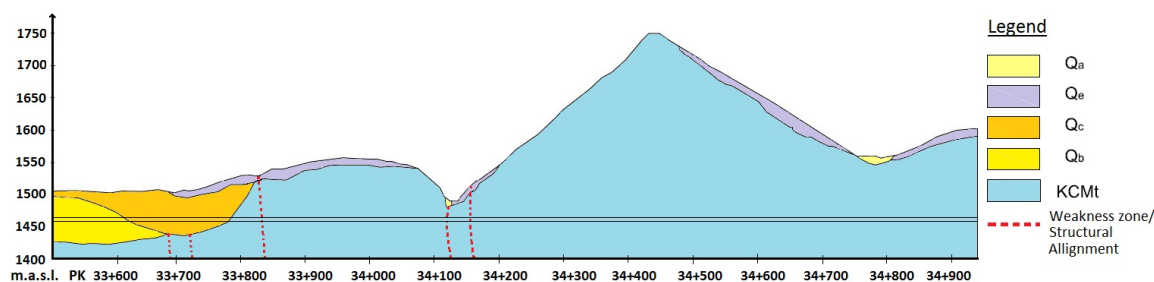


Figure 6.1: Simplified geological profile of PK 33+500 - PK 34+900 based on as built maps (HLC, 2011). Numerical analysis is conducted on a cross section perpendicular to PK 34+405. Qa is alluvial deposits, Qe is colluvial deposits, Qc is alluvial fans, Qb is basaltic lava flows of the Tinguiririca volcanic complex, KCM-t is of the Coya Machali formation.

According to the as built maps (HLC, 2011) the tunnel passes through KCMt in the alignment between PK 34+390 and PK 34+405.

6.3 Structures and Discontinuities

Characteristic rock stratification seen in the area is illustrated by the image in figure 6.12. The discontinuities along the Portillo tunnel are represented by the stratification, several sub-vertical discontinuity sets (S2, S3 and S5) and a secondary sub-vertical set (S4). Strike and dip direction of the discontinuity sets in the area are presented in table 6.1 (Golder Associates, 2016).

Due to the orientation and gentle dip of the stratification it may have affected and controlled the contour of the crown. S2 and S5 may have affected the contour of walls in different parts of the tunnel depending on its orientation. In addition three major

Table 6.1: Joints and minor fractures of the Portillo-Azufre tunnel branch. Table from Golder Associates (2016).

Set or family	Strike	Dip	Comment
S1	N7°W	21°WSW	Stratification
S2	N55°E	84°NW	Main sub-vertical set
S3	N57°W	87°NE	Main sub-vertical set
S4	N72°E	52°W	Secondary sub-vertical set
S5	N12°E	84°E	-

discontinuity planes affects the Portillo tunnel, none which corresponds with the joint sets in table 6.1.

Table 6.2: Fault and shear zones of the Portillo-Azufre tunnel branch. Table from Golder Associates (2016).

Set or family	Strike	Dip
F1	N82°W	86°S
F2	N26°E	26°SE
F3	N74°E	87°SSE

F2 was expected to impact longer stretches of the tunnel due to its orientation presented in table 6.2. In addition to the presented fault/shear zones, at least two interbedded zones where weaker material could be expected was observed. It was inferred that they would appear as stratification planes, affecting stability in the crown (Golder Associates, 2016).

PK 34+390 to PK 34+405

The mapping schemes from the construction phase have been studied in the area from PK 34+301 to PK 34+537. The schemes show a variation of 3 to 5 joint sets, illustrated in the joint rosette in figure 6.2. There are registrations of fallouts because of unfavorable joint orientation and overexcavation several places along this stretch.

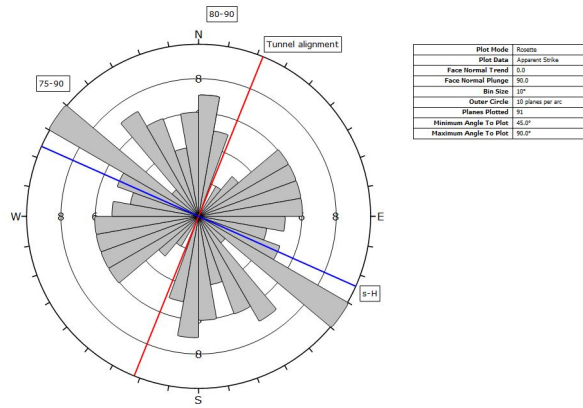


Figure 6.2: Joint Rosette from PK 34+258 to PK 34+500 based on 115 measurements from the construction phase. Approximate tunnel orientation shown in red is 22° and direction of largest horizontal stress σ_H 114° shown in blue.

A zone with similar characteristics as the weak zone at PK 34+395 appears at PK 34+354 with a dip of approximately 30° . At this chainage the rock mass changes from andesite and tuff, to tuff. At PK 34+382 the dip changes to $40\text{-}50^\circ$. The dip direction of the zone is about 280° along this stretch. It is not clear from the schemes whether the dip direction is measured according to north or the tunnel axis. From images and personal communication the zone is about 0.5 to 1 m thick. At PK 34+428 it is not registered anymore (HTC, 2010).

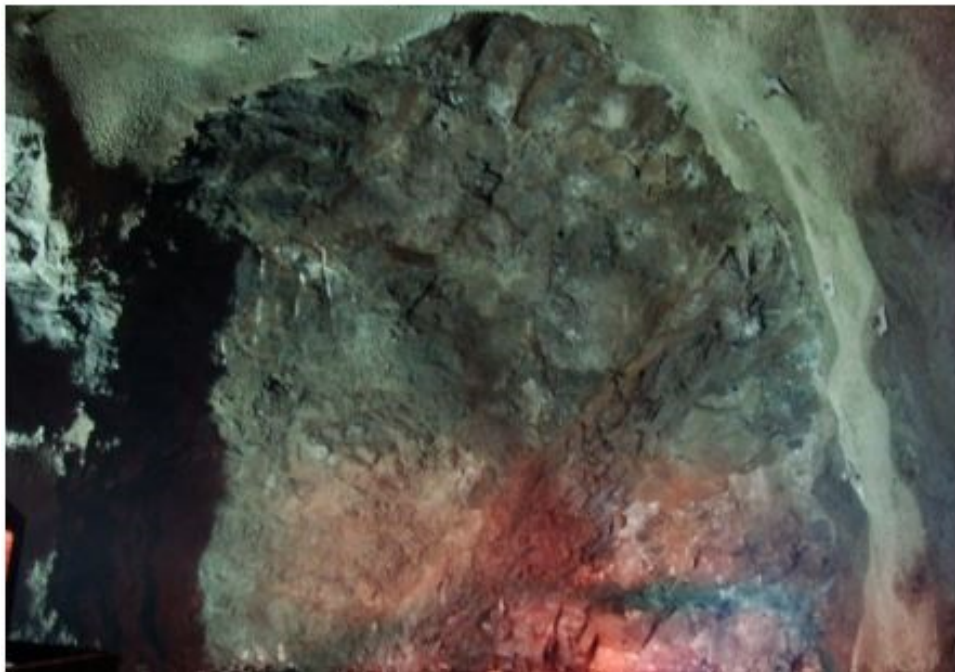


Figure 6.3: Image of PK 34+395-PK 34+390 from the construction phase (TE, 2010)

The zone is filled with highly weathered and argillaceous material, limonite and oxides mainly, in addition there are some registrations of calcite. It is highly broken and has a red/brown characteristic color. At PK 34+395 – 34+388, inflow of 1-2.5 l/min x m

is registered. This type of inflow is registered a few other places as well. Based on information from the mapping schemes and communication with co-supervisor the zone is inferred to cross the tunnel as illustrated in figure 6.4. The two cross sections marked in the figure are modelled later.

Due to the repeating registrations, it is likely to believe that different layers with the same characteristics cross the tunnel. A similar zone is visible around PK 34+517 to PK 34+500 in the upper right transition between walls and roof. At PK 34+305 the same type of material appears in the lower left corner

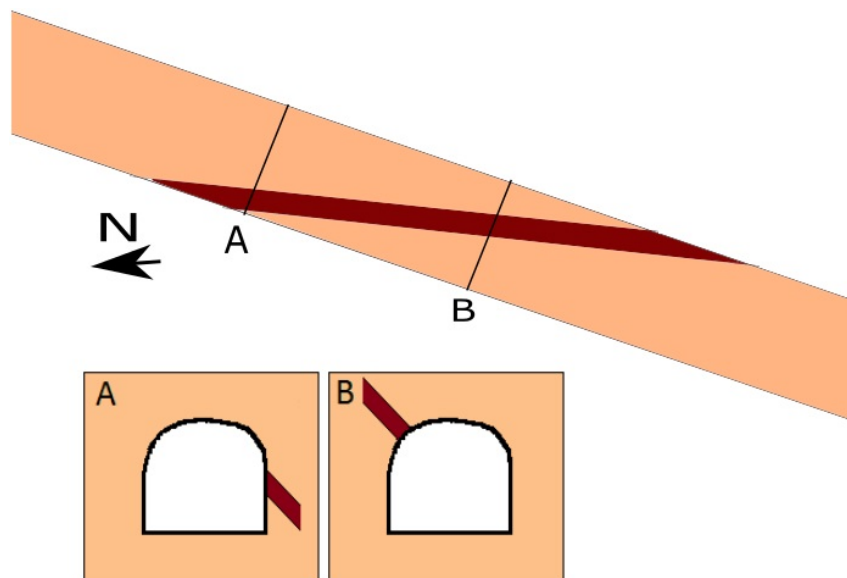


Figure 6.4: Illustration of the weakness zone between PK 34+350 to PK 34+420. The tunnel orientation is $N22^{\circ}E$, dip direction of the zone is ca. $280^{\circ}W-NW$. The sketch is not to scale, and the weakness zone is wider than in reality.

The support class is mainly IVa and IVc. At PK 34+350 it changes to IVc, and continues like that until PK 34+400 where it goes back to IVa. However, from observations in the tunnel the support class at PK 34+385 is IVa (personal communication with Thomas Schönborn).

6.4 Laboratory Results

Point load strength, tensile strength and slake durability of sedimentary volcanic rock have been tested by FCFM (2013), between chainage PK 40+522 and PK40+758. These samples were received in August 2013, two tears after completion. From the geological map, these rocks belong to KCM-t (Golder Associates, 2006). The in situ hydraulic tensile rock strength was in the range 1.6-4.4 MPa. PLI was conducted on irregular samples, and tested both dry and saturated for 48 hours. In general PLI is classified as high. At PK 40+640 the samples stand out with a saturated point load strength of 0.66 and 2.26 MPa. These samples have alteration products of clay, while the other samples mainly contain

hematite or no alteration. The mean point load strength of saturated samples without PK 40+640 is 6.32 MPa. Slake durability was conducted on samples from chainages PK 40+540 (very high) and PK 40+640 (high to medium high) (FCFM, 2013). The difference between saturated and dry samples were small, and which was stronger varied. The results are listed in appendix F.

6.5 Stress Situation

The stress situation along the tunnel is estimated based on information from the World stress map, other measurements and results from hydraulic fracturing tests.

6.5.1 Regional stress

The Andes mountains are a result of the ongoing subduction of the Nazca plate beneath the South American plate (Pankhurst and Hervé, 2007). As illustrated by the World Stress Map for South America in figure 6.5, the Andes mountains are affected by tectonic activity. The stress regime in the area is dominated by thrust faulting SW-NE and an unknown regime (black lines).

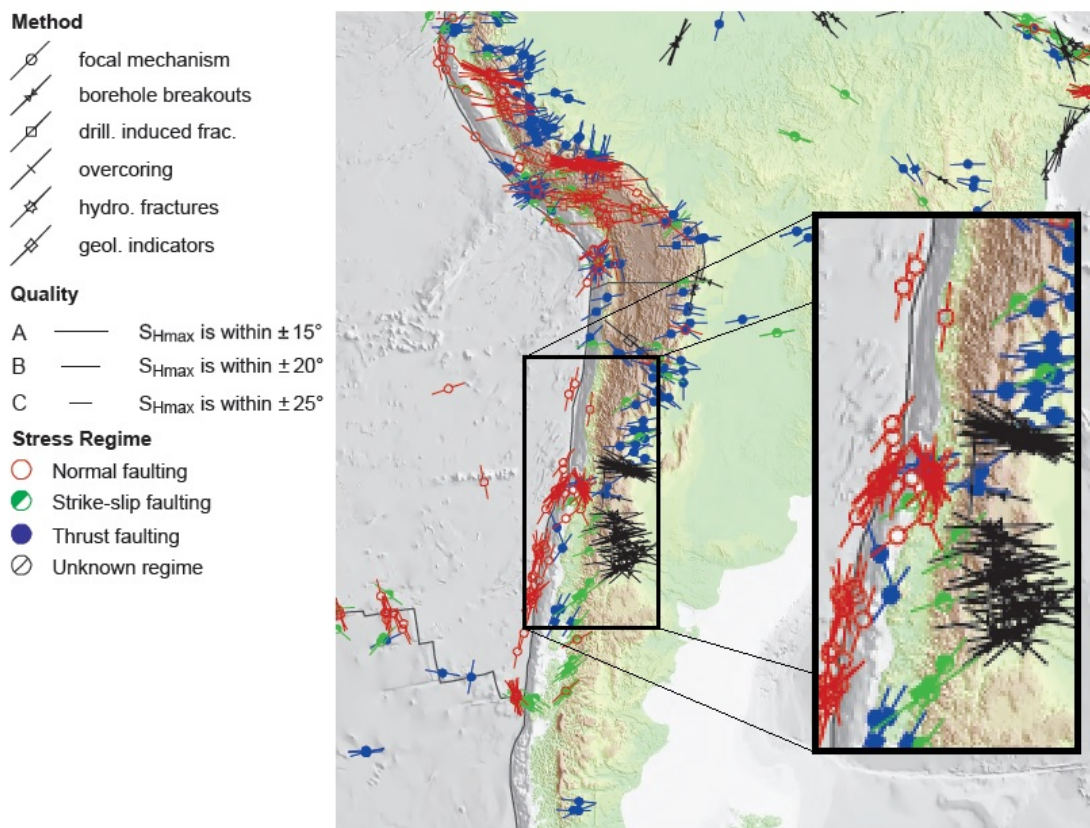


Figure 6.5: World Stress Map, Chile/South America (Heidbach et al., 2016).

Due to the compression it is natural to expect high horizontal stresses in the area. El Teniente mine is located approximately 80 km north of La Confluencia. Several rock stress measurements and numerical analysis have been conducted to estimate local and regional stress field (McKinnon and Garrido de la Barra, 2003; Windsor et al., 2006a,b). Many of the measurements were affected by the mining, but some deep measurements compared well with stress calculated due to overburden. The smallest principal stress is close to calculated vertical stress in many of the measurements. However most of the measurements are conducted at overburdens from 400 m and more, which reduces the compatibility with this project. It was found that the tectonic stress component far field from the cite was oriented close to North-South, consistent with most recent faulting, but perpendicular to the regional crustal shortening direction (E-W) (McKinnon and Garrido de la Barra, 2003). The average far-field value of maximal horizontal stress σ_H found by numerical modelling, was 15.8 MPa while the average minimal horizontal stress σ_h was 10.2 MPa. However the stresses in this simplified model varied from 5.9 to 45.5 MPa indicating that estimation of tectonic stress is complicated.

6.5.2 Hydraulic fracturing

As part of the site investigations for La Confluencia, 7 hydraulic fracturing test, including 7 impression packer test were conducted in October 2008. Testing was carried out in borehole HTS-02 at 1320 m.a.s.l, near the location of today's vertical pressure shaft. The tests were carried out between 203.5 and 236.5 m depth, in volcanic breccia belonging to the KCMA rock unit (MeSy, 2008). Stress depth relations were found with two different methods, the HTPF-or PSI method and Hubbert and Willis method (MeSy, 2008). The test yielded reliable results for σ_h and σ_H . In addition, results from numerical analysis showed that the vertical stress could be regarded as a principal stress at the given depth. The calculations are based on a rock density of $2.67g/cm^3$ and are valid between 203.5 and 236.5 m depth. An east-west orientation of $N114^\circ \pm 4^\circ E$ was found for the maximum horizontal stress σ_H . In table 6.3, the direction found by the Hubbert and Willis method is included. The average direction is $N88 \pm 34^\circ E$ (MeSy, 2008). Calculation of the ratio k between the average horizontal stress $\sigma_{h(avg)}$ and σ_v , is included in table 6.3. The average ratio is $k = 1.44$.

Table 6.3: Stress field based on hydrofracturing tests calculated after the Hubbert and Willis (1957) method. σ_v is calculated with a density of $2.67g/cm^3$. The table is modified from MeSy (2008).

Test no.	Depth [m]	σ_v [MPa]	σ_h [MPa]	σ_H [MPa]	Orientation [°]	$\frac{\sigma_{h(avg)}}{\sigma_v}$
1	203.5	5.33	4.17	8.54	incl.	1.19
2	207.5	5.43	5.00	7.27	88	1.13
3	216.8	5.68	5.38	11.17	61	1.46
4	226.5	5.93	5.10	9.43	154	1.23
5	230.0	6.02	6.92	11.83	68	1.56
6	233.4	6.11	7.78	16.74	81	2.01
7	236.5	6.19	5.95	12.45	74	1.49

6.5.3 Estimating stress at PK 34+405

The Hubert and Willis method has several simplifications, but since the data is used for stress estimation several kilometres away, the results are considered accurate enough for the purpose of estimating stress at PK 34+405. Due to the compressive regime in the Andes mountains, the horizontal stress is expected to be larger than the vertical stress in the area. The influence of tectonic stress must be considered in the estimation of the horizontal stresses. From the hydro-fracturing tests the ratio k between horizontal stress and vertical stress was found to be 1.44. This value is reasonable, compared to figure 2.2. The overburden at the location of the hydro-fracturing tests is 203.5-236.5 m, quite similar to the overburden of 235 m at PK 34+395. The distance from where the hydro-fracturing tests were conducted to PK 34+395 is ca. 8 km.

In the mapping schemes between PK34+387 and PK 34+404, SRF is set to 1, which after the Q-method (NGI, 2015) describes competent rock and favourable stress situation. From the discussion above, and no other available stress measurements closer to the area, it is assumed that the same horizontal stresses as in table 6.3 can be used. The average horizontal stress is calculated and presented in table 6.4. Vertical stress is calculated from equation 2.4, using a rock mass density of $2.57g/cm^3$ and the given overburden (HLC, 2011).

Table 6.4: Estimated in situ stress at PK 34+405.

Location.	H [m]	$\rho[g/cm^3]$	σ_v [MPa]	σ_h [MPa]	σ_H [MPa]
PK34+405	235	2.56	5.9	5.8	11.1

Due to the varied topography in the area it is possible that the area is influenced by de-stressing. From the field observations and data from mapping during construction, there is no evidence of very high or abnormal stresses in the tunnel-periphery in this area. It is therefore natural to use the same stress as the hydrofracturing yielded.

6.6 Rock Support

Five different support classes, some with subgroups, were designed for the tunnel. Only the two relevant support classes are presented here. The invert is covered with 200 mm of RCC concrete, except for some lengths with heavier support. From observations in the tunnel, approximately 90 % is shotcrete covered. The bolting ranges from spot bolting to patterns of 1.5×1.5 m. In figure 6.6 the support class IVc, used at PK34+395 according to the mapping schemes (HTC, 2010; TE, 2010), is illustrated. Support class IVa is given in figure 6.7.

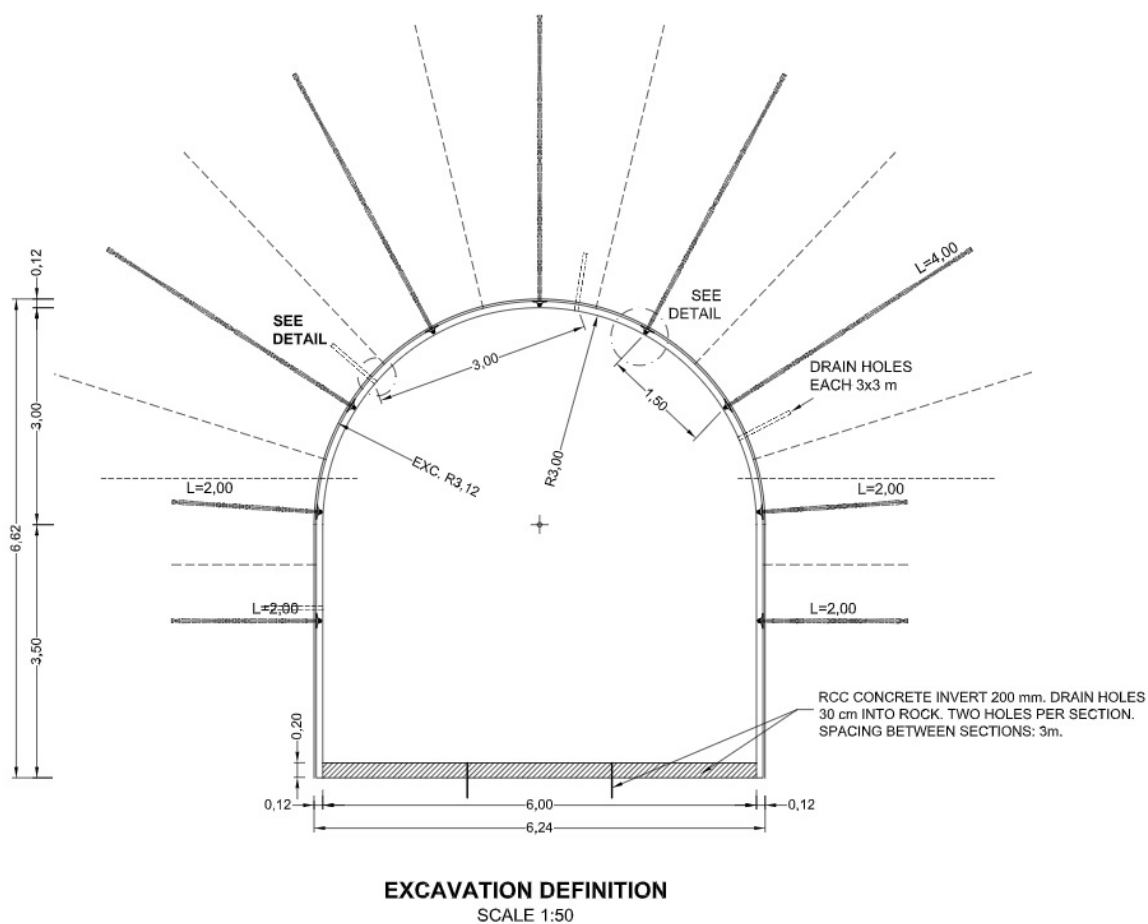


Figure 6.6: Support class IVc and tunnel geometry (HLC, 2010).

Resin or cement fully grouted bolts are used. For IVc a combination of 2 and 4 m long bolts are used, in IVa only 2 m. According to the drawing the shotcrete is applied in two layers, and the bolts installed between. The shotcrete layer is 3 cm thicker for support class IVa. IVc is used for poor rock conditions, with intensively fractured rock, rocks with weak strength, slickensided surfaces or gouge and when the risk of ravelling due to highly erodible rock or poor durability is high (HLC, 2010).

Support class IVa is used for slightly better rock conditions, where it is probable that slabbing, rock falls or ravelling may happen, but where the stand up time is sufficient for

support to be installed safely.

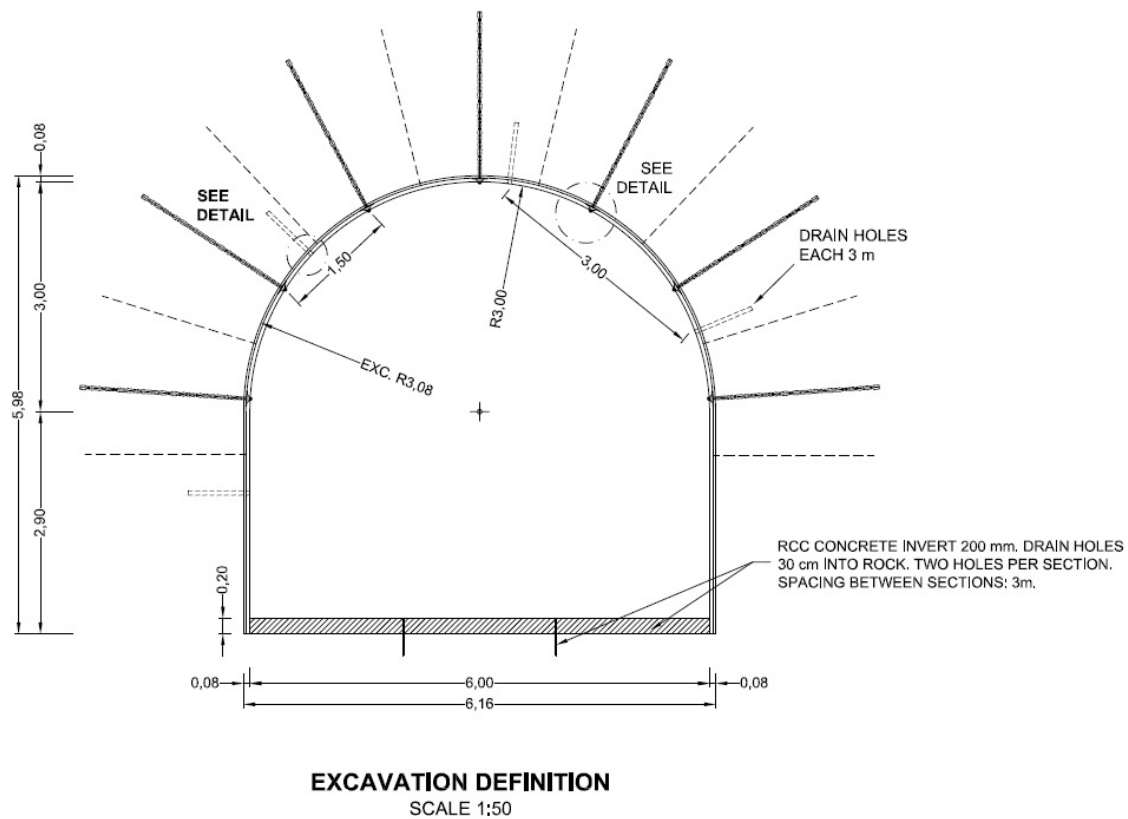


Figure 6.7: Support class IVa and tunnel geometry (HLC, 2010).

6.7 Field Observations

A field visit was carried out on April 28th-29th, 2017. Both the Portillo and Tinguiririca tunnel were driven through, and the surface area close to PK 34+750 was examined more closely. The description focus on observations from the Portillo tunnel and from the surface, since this is the area covered by the thesis. All the images are taken on the inspection 28.04.2017.

6.7.1 Portillo Tunnel

The Portillo tunnel is mostly covered with shotcrete and some shorter sections with concrete lining. This reduces the possibility for strike and dip measurements within the tunnel. It was not observed anything unusual in the area around PK 34+400, where damages previously had been detected. The shotcrete was checked for drumminess, but appeared to be in good condition. Further downstream in the tunnel some shotcrete cracks could be seen, most likely related to poor adhesiveness of the second layer of shotcrete.

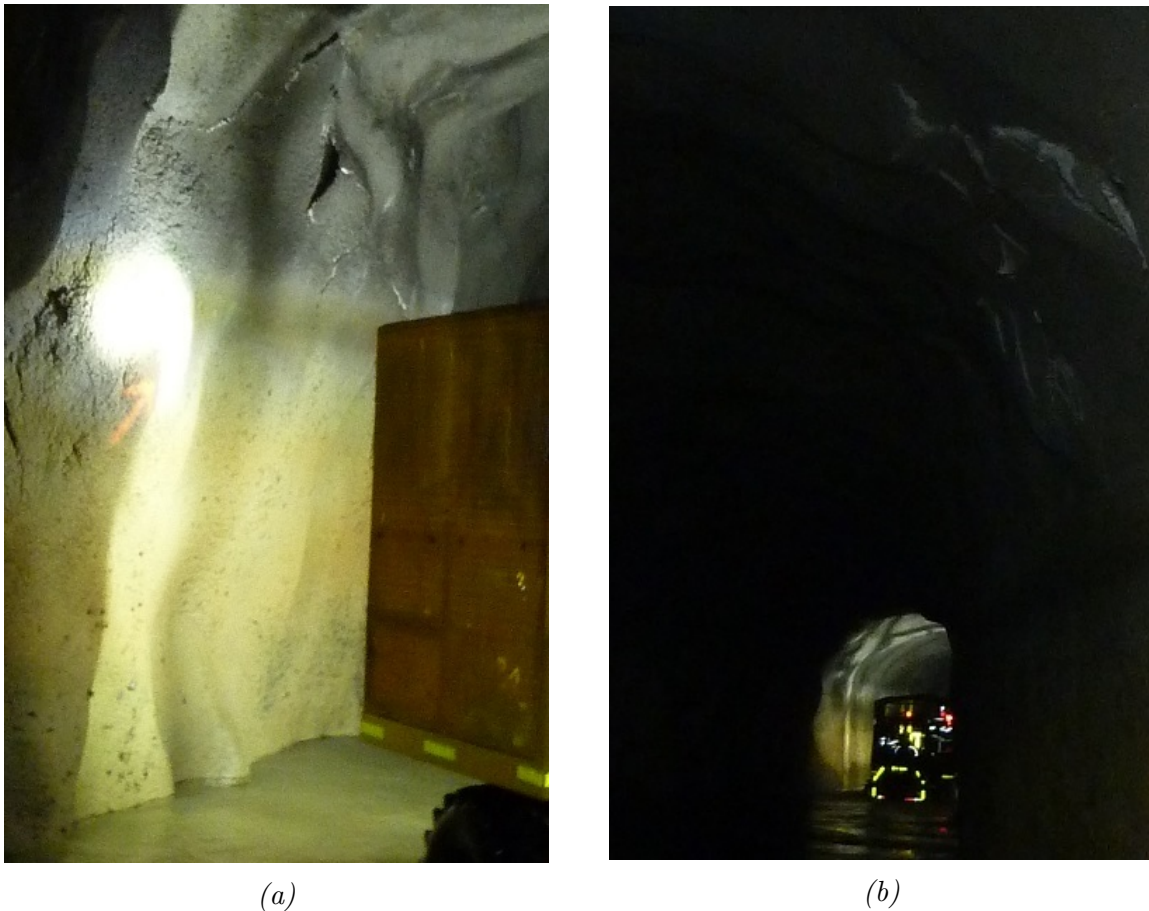


Figure 6.8: Shotcrete cracks in the Portillo tunnel, looking downstream. The cracks in (a) are likely due to poor adhesion. In (b) the cracks are possibly related to poor adhesion or stress concentration.

In the case of cracks initiated by swelling pressure, the cracks normally first appear as radial hairline cracks. In the area close to the landslide deposits, it is possible that the shotcrete cracks in the right corner of the profile (looking downstream) have appeared due to stress concentrations. This area is located very near the surface of the hillside due to the landslide deposits discovered during construction. In addition, the overburden is relatively high, which gives conditions where high tangential stresses may develop close to the surface. The profile of the tunnel has signs of hard blasting, with over-excavation and a ragged profile.

6.7.2 Outcrop at PK 34+750

The outcrop near PK 34+750 was chosen due to its accessibility by car. It is located on the left side of the Riquelme stream in a distance of about 100 meters above the Riquelme intake. Both the intake and the location of the outcrop can be seen in figure 6.9. The tunnel is placed further into the hill slope. The surface at PK 34+400 is not visible in the image, but located on the left side of the left hillside. The observations in the outcrop was mainly focused on stratification, structures, rock composition and weakness zones.



Figure 6.9: Overview of field observation area, Riquelme intake. Observations were made in the outcrop located around PK 34+750, indicated by the red ring.

Two structurally different rocks are observed. In figure 6.11, what is inferred to be a relatively massive andesitoid rock is seen. This interpretation is done based on the fine grained structure and white needle formed minerals seen in figure 6.10, in addition to the geology in the area. Fracture planes are also marked in the figure. It is also possible that it is granodiorite. Some fracture planes are covered with calcite. The near vertical structures marked with red and yellow in figure 6.11, are likely the same structures as can be recognized in the back of figure 6.9. The weakness planes are smooth to rough and planar. Fresh planes are not observed.



Figure 6.10: Close-up of needle formed white minerals observed in the more massive rock mass in the outcrop.

Strike and dip measurements at the outcrop resulted in the joint rosette seen in figure 6.11. The measurements are listed in appendix H. It should be noted that very few measurements were taken. The rosette from the daylight mapping and from the mapping schemes are roughly corresponding. The dip angle varies between 74-88°S-SE except for one measurement with strike N10°E and dip angle 50°E.

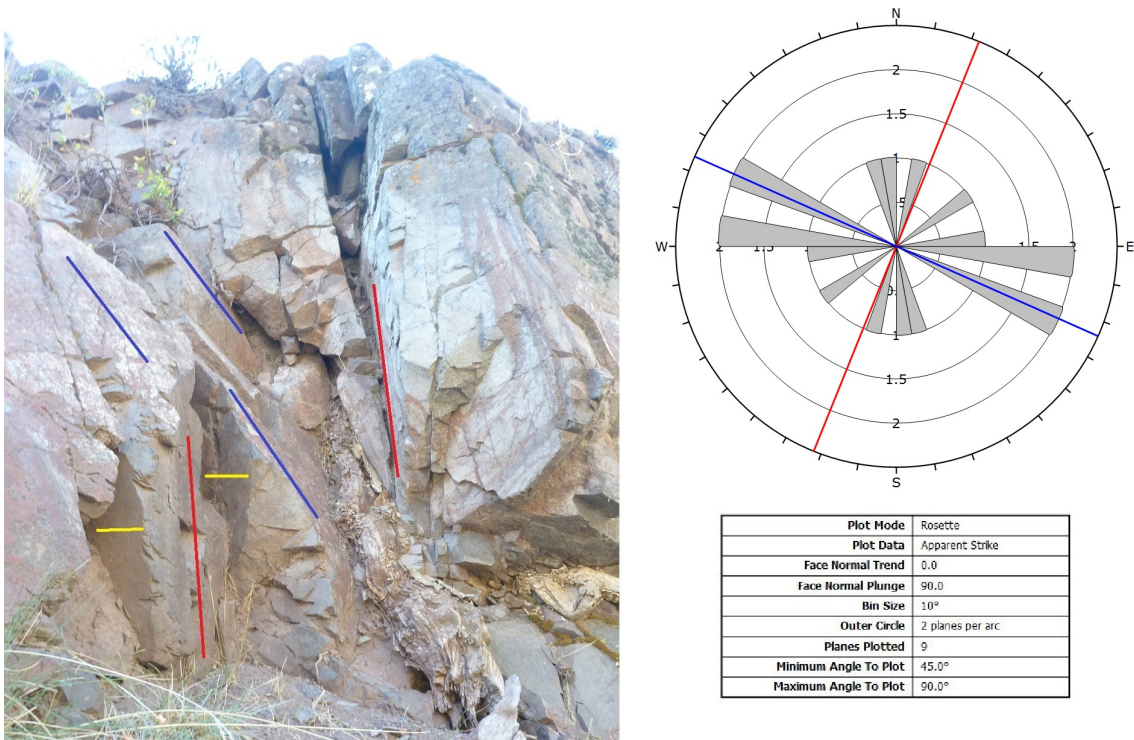


Figure 6.11: Left: Observed structures in the rock mass. Right: joint rosette based on mapping at the outcrop. A total of 9 measurements are used. Each circle represents 0.5 measurements. Approximate tunnel orientation shown in red is 22° and direction of largest horizontal stress σ_H 114° shown in blue.

At the point where figure 6.11 is taken, only massive rock is observed. A few meters further up the river a pronounced zone of intensively broken material of about 25 cm thickness becomes visible, see figure 6.12a. The material in this zone is highly weathered, brownish, not consolidated and soil-like with small rock fragments (2-5 cm). Beneath is an approximately 2 meter thick layer of red/brown highly weathered rock. Massive rock can be observed in the river underneath the weak zone. The quality above the zone is gradually increasing. Strike and dip measurements were also taken on this zone, but as it was only observed one place it was difficult to determine the directions. The dip angle is between 30 and 60°, possibly to NW. From the geological maps these rocks belong either to the granodioritic complex or KCM-t.



(a)



(b)

Figure 6.12: Weak zone in (a) observed at the outcrop and is dipping towards north approximately. Image (b) shows the stratification closer to the end of the tunnel.

From table 6.1 the stratification is quite shallow dipping towards W-SW, and it is possible that the weak layer belongs to the stratification. To interpret the propagation of the zone towards the deep more measurements should be taken. The zone is not consolidated, and this may be the case also deeper in the ground.

Chapter 7

Laboratory Methods

The project work carried out prior to the thesis aimed to assess swelling and slaking properties of volcanic rocks. X-ray diffraction (XRD), differential thermal analysis (DTA), free swelling and swelling pressure tests were conducted on four samples from the Portillo tunnel, named after the chainage they were sampled from. In the thesis further testing of mineralogy and strength properties are done. XRD, thin section analysis, density, Young's modulus, Poisson's ratio and Point Load Strength test are done. The rock mechanical properties are important input parameters for the numerical analysis. Both the methods used in the project work and in the thesis are described.

7.1 Swelling

7.1.1 Free Swelling

The free swelling test is a quick method to assess the swelling potential of a material (Nilsen and Broch, 2012). Bulk powder is prepared by crushing material down to the 2.5 mm fraction, before 40 grams are milled down in a coil mill for 2.5 minutes. 10 ml (V_0) of powder is loosely filled into a measuring cylinder, before it is carefully sprinkled into another cylinder filled with 45 ml of distilled water. The volume (V_1) of powder after sedimentation is recorded and the swelling index is found from equation 7.1. (Sørlokk et al., 2007; Mao et al., 2011a).

$$Fs = \frac{V_1}{V_0} \times 100\% \quad (7.1)$$

Classifications of free swelling and swelling pressure are provided in appendix E.

7.1.2 Swelling Pressure

The laboratory at NTNU/SINTEF has developed a procedure for testing of axial swelling pressure on remoulded specimens under conditions of zero volume change (Mao et al., 2011a). One modification is done on the sample preparation procedure as bulk samples

are used in stead of material with particle size less than $20 \mu\text{m}$. The powder is prepared as for free swelling. The components of the traditional apparatus at NTNU is shown in figure 7.1.

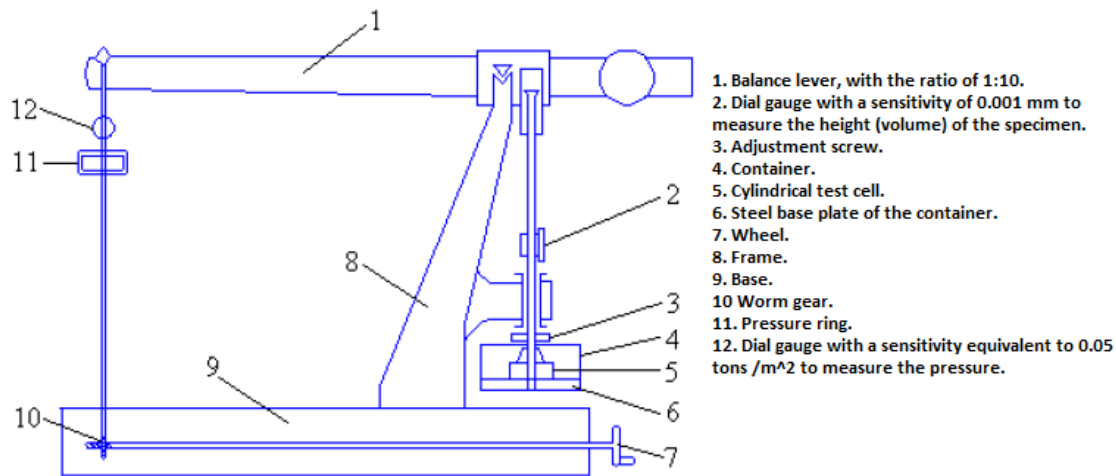


Figure 7.1: Sketch of the traditional apparatus setup used by NTNU to measure swelling pressure (Mao et al., 2011a)

An updated version of this apparatus has been made (Mao et al., 2011a), shown in figure 7.2. To ensure the specimen volume is kept constant throughout the test, a height transducer and inductive sensor have been installed instead of the traditional dial gauges, that measures height of specimen and pressure. The manually operated wheel used for worm gear adjustment is replaced by a automatic step-motor. Together with the software developed, this gives the possibility to continuously compensate for the deformation of the apparatus when it suppresses the volume change in the specimen, as well as to record the swelling pressure at all times throughout the test. The test cell consists of a porous glass filter at the bottom, which the sample is placed on top of, and a copper filter on top. A stamp is placed on top of the copper filter before the cell is mounted in the apparatus as described below. The procedure used for measuring swelling pressure on a remoulded specimen is as follows, partly as described by Mao et al. (2011a):

1. 20 grams of material is placed into the 20 cm^2 test cell shown in 7.2. Care is taken to get a even surface;
2. The test cell is placed into the apparatus as shown in 7.2, and connected to the pressure ring;
3. The balance lever is leveled slightly above horizontal position;
4. The height transducer is installed;
5. The specimen is compressed at 2 MPa for at least 24 hours, by loading the balance lever with steel disks;
6. The specimen is unloaded for 2 hours;
7. A pressure spring is installed as shown in 7.2;

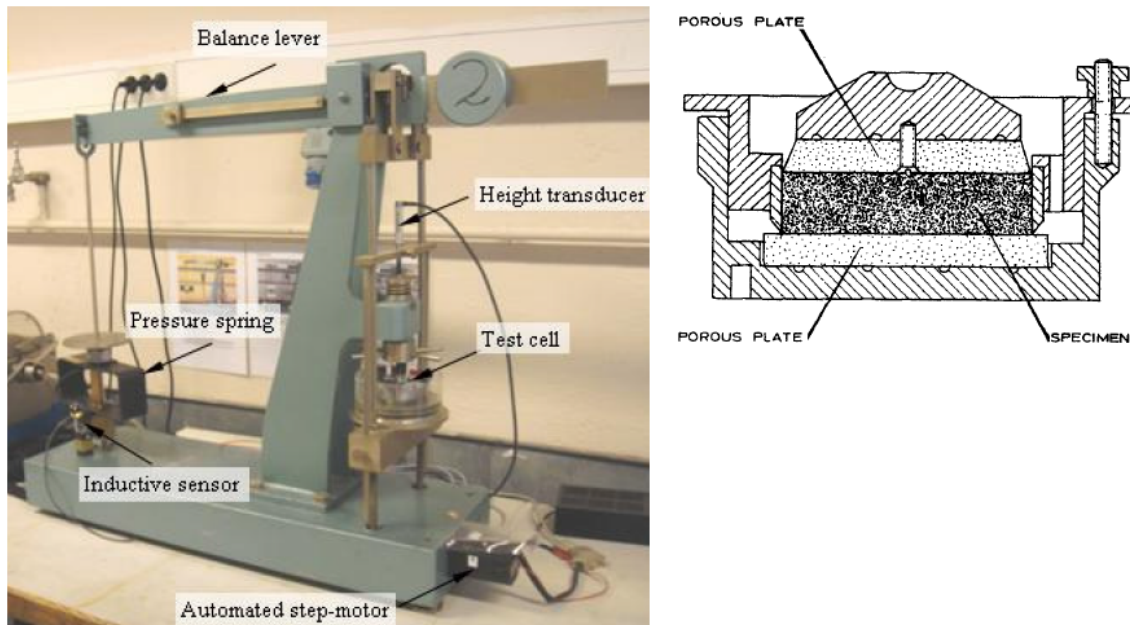


Figure 7.2: Right: Improved apparatus setup for swelling pressure test at the NTNU/SINTEF laboratory (Mao et al., 2011a). Left: sketch of the test cell (ISRM, 1979b).

8. The container around the test cell is filled with distilled water until it reaches a depth of 10 mm and at the same time the automated motor starts, to continuously keep the volume of the specimen constant;
9. The swelling pressure is registered for 24 hours or until the pressure has stabilized. The software register the whole process and the swelling pressure curve and maximum pressure can be read of after.

In addition disks are tested with a similar procedure. 34 mm cores are cut into discs and grinded down to a thickness of 5 mm to fit perfectly in the test cell. The disks are shown in figure 8.1. The same apparatus as for powder swelling is used but with a smaller test cell. The test cell is cylindrical with an area of 10 cm². The disk is placed in the test cell, and the same procedure as above is followed, except that the applied compression weight is now 4 MPa (due to the smaller area of the disk).

7.2 Mineralogy

7.2.1 DTA

Differential Thermal Analysis (DTA) is based on the exothermic or endothermic reactions that can happen when minerals are heated. At certain temperatures some minerals, such as clay, quartz and pyrite change their crystal structure, giving a characteristic curve that can be used to identify the minerals qualitatively by comparing the curves to known minerals (Nilsen and Broch, 2012). The apparatus at the NTNU/SINTEF laboratory

heats the minerals to a temperature of about 600 °C. Montmorillonite can have several peaks in the temperature range from 20-1100 °C. The first stage involves endothermic release of water adsorbed on the inner and outer stages, and the second stage endothermic release due to dehydroxylation, the third stage is characterized with an endothermic event followed by an exothermic event (Fajnor and Jesenák, 1996). The first stage normally gives strong manifestations between 100-250 °C, the second at 600-700 °C, and the third at 900 °C (Sørlokk et al., 2007). The two latter effects cannot be observed by the apparatus at the NTNU/SINTEF laboratory, because of the limited temperature range.

7.2.2 X-ray Diffraction

X-ray diffraction analysis (XRD) is a method used for semi-quantitative analysis of the minerals in a rock sample (Nilsen and Broch, 2012). X-rays are diffracted from the different planes in a crystal, due to similar dimensions of X-ray wavelength λ and atom spacing in the minerals. At a certain angle of incidence θ , interference between the X-rays is possible. This happens when the additional path length traveled by the second wave is equal to a whole number of wavelengths n . This distance is related to the spacing d between the atom planes in the crystal, as expressed by *Bragg's equation* (Nesse, 2000):

$$n\lambda = 2d \sin \theta \tag{7.2}$$

The sample and detector goes through a range of angles and the intensity of the reflected X-rays is continuously recorded on a computer. The peaks that are recorded are characteristic for each mineral, and by examining the result the minerals in a sample can be identified. The intensities are approximately proportional to the quantity of the different minerals (Nesse, 2000). Uncertainties are related to overlapping peaks and masking of weak peaks by larger peaks. There are also uncertainties related to identification of certain minerals (Nilsen and Broch, 2012), such as clays, which can sometimes only be determined by relative amount of the different types (Nesse, 2000)

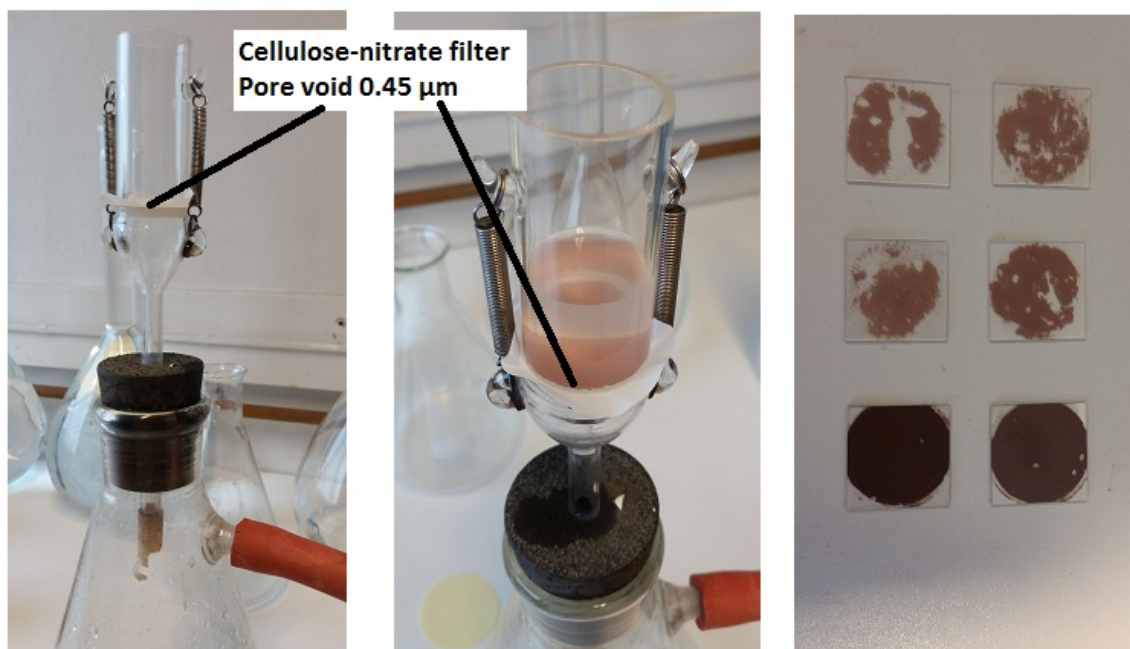


Figure 7.3: Some of the steps for extracting the fraction below $6\ \mu\text{m}$ before ethylene glycol treatment. On the left hand the equipment is shown before the sample is pored over. The desired fraction is left on top of the filter. On the right hand the desired fraction has been transferred to a glass plate.

When bulk samples are tested it can be difficult to discriminate between mica and clay minerals. Glycolation is used to identify swelling clays, due to an ability to expand the crystal lattices which gives a representative shift in the diffractograms (personal communication with L. Tjihuis at the laboratory). Intact rock pieces representing the bulk volume of the sample are immersed in approximately 200 ml of water. If the rock pieces do not disintegrate, ultrasound bath can be used to achieve this. The aim is to get the small fractions out of the sample. The sample is moved to a 250 ml glass-bulb, filling it up to a mark. Stokes law is used to calculate at which depth only the $< 6\ \mu\text{m}$ fraction is found. The sedimentation takes 1 hour 45 minutes, and after this time the upper 20 cm consists of the desired fraction. A vacuum pump is used to extract the upper 20 cm. Figure 7.3 shows the next steps where the "small fraction-water" is pored over a cellulose-nitrate filter to extract the smallest particles, which are later transferred to a glass plate. Two plates are made for each sample. One of the plates is put in a bowl with a "shelf" for the samples. Beneath is ethylene-glycol, which evaporates above 60°C , and expands the crystal lattice. The bowl is placed in an oven at 60°C for 20 hours. Then XRD is carried out and the glycolated sample is compared to the non-glycolated, to determine the presence of swelling clays. At NTNU, the analysis is conducted with a Bruker D8 ADVANCE. Identification of minerals is done with DIFFRAC.SUITE.EVA software combined with PDF-4+ database. Quantification of the minerals is done by Rietveld refinement in Topas with an accuracy of 1-2 %.

7.2.3 Thin Sections

Thin sections analysis with light microscope can be used to assess mineralogy and texture of rock samples, and hence improve understanding of rock properties (Brattli and Broch, 1995). Thin sections have been prepared at the *Sliplaboratorium* at NTNU. Samples are cut to the customized size of $20 \times 30 \times 10\text{mm}$ with a diamond saw. The customized piece is grinded at one side and glued to a glass slide. After drying of the adhesive, the sample is further grinded until the desired thickness is achieved. For a normal thin section, this is about 30-35 μm . If a polished thin section is preferred, the thin section is further polished until a thickness of 25-30 μm . The samples are prepared in ethanol, due to the content of swelling minerals (personal communication with K. Eriksen at the Sliplaboratorium). The analysis is conducted to identify the minerals found from X-ray diffraction in the previous work.

7.3 Density

Two methods are used to find the density of the samples. For samples in the form of a cylinder the diameter and length are measured at several points to calculate the bulk volume. The weight is measured and $\rho = m/V$ can be calculated.

For specimens which are not in the form of a cylinder a pycnometer is used. The equipment needed is a weight of sufficient accuracy, a glass container and a glass plate. The following procedure (Dahl, 2003) has been used:

- The glass container is placed on the weight and tared. The container is filled approximately $2/3$ full of the sample and the weight of the specimen m_1 is registered.
- The container with specimen is filled with tap water until the container is full, making sure that no air bubbles are trapped. The glass plate is used to adjust the water level. Make sure all water on the outside of the container is dried and tare the weight again. Weight of container, water, sample and glass plate m_2 is registered.
- The sample is removed from the container, which is cleaned. The empty container is filled with tap water, making sure no air bubbles are trapped. The water level is adjusted with the glass plate, and the container is dried on the outside before weighing. The weight is tared and weight of container, water and glass plate m_3 is measured.
- The density of the specimen is calculated as: $\rho_s = \frac{m_1}{m_1+m_3-m_2}$.

7.4 Rock Mechanical Properties

7.4.1 UCS, Poisson's ratio and E-modulus

In the uniaxial compressive test an unconfined core is loaded in the axial direction until failure occurs ISRM (1979a). The load at the failure point is registered and uniaxial compressive strength decided. Small samples are less likely to include all the factors that influence rock strength, and will hence be stronger than larger samples and the classification tables are based on cores with 50 mm diameter a strength correction must be applied to convert the result for cores with diverging diameters. This is done by equation 7.3 (Nilsen and Palmström, 2000). D is the diameter of the actual sample in mm.

$$\sigma_c = \sigma_{c50} \times \frac{50^2}{D} \quad (7.3)$$

At NTNU the test is carried out with a GCTS – RTR-4000 Rapid Triaxial Rock Testing system

7.4.2 Point Load Strength Test

The Point Load Strength test is an index test for strength classification of rock materials. The test can be performed on rock specimens in the form of cores, blocks or irregular lumps (ISRM, 1985). In this thesis the test is carried out on irregular lumps. Therefore only the requirements for irregular lumps are described. The machine and procedure used for the testing is according to the description in ISRM (1985). The samples are loaded by two spherically-truncated, conical platens, until breakage is induced. A caliper is used to measure the distance D between specimen-platen contact points, and the distance W for axial and irregular lump test, see figure 7.4 for an illustration. The load is manually and steadily increased until failure, preferably at between 10-60 sec, and the maximum load P is recorded by the apparatus. For the test to be valid, the fracture surface must pass through both loading points.

A sample is comprised of a set of rock specimens with similar strength properties, for which a single Point Load Strength value will be determined. There should be at least 10 rock pieces with the correct size and shape requirements, per sample, and more if the sample is heterogeneous or anisotropic. The sample should be either fully saturated or at its natural water content. The size of the lumps should be $50 \pm 35mm$, and with shape as shown in the figure. The ratio D/W should preferably be close to 1.0 but between 0.3 and 1 is accepted. The distance L must be at least 0.5 W . When the sides are not parallel W is calculated as the mean of W_1 and W_2 . The load is applied so that the platens make contact with the smallest dimension of the lump. The dimensions of each rock piece must be recorded for all the tests (ISRM, 1985). In figure 7.4 the requirements for the axial

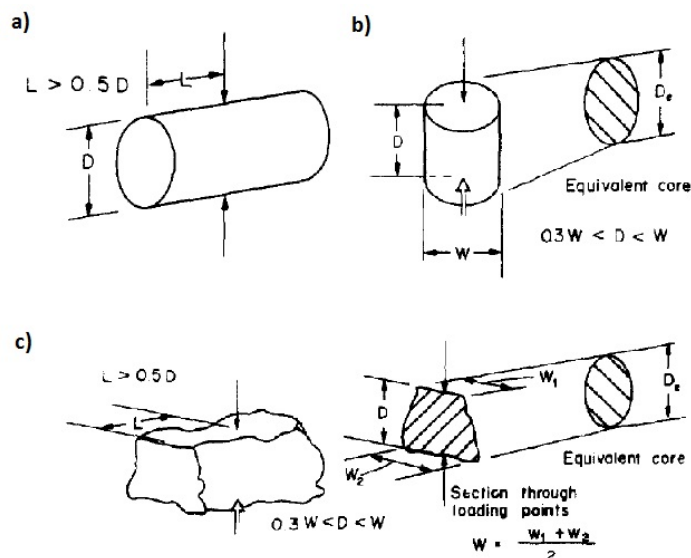


Figure 7.4: Required specimen shape for PLI for a) diametrical test, b) axial test and c) irregular lump test. Figure modified after ISRM (1985).

and diametrical test are also shown. The Uncorrected Point Load Strength I_s is given by equation 7.4 where D_e is the equivalent core diameter as shown in figure 7.4.

$$I_s = P/D_e^2 \quad (7.4)$$

For irregular lumps $D_e^2 = 4A/\pi$ and $A = W \times D$, which is the minimum cross sectional area through the platen contact points.

Because I_s varies as a function of D and D_e , a size correction must be applied to obtain a PLI-value that can be used for rock strength classification $I_{s(50)}$. This can be done in two ways (ISRM, 1985):

1. Register P over a range of D and D_e values, and plotting the results in a log-log plot which will normally result in a straight line. Outliers can be removed. Inter- or extrapolation may be used to find P_{50} , and $I_{s(50)}$ can be found by $P_{50}/50^2$.
2. Applying the "Size Correction Factor F " in equation 7.5 to equation 7.6.

$$F = (D_e/50)^{0.45} \quad (7.5)$$

$$I_{s(50)} = F \times I_s \quad (7.6)$$

The point load strength test is executed with a GCTS mobile point load machine at NTNU.

7.5 Slake Durability Index

The slake durability test is used to evaluate the rock samples resistance to weakening and disintegration when subjected to two cycles of drying and wetting (ISRM, 1979b). The method and apparatus at NTNU is in accordance with the ISRM standard *Suggested Method for Determination of the Slake-durability Index* (ISRM, 1979b). The apparatus consists of a test drum comprising a 2.00 mm mesh cylinder, of unobstructed length 100 mm and diameter 140 mm, fixed on a solid base. The drum is fixed with a horizontal axis and rotates freely in a trough, which is filled with distilled water at 25°C until 2 cm below the drum axis. There is 40 mm unobstructed clearance between the trough and the base of the mesh. The drum rotates at a speed of 20 rpm for 10 minutes and the speed should be kept constant within 5 % for the whole time. The procedure is described as follows:

- A representative sample of ten rock lumps of size 40-60 g, with a total sample mass of 450-550 g, is prepared. The lumps should be about spherical, corners should be rounded and maximum grain size should not extend 2 mm.
- Before the first cycle the sample is placed in a clean drum and dried to a constant mass of 105°C. The mass A of samples and drum are weighed together on a scale with accuracy of 0.5 grams.
- The lid of the drum is mounted, and the drum is placed into the apparatus. The trough is filled with distilled water before the cycle runs for 10 minutes. The lid of the drum is removed, and the sample is dried for approximately 4 hours. The dry weight B of sample and drum is noted.
- After cooling the next cycle is started. The weight C is recorded after drying of sample and drum. The weight D of the drum alone is also noted and the slake-durability index after two cycles I_{d2} is calculated as in equation 7.7.

$$I_{d2} = \frac{C - D}{A - D} \times 100\% \quad (7.7)$$

Chapter 8

Results of Laboratory Work

In this chapter both results from the project work and thesis are presented. Mineralogy of four samples from the Portillo tunnel has been examined with X-ray diffraction, in addition to a study of thin sections in the microscope. The point load strength test was conducted on 3 samples, and uniaxial compressive strength, E-modulus and Poisson's ratio have been tested on one core from PK 34+405. Density of two of the samples are found. A discussion of the results are given after they are presented.

8.1 Sample Description

PK 34+405, PK 36+555 and PK 37+060 are all reddish brownish of colour, consisting of more or less intact cores of diameter 10 cm. Sample PK 34+405 and PK 37+060 have similar appearance with angular to rounded fragments with size from barely visible to 3-6 mm long grains. PK 36+555 is more fragile and starts disintegrating in contact with water. PK 34+385 differs structurally from the others, as it is taken from a weakness zone, and is decomposed and highly weathered. The structure is soil-like with some fragments of intact rock. In figure 8.1 an image of the three solid samples, prepared as disks for swelling pressure tests, is provided.



Figure 8.1: Samples prepared as disks for swelling pressure test. Left: PK 34+405, Middle: PK 36+555, Right: PK 37+060.

The appearance of PK 34+405 and PK 37+060 is quite similar, but with a slight color

difference. PK 36+555 stand out with its white dots, which become more visible after drying. In discussion with co-supervisor T. Scönbörn, the samples are believed to be andesitic tuff with varying composition due to a porphyritic texture and the geological history.

8.2 Swelling

In table 8.1 results from both free swelling and swelling pressure on disks and powdered samples are presented.

Table 8.1: Results from the swelling pressure and free swelling tests. Classification after (Mao et al., 2011a) given in appendix E. L=low, M=moderate, H=high, V-H = very high.

Sample	Powder [MPa]	Powder (dried) [MPa]	Class.	Disk [MPa]	Class.	Free swell [%]	Class.
PK 34+385	-	0.207	M	-	-	132	M
PK 34+405	0.076	-	L	0.025	L	83	L
PK 36+555	0.310	0.272	H/M	1.11	V-H	135	M
PK 37+060	-	0.101	M	0.01	L	120	M

Both PK 34+405 and PK 37+060 had higher swelling pressure in powder form than on disks, but still low/close to low. PK 34+405 is classified as inactive according to the free swelling test. PK 36+555 had a remarkable high disk swelling pressure. The swelling pressure charts are given in appendix A.

8.3 Mineralogy

8.3.1 DTA

The results show peaks coinciding with the temperature interval corresponding to kaolin, except for PK 34+405 which had no such peak. There are minor peaks in the lower temperature area where the first peaks of montmorillonite can be seen, but they can not confirm the presence due to their small size. The samples were dried at 105 °C for 24 hours prior to testing, as part of preparation for other tests. The DTA charts are provided in appendix C.

8.3.2 X-Ray Diffraction

The mineralogy of the samples were first examined by normal X-ray diffraction procedure in the project work. The results are presented in table 8.2. Later all four samples were glycolated. Ultrasound bath were used to achieve the desired fraction from PK 34+405

and PK 37+060, while it was achieved from water submersion only for PK 34+385 and PK 36+555.

Table 8.2: Mineralogical composition of rock samples derived from X-ray diffraction on bulk material. All the values are in mass ratio and normalized until 100 %.

Mineral	PK 34+385	PK 34+405	PK 36+555	PK 37+060
	[%]	[%]	[%]	[%]
Plagioclase	39	66	17	21
Quartz	13	11	7	17
Pyroxene	2	7	5	3
Chlorite	8	7	24	16
Laumontite	16	1	-	-
Hematite	8	4	8	8
Calcite	11	2	23	4
Mica	3	-	-	-
Magnetite	-	<1	-	-
Analcime	-	-	-	31
Kaolinite	-	-	16	-
Siderite	-	<1	-	-
Chalcopyrite	-	-	-	<1

Treatment with ethylene-glycol shows a shift in d-values for all samples, indicating the presence of montmorillonite. The exact type of smectite is uncertain due to a limited selection of samples in the database. The diffractograms can be seen in appendix B.

8.3.3 Thin Sections

PK 34+385

Since the thin section is made of non-consolidated rock mass, transparent holes can be observed. Otherwise the sample is dominated by a white/grey and mostly brown to dark brown matrix. Calcite, colorless in plane polarized light and with characteristic twinning, is observed as bands in one corner. In cross polarized light the high interference colors and oblique extinction is characteristic. Opaque grains with splinters of red/bronze/orange color are observed. Images from the microscope are provided in figure 8.2.

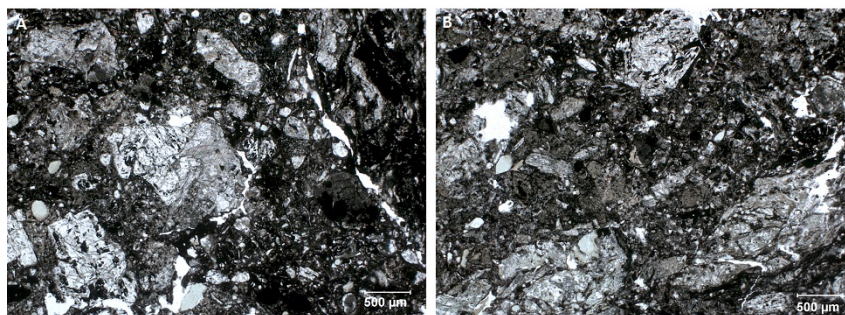


Figure 8.2: Microscopy images of thin section PK 34+385 in plane polarized light.

PK 34+405

The thin section of PK 34+405 has differing grain size. The texture is porphyritic, with large grains in a more fine-grained matrix. The matrix is composed of colorless, grey and brown minerals. Calcite is colorless in thin sections, with characteristic twinning. In figure 8.3 calcite, quartz and pyroxene grains can be observed, in addition to opaque grains/matrix.

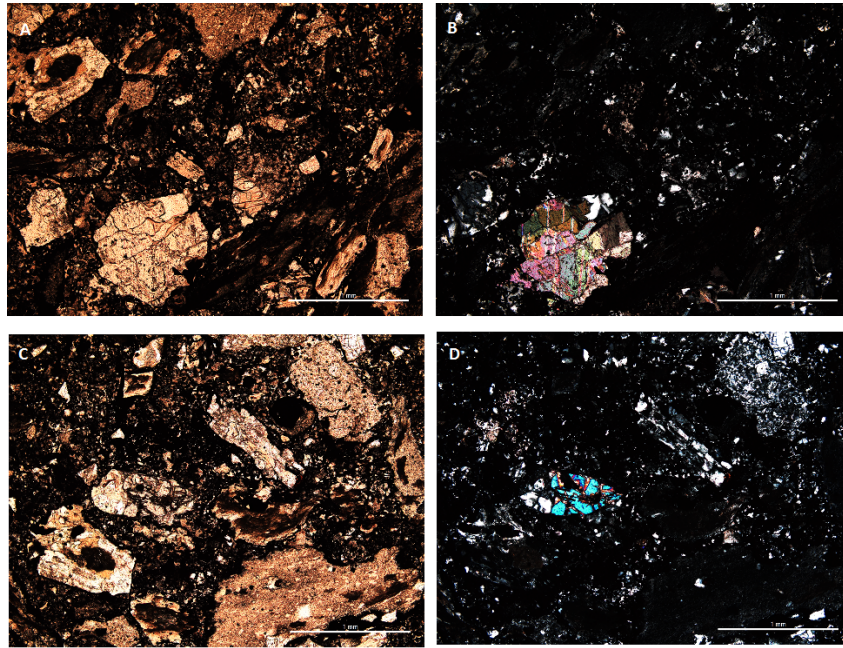


Figure 8.3: Microscopy images of thin section PK 34+405. A and B, calcite in plane polarized and cross polarized light respectively. C and D, pyroxene, plane polarized and cross polarized light respectively. The scale is 1 mm

PK 36+555

The thin section of PK 36+555 is poorly sorted. The texture is porphyritic, with large grains in a more fine-grained matrix. The matrix is composed of colorless, grey and brown minerals. Calcite is colorless in thin sections, with characteristic twinning. In cross polarized light the high interference colors and oblique extinction is characteristic. In figure 8.4 image C and D, reflected and cross polarized light respectively, calcite with inter-growth of other minerals are seen in the lower right corner. The fine-grained brown minerals in the middle are representative of the matrix.

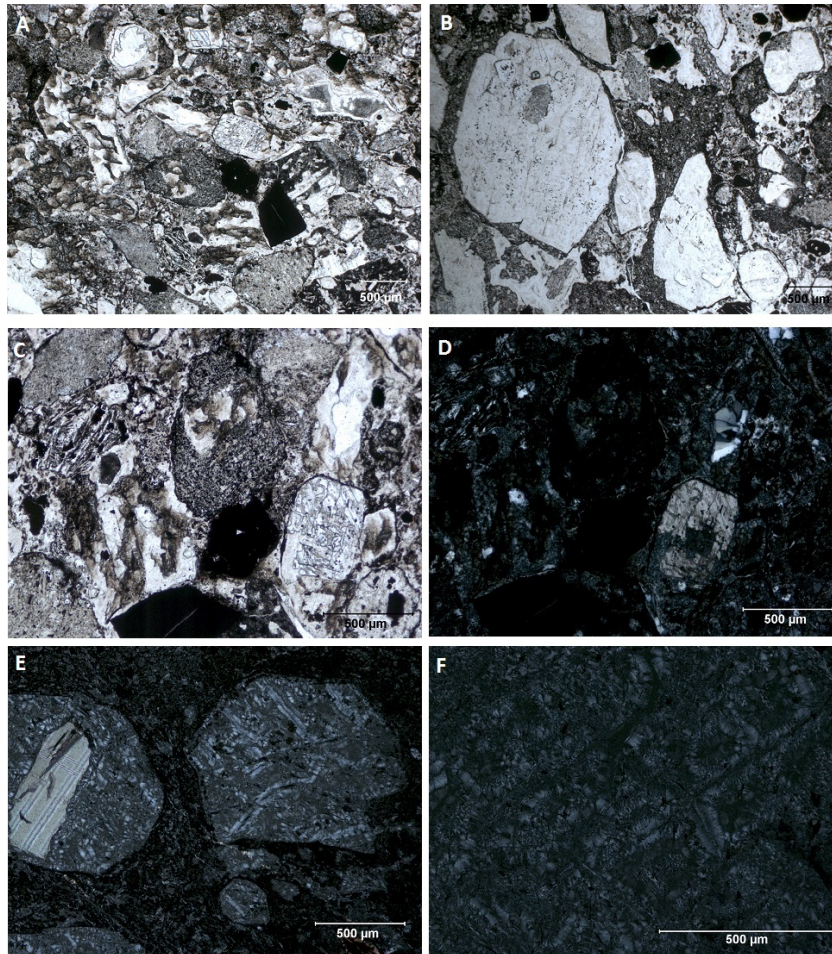


Figure 8.4: Microscopy images of thin section PK 36+555. A: Plane polarized light, overview image showing the texture and variation of grain size. B: variation in grain size. C: Altered calcite grain in the lower right corner, and two black hematite grains in the fine-grained matrix. D: Same as C in cross polarized light. E: Serpentine or chlorite, in what might have been pyroxene. Inclusion of calcite on the left side. F: Zoom in on the structure of the large grain on the right in image E.

In image D a quartz grain is possibly seen above the calcite grain. Some opaque grains are seen. Other from calcite, the rest of the minerals do not show clear distinguishing signs. Image D show two large grains, one with a calcite inclusion. They have a fibrous nature, and can be representative of either chlorite or serpentine, and might represent altered pyroxene. The whole thin section is highly altered, which complicates the identification. Decomposed volcanic glass may also be present.

PK 37+060

The thin section is dominated by different grain sizes and has some bonds. The matrix is mainly fine-grained with some veins and larger grains. A lot of the matrix appears to be opaque, as shown in 8.5. Calcite is observed as in figure 8.2 and 8.4. Image E and F show the structure of two different grains. E is "cloudy" and may consists of different crystals, maybe altered. F is fibrous with elongated crystals.

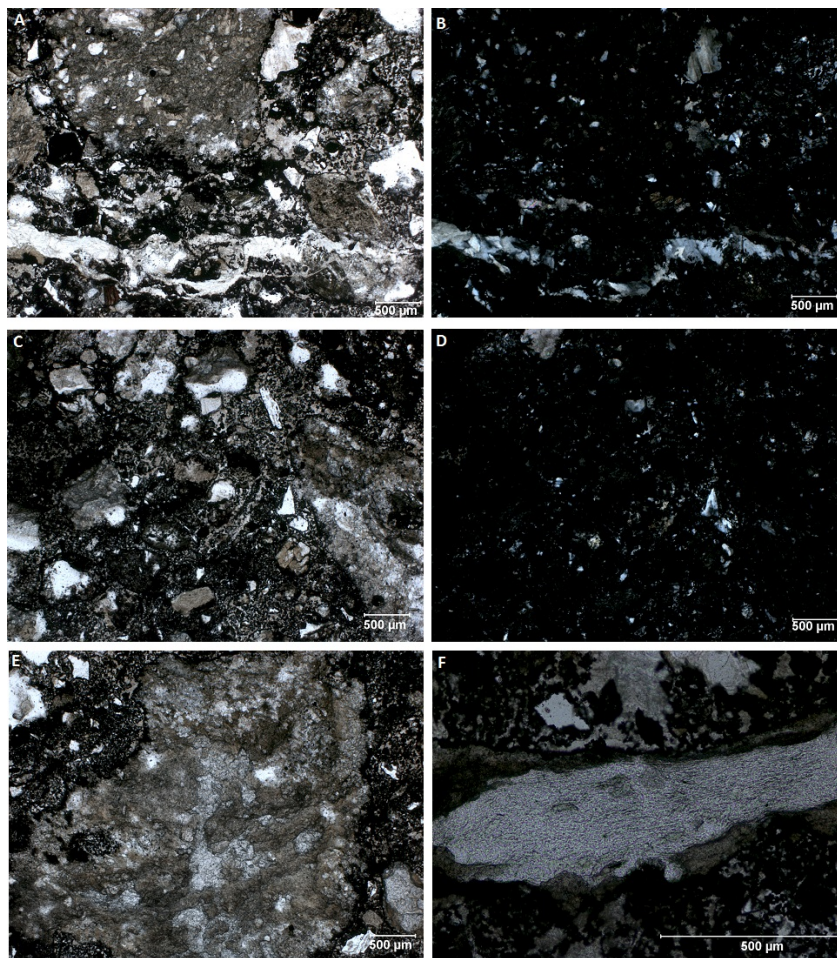


Figure 8.5: Microscopy images of thin section PK37+060. A/B and C/D are the same image in plane polarized and cross polarized light.

8.4 Density

The density of PK 34+405 was examined both in the form of a cylinder and with a pycnometer, PK 37+060 only with the pycnometer, results are presented in table 8.3.

Table 8.3: Density from cylinder and pycnometer

Sample	sat/dry	ρ_{syl}	ρ_{pyc}
PK 34+405	dry	2.48	2.56
PK 37+060	dry	-	2.50
PK 34+405	sat	2.50	2.57
PK 37+060	sat	-	2.50

For the first pycnometer test the samples had been stored in air temperature with natural fluctuations in humidity for approximately 4 months. The samples were immersed in water for a few minutes during the pycnometer test. On the second round of measurements the samples had been stored in tap water for 22 days. Further in the text calculations are made with a density of $2.57g/cm^3$ for PK34+405.

8.5 Rock Mechanical Properties

8.5.1 Point Load Strength

Irregular samples, mostly in the form of an annular sector was tested. PK 34+405 and PK 37+060 were stored in tap water for 22 days, while PK 34+555 was tested dry. The latter because this sample disintegrate in contact with water. PK 36+555 was prepared by dividing large pieces with a hammer. From visual examination the samples were fully saturated. The saturated samples PK 34+405 and PK 37+060 can partly be broken by hand after 22 days in water. The results of the point load test are given in table 8.4.

Table 8.4: Results from Point load strength test [MPa]. Calculated min, max, mean and standard deviation values when the two highest and lowest values are excluded before calculation. Classification in appendix E.

Sample	Min $I_{s(50)}$	Max $I_{s(50)}$	$I_{s(50)}$	Std.	Classification
PK 34+405	1.2	2.2	1.7	0.3	Low
PK 36+555	0.7	1.2	0.9	0.2	Very low
PK 37+060	1.7	3.1	2.6	0.5	Medium

Figure 8.6 show PK 34+405 and PK 37+060 prior to testing, and loading direction. 18 out of 22 pieces from PK 34+405 yielded valid result. Of the samples from PK 36+555, 13 out of 15 were valid. 14 pieces from PK 37+060 were tested, of these 11 were valid. The size correction factor was applied to find $I_{s(50)}$. To obtain the correct point load strength value, the two highest and lowest values of $I_{s(50)}$ among the 10 or more tests are deleted, and the mean is calculated from the rest.

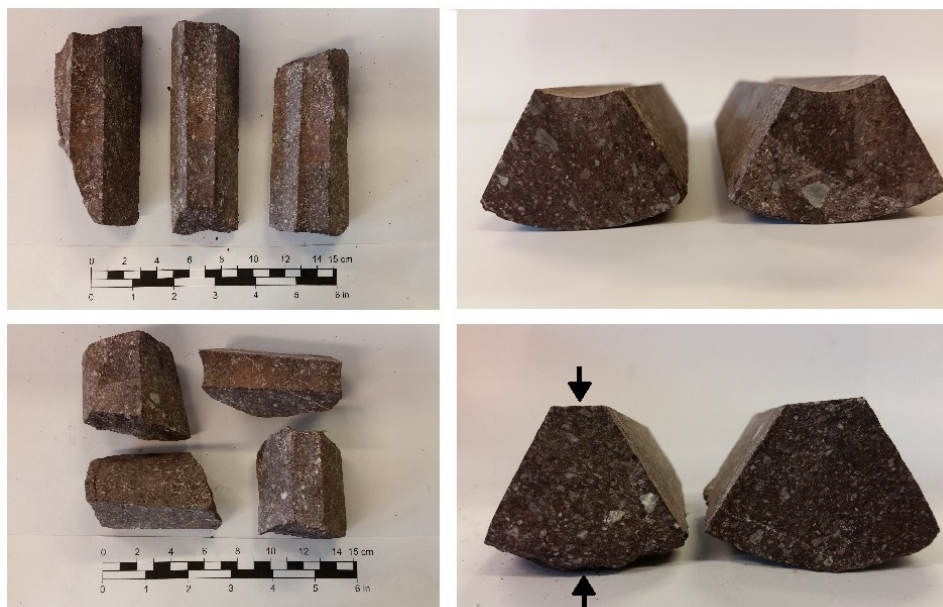


Figure 8.6: Samples prepared for PLI-test. The irregular lumps have either the shape of the top right or bottom right image. Loading direction is shown in lower right corner.

No preferred failure orientation were registered. A table of all other values can be seen in appendix D.

8.5.2 UCS, E-modulus and Poisson's ratio

It was only possible to prepare one successful core out of several attempts and only one UCS test was carried out. The diameter of the core was ca. 36 mm. The sample was saturated for 22 days, and no preferred orientation was seen. The length/diameter ratio of the core is 2.9, which is above the smallest recommended ratio of 2.5. The test was controlled by setting a fixed strain rate of 20 micro-strain/second instead of controlling the load rate. Failure mode appears to be shear failure as figure 8.7 show. The curve of stress plotted against strain is also provided in the same figure.

Table 8.5: Results after uniaxial compressive test on PK 34+405. E-modulus is calculated as tangent modulus at 50 % of UCS.

Parameter	PK 34+405
UCS [MPa]	41.9
E-modulus [GPa]	15.12
Poisson ratio ν	0.23

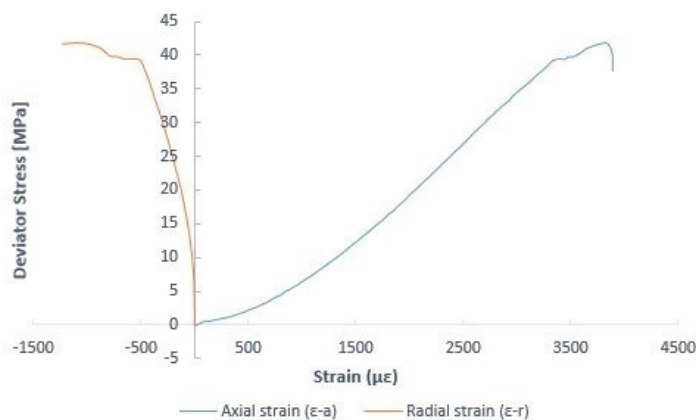


Figure 8.7: Result from uniaxial compressive test. Axial stress plotted against axial and radial strain. Image of PK 34+405 showing the failure mode, which appears to be shear failure.

By reversing equation 7.3 a corrected σ_{c50} of 39.2 is found. The uniaxial compressive strength is classified as medium.

8.6 Slake Durability Index

The slake durability test has been carried out in the project work, as well as in the thesis. The results are given in table 8.6. In the project work the rock lumps was prepared by cutting cores into appropriate size. In the thesis 10 rock lumps of appropriate size was selected from the remains after point load strength testing of PK 34+405 and PK 37+060. These samples had been stored in water for 22 days, which means that they had already been exposed to one cycle of wetting and drying. The procedure and calculation of slake durability index is still followed, to compare with previous results.

Table 8.6: Results from slake durability test. ¹ Tested in project work. ² Tested in thesis. Classified according to the classification in appendix E.

Cycle	I_{d1} [%]	I_{d2} [%]	I_{d3} [%]	I_{d4} [%]	Classification
PK 34+405 ¹	99.7	99.5	-	-	Very high
PK 36+555 ¹	51.3	41.4	-	-	Low
PK 34+405 ²	98.6	97.8	96.9	96.5	High
PK 37+060 ²	98.9	97.7	97.5	97.2	High

Figure 8.8 and 8.9 show the samples before and after testing. Spring water was used as slaking fluid, and the edges of the rock lumps were not rounded before testing. Some grains were larger than 2 mm.

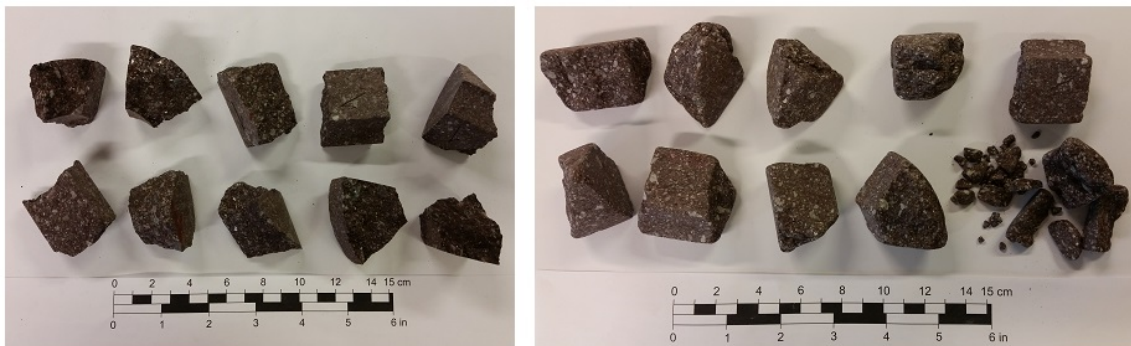


Figure 8.8: PK 34+405, samples before and after 4 cycles of slake durability test.



Figure 8.9: PK 37+060, samples before and after 4 cycles of slake durability test.

Rounding of the edges as well as some broken pieces are seen. From observations of the slaking fluid, particles were kept in suspension for at least 24 hours, as the bottom was not visible. After emptying of the slaking fluid, the bottom of the trough was covered with fine-grained material. In figure 8.10 the results from the slake durability test is plotted together with results from the project work.

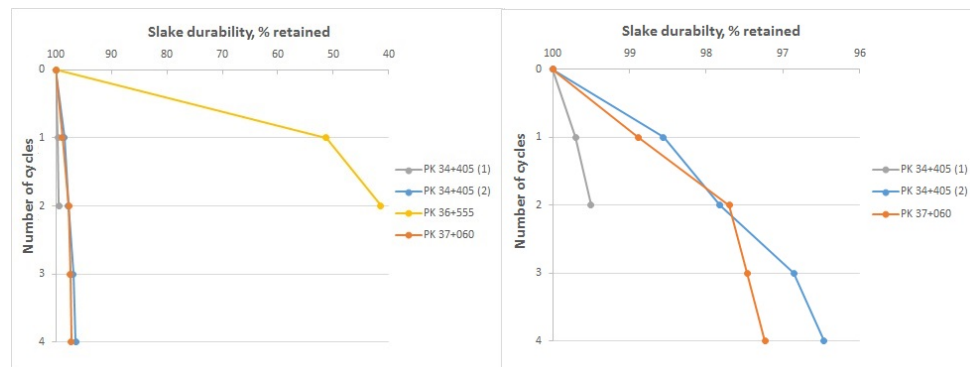


Figure 8.10: Number of slaking cycles plotted against slake durability in %. Left: all the samples are plotted together. Right: the three samples with high durability is emphasized.

8.7 Discussion of Results

8.7.1 Mineralogy

Neither normal XRD, nor DTA could confirm the presence of montmorillonite, and this result show the importance of glycol treatment in the identification process. As the first peaks of montmorillonite normally becomes visible around 100°C it is possible that drying the samples at 105°C have influenced the DTA result. The thin section study was meant to assess if the minerals found in XRD-analysis could be confirmed. Calcite was observed inn all the samples, except that, alteration and the fine grained nature of the matrix complicated the identification process. The optical properties of clay minerals such as kaolinite and smectite are in general difficult to identify with a normal light microscope due to their fine-grained nature. In thin section, they typically occur as fine-grained gray or brown earthy aggregates (Nesse, 2000). Plagioclase which is a large constituent of all the samples according to XRD was not observed in the thin section. Scanning electron microscopy (SEM) can be used to assess alteration of minerals and crystallinity (Brattli and Broch, 1995). The mineralogy of the clay minerals may play an important role for the time rate of swelling, together with hematite which has been inferred to influence the swelling potential either as coating on the clay minerals or as a cementing agent (Carter et al., 2010). These features should also be assessed with SEM.

8.7.2 Swelling

The amount of montmorillonite is not given from the mineralogical tests, but all the samples swell in different extents in powdered form. There are some differences between free swelling and swelling pressure results. The swelling pressure of samples classified as medium on free swelling, have swelling pressures ranging from 0.01 to 1.11 MPa on disk. In powder form the variation is smaller. This show the importance of a variation of tests. In the Chilean rocks, it was seen that powdering of intact rock samples was necessary to observe the full swelling potential (Carter et al., 2010). It is therefore surprising that the disk of PK 36+555 has such high swelling pressure compared to powder. The high pressure may be because the sample has already been subjected to mechanical disturbance as it possibly was taken from a weakness zone, but this does not explain the lower pressure in powdered form. The other samples behave according to the experiences in Chile.

8.7.3 Density, UCS, PLI

The density calculated from the pycnometer is approximately 3 % larger than for the cylinder. It is likely that this can be attributed to surface water and/or a small degree of water absorption in the pycnometer method. There is minor difference between the samples tested before and after 22 days in water.

A correlation between UCS and PLI should be established, to obtain input data for numerical modelling. From table 2.1, a correlation factor of 14 is recommended for rocks with compressive strength between 25-50 MPa, and $I_{s(50)}$ between 1.8 and 3.5. With this correlation σ_c can be estimated to 23.8 MPa and 36.4 MPa for PK 34+405 and PK 37+060 respectively. This result does not comply with the result of UCS for PK 34+405, which gives a correlation factor k of 23. The uniaxial compressive strength was only tested on one core. The load on the sample increased slowly, and might have resulted in a larger UCS.

Before the samples were stored in water, the strength appeared visually as similar. After water storage PK 37+060 appeared stronger than PK 34+405, also reflected in the result as it is almost 1 MPa stronger. The former was of the shape as the image in the lower right corner of figure 8.6 show, while the latter was mainly curved. Parts of the small pieces of PK 34+405 could be broken off by hand. The number of samples tested differ between the two, 18 and 11 valid tests respectively. The minimum, maximum, mean and standard deviation from the tests are given in table 8.4. The standard deviation may be a result of few samples or represent normal variation between the samples. Irregular samples give the least accurate results in the PLI test. The samples are small with an average D of 28.5 mm. Tests on specimens smaller than D=25 mm require caution to ensure sufficient measuring sensitivity (ISRM, 1985). The log-log plot in figure 8.11 also show the results. It is not possible to draw a regression line to obtain I_{s50} , due to small variation in D_e values

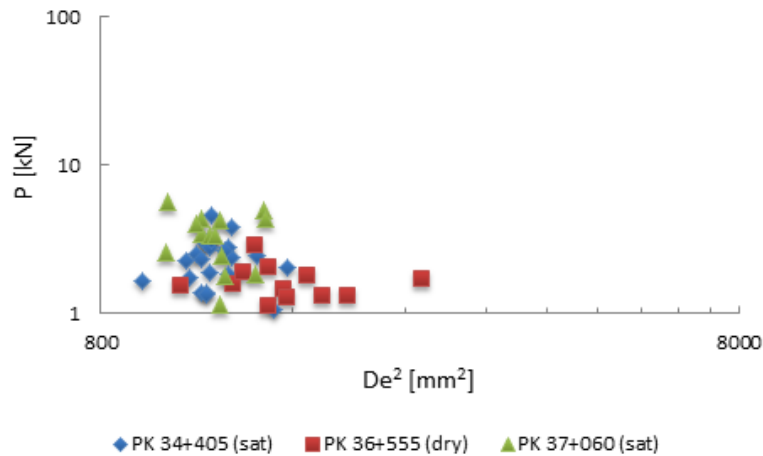


Figure 8.11: Graphic presentation in log-log plot of results from the point load strength test.

These considerations show that there is some uncertainty in estimating the compressive strength from PLI. It is recommended to gather more samples for UCS testing to establish a certain correlation factor.

8.7.4 Slake durability

As table 8.6 and figure 8.10 show the second test for PK 34+405, after water storage, does not reduce the slake durability significantly compared to the first test, even though the sample appears weaker. It is possible that the time frame of the test is too short for the slaking fluid to affect the mechanical properties of the samples and that the test does not reflect the ability the rock mass has to withstand repeated wetting and drying cycles, when the rock is of a certain quality. None of the factors deviating from the standard are believed to have affected the result, because of the high values. Rounding off the edges before the testing could have resulted in even higher results.

Chapter 9

Estimation of Rock Mass Properties

Since a limited number of laboratory tests have been conducted, some additional considerations are presented in this chapter to decide input values for the numerical analysis. Field visits, data from the construction phase and literature studies are helpful methods for estimating relevant parameters. Both properties of the surrounding rock mass and the weakness zone must be considered. From the construction mapping the rock mass in the tunnel is registered as tuff, bordering against andesite (HTC, 2010; TE, 2010).

9.1 Rock Mass Properties at PK 34+405

The laboratory values are compared to other values that have been suggested for tuff and andesite. The values for andesite are considered because it has been reported in the vicinity of the section in question. In table 9.1 variation in compressive strength and the input m_i factor for the Hoek-Brown criteria is presented. The variation in strength can be significant.

Table 9.1: Variations of the compressive strength and the factor m , for andesite and tuff. Table based on ¹Lama and Vutukuri (1978) and Hoek et al. (1992) in (Palmström and Stille, 2010), ²(Marinos and Hoek, 2000).

Rock type	Variation in σ_c [MPa]			Rating of the factor m_i	
	Low	Average	High	¹	²
Tuff	3 ¹	25 ¹	150 ¹	15	13±5
Andesite	75 ¹	140 ¹	300 ¹	19	25 ± 5

(Dinçer et al., 2004) tested a number of tuff, basaltic and andesitic rock samples from the Bodrum peninsula in Turkey to assess the correlation between Schmidt hardness, uniaxial compressive strength and Young's modulus. Some of the results are presented in table 9.2. Also within these data the variation was large. The rocks were altered and in thin section analysis it was found that plagioclase had been transformed to sericite and kaolinite. No notice on the water content is included. For more information about the testing procedures it is referred to Dinçer et al. (2004).

Table 9.2: Average values of UCS, Young's modulus and unit weight from andesites and tuff from Bodrum Peninsula, Turkey (Dinçer et al., 2004).

Rock type	σ_c [MPa]	Young's Modulus [GPa]	Unit weight [kN/m^3]
Tuff	41.97	6.92	18.44
Andesite	82.52	13.62	22.53

When the weakest samples are excluded, the average PLI from PK 40+522 to PK40+758 was 6.32 MPa. From the map of the surface these rocks are from the same unit as the rocks around PK 34+400. According to table 2.1 a correlation factor k_s of 20 is recommended for rocks with PLI between 6-10 MPa. Because this results in a significant difference from the laboratory results it can be considered to use the factor of 16 suggested for rocks with PLI from 2.5-6 MPa.

As already discussed in section 8.7, a correlation factor of 14 is recommended when PLI is between 1.8 and 3.5. Since this result does not comply with the result of UCS which gives a correlation factor 24.6, and it is suspected that the sample geometry affected the result it is suggested to test four different cases of rock strengths. All the values are rounded to nearest whole number.

1. Case 1: The results from point load strength testing with a correlation factor of 14 is used. UCS = 24 MPa.
2. Case 2: The results from the uniaxial compressive strength test is used. Size corrected UCS = 39 MPa.
3. Case 3: The results from point load strength testing by FCFM (2013) with a correlation factor of 16 is used. UCS = 101 MPa.

These numbers reflect the variation seen in table 9.1 except for the lower range off tuff strength. The laboratory values obtained in the thesis is very close to the average value of the tuffs tested by Dinçer et al. (2004). The constant m_i is set to 15 as recommended in table 9.1.

9.2 Weakness Zone at PK 34+405

Estimating the strength of the weakness zone is difficult due to lack of data. A possible approach suggested by supervisor K.K.Panthi, is to reduce the strength according to the degree of weathering. The core from PK 34+385 can be classified as highly weathered to completely weathered according to table 2.2. From figure 2.4 a reduction between 75 and 90 % can be applied. However, the initial strength should be known for this to be applicable. As an alternative the average PLI of 0.9 MPa for PK 36+555 is used, as this sample also is assumed to originate from a weakness zone (personal communication with Thomas Schönborn). With a correlation factor of 14 this results in a strength of 13 MPa.

It should be noted that is not recommended to do the test for samples with UCS below 25 MPa. This value is comparable to the properties of the weakness zone that was modelled at Buon Kuop (section 5.3.2) which had a strength of 12 MPa, a GSI of 25 and m_i of 7. Since the core from PK 36+555 is an intact rock, the strength of the weakness zone is probably lower. However the cracks in the shotcrete was not discovered before after two years of operations. It is possible that the strength of the material has been reduced as the rock mass was subjected to water. For example, at Hanekleiva an E-modulus of 3.1 GPa was assigned to the original material in the weakness zone. After strength reduction the E-modulus was reduced by 35 % to 2.0 GPa. A strength of 13 MPa is therefore applied to the weakness zone. The numerical analysis will show if these considerations are reasonable, or that if the strength properties should be adjusted.

A low value of m_i is chosen, because the content of clay is likely to reduce the friction significantly. In the NGI (2015) friction angles from 6-16° are suggested in the presence of clay. A value of 8 is assigned to the weakness zone, since this is the lowest recommended value for tuff in table 9.1.

Chapter 10

Stability Assessment

Since the tunnel is completed, this analysis is mainly carried out to assess the input values for the numerical analysis and to have some means of comparison. Evaluation of results from rock mass classification, calculation of tangential stresses and possible tunnel deformation are done. A GSI value is estimated based on the mapping results and field visit.

10.1 Rock Mass Classification

10.1.1 Q-values from mapping

In table 10.1, Q and RMR values from mapping schemes are provided. These values and the mapping schemes describe a rock mass of poor quality, with three to four joint sets. The joints are described as relatively smooth, and have infilling of clay, limonite, zeolite and calcite. The stress situation is favourable and minor water is observed. In relation with the weak zone water is registered. The rock mass is moderately to highly weathered.

Table 10.1: Q-value from construction mapping

Chainage	RQD	J_n	J_r	J_a	J_w	SRF	Q	RMR
PK 34+404.2-401.0	55	9	2.0	4.0	1.0	1.0	3.1	54.1
PK 34+395.4-394.0	40	15	1.5	4.0	1.0	1.0	1.0	44.0
PK 34+390.4-387.0	45	12	1.5	6.0	1.0	1.0	0.9	43.4

Excavation support ratio of 1.6, and a tunnel height of 6 m gives an equivalent dimension of 3.75. The support scheme provided in the Q-system assigns this type of excavation in very poor to poor rock mass to support class 3-4. 5-9 cm of fiber-reinforced shotcrete with minimum energy absorption 500 J and systematic bolting with average bolt spacing of 1.6 m is suggested.

10.1.2 GSI

From the values in table 10.1, information from the mapping schemes and the field observations described in section a GSI ranging between 35 to 50 is a reasonable estimate. Since only one value will be used in the stability analysis, this is estimated to 40. This corresponds well with the relationship between RMR and GSI that also can be used.

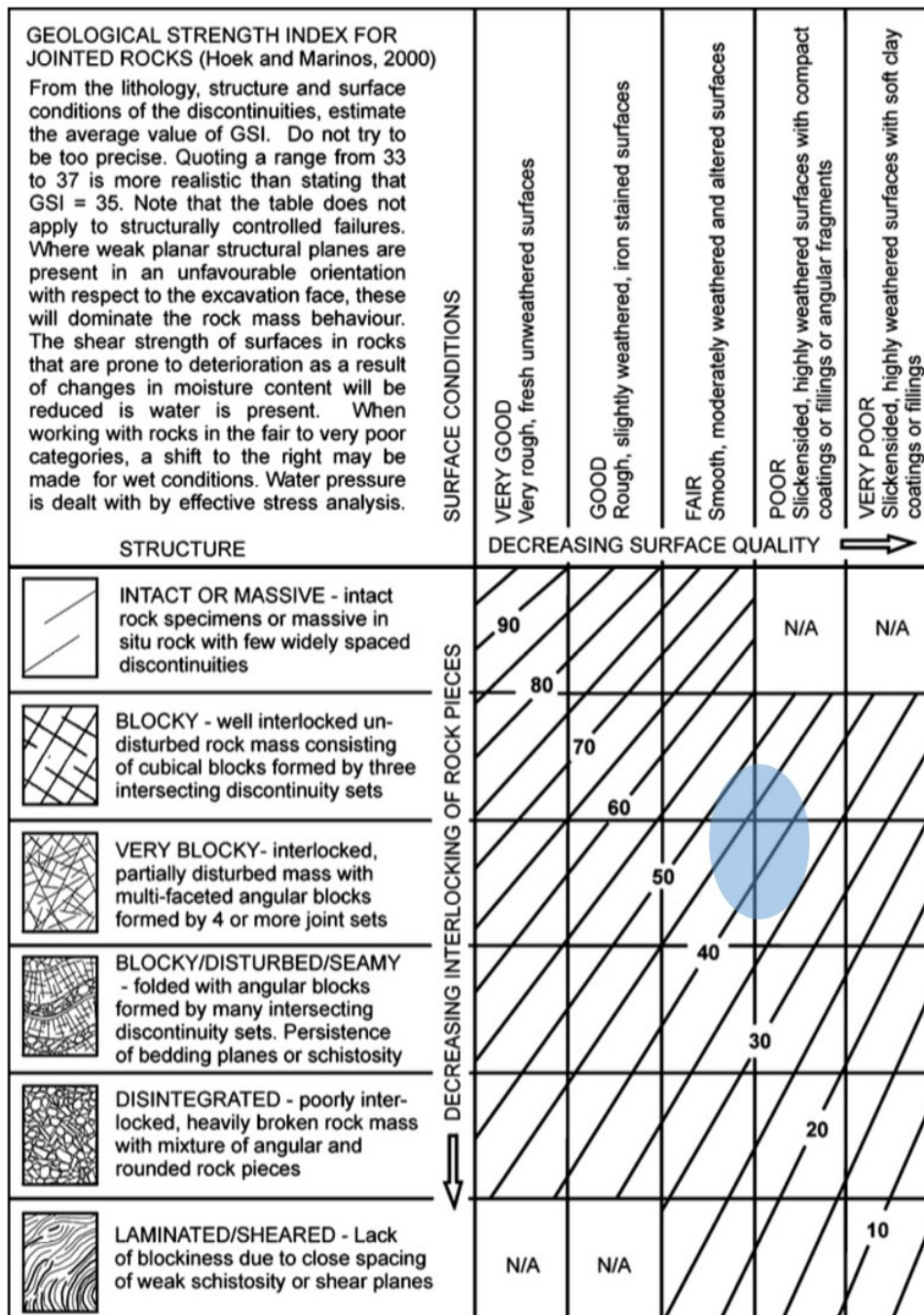


Figure 10.1: Estimated GSI value

For the weakness zone a reduced GSI should be applied. From the sample from PK 34+385 and the mapping schemes the rock mass is disintegrated with very poor surface

conditions. Based on this a GSI of 15 is assigned to the weakness zone.

10.2 Estimates of Deformation and Support

Due to the variation in strength from weak to stronger rock in the proposed cases, the tunnel deformation is assessed by the Hoek and Marinos method (Hoek and Marinos, 2000), after recommendation from supervisor K.K. Panthi. In table 10.2, sidewall deformation and radius of plastic zone in a circular tunnel, calculated with equation 3.23 and 3.24, are presented. Rock mass properties and the estimated value of m_i for the cases suggested in chapter 9 are used. Since cohesion and friction angle in the rock mass/weakness zone have not been assessed, strength must be estimated in another way than by equation 3.22. Equation 3.25 defined by Panthi (2006) is used in stead.

Table 10.2: Estimation of deformation and width of plastic zone without support pressure. A tunnel radius of 3 m and in situ stress of 5.9 MPa is used. Method by Hoek and Marinos (2000).

Parameter	Case 1	Case 2	Case 3	Weakness zone
σ_{ci}	24	39	101	13
σ_{rm}	2.0	4.1	16.9	0.8
Strain ϵ [%]	1.81	0.42	0.02	11.4
Deformation δ [cm]	5.44	1.27	0.07	34.22
Diameter plastic zone d_p [m]	3.75	3.75	3.75	3.75

From figure 3.5 a strain of less than 1 % is associated with very few stability problems, and rock support can be decided according to rock mass classification schemes. The deformations for case 1 to 3 is acceptable, but the weak material is clearly not stable. A strain of 34.44 % on the other hand would result in severe stability problems/collapse. However, due to several reasons this calculation is not very relevant. The weak zone has a limited thickness and is surrounded by rock mass of better quality, the tunnel is not circular and the stress situation not isostatic and only the vertical stress is taken into consideration. Support pressure can be estimated according to table 3.1. The installed support was initially 8 cm of shotcrete. After cracks in the shotcrete was discovered an additional 20 cm of shotcrete was installed (personal communication with co-supervisor Thomas Schönborn). In table 10.3 the deformation in the weakness zone with different support pressures is presented. As the weak material is not covering the whole tunnel, these estimates are given just to have some perspective on the support.

Table 10.3: Estimation of support pressure of shotcrete after Hoek (2007a) and associated deformation in cm in the weakness zone.

Thickness [cm]	$p_{i,max}$ [MPa]	ϵ weak zone [%]	δ weak zone [cm]
30 cm	3.7	0.12	0.35
15 cm	1.9	1.43	4.29
10 cm	1.26	2.97	8.90
5 cm	0.6	6.08	18.24

In addition the support is not affected by bending moments which clearly affects the shotcrete as shown in the numerical analysis. From Kirch's equations the maximum tangential stress around a circular tunnel with this stress situation is 27.4 MPa, while the minimum tangential stress is 6.6 MPa.

Chapter 11

Numerical Analysis

The finite element program RS² is used for a 2D analysis of a cross section in the area between PK 34+390 and PK 34+405 in the Portillo tunnel. A plane strain analysis with Gaussian elimination, and the Hoek Brown criteria is used. The main focus is to analyse displacements and support performance in relations with a weakness zone. Therefore the material is analysed with plastic properties.

The cross section is referred to as PK 34+405 from now on, as the overburden at this point is used. The analysis aim to model the manifestation of shotcrete cracks and deformations of approximately 10 cm that occurred after two years of operation. The section is simulated with a weakness zone with swelling pressure of the same characteristics as the material from PK34+385. Properties of the surrounding rock mass as suggested in chapter 9 are assessed.

11.1 Model Set-up

11.1.1 Geometry, mesh and displacements

A graded mesh with 3 noded triangles, a gradation factor of 0.1 and 110 excavation nodes is used. The geometry of the model is drawn according to support class IVc from HLC (2011), and is illustrated in figure 11.1. This includes space for installation of different types of support. A 1.5 m blast disturbed zone is added around the excavation. The external boundary is extended by a factor of three times the tunnel width. The sides of the boundary are restrained in x-direction and the top and bottom in y-direction. The corners are restrained in both directions. The tunnel is excavated in one stage.

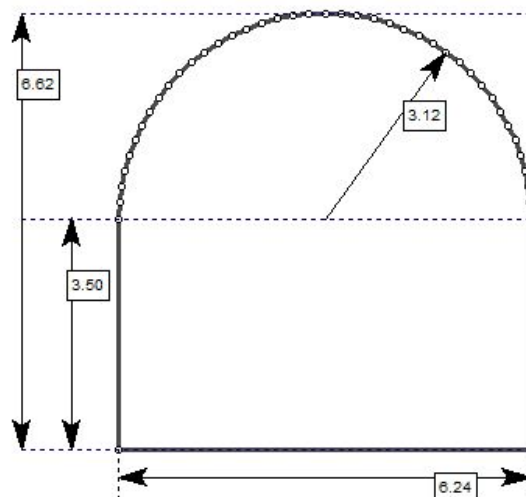


Figure 11.1: Geometry of the tunnel. The geometry is according to drawing of support class IVc.

The weakness zone is modeled as a 1.5 thick zone with dip angle of 40° . Because of the way the zone strikes the tunnel is modelled in two separate models. This is applied as illustrated in figure 6.4. Figure 11.2 show the setup of the model.

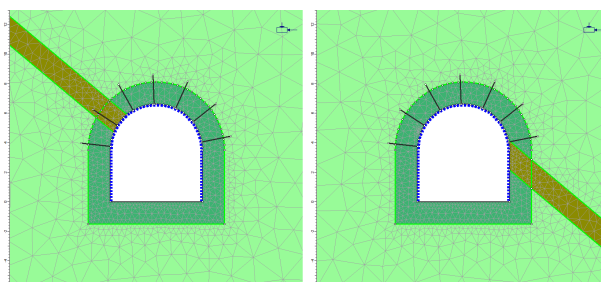


Figure 11.2: Model set-up for numerical analysis with weakness zone and support installed according to IVa.

11.1.2 Rock stress and loads

Mean values from the hydraulic fracturing measurements are used as "Field Stress Properties" in the analysis. An overburden of 235 m gives a vertical stress of 5.9 MPa and a horizontal stress of 11.1. The out of plane component corresponds with the minimum horizontal stress of 5.8 MPa.

Because of the relatively high overburden and high horizontal stress the field stress is set to constant. The orientation of the maximum horizontal stress is described in section 6.5.3. Since the tunnel is oriented approximately $N025^\circ$, σ_H will be oriented perpendicular to the tunnel and no correction for orientation is necessary as it is assumed to be a principal stress. Groundwater is not taken into account. The swelling pressure is applied as an uniform load normal to the excavation boundary.

11.1.3 Rock mass properties

In chapter 10 three different sets of material properties are proposed. These are used as input to decide the most likely conditions in the tunnel. The dilatation parameter is a measure of the volume increase of a material when it is sheared (Rocscience, 2017b). For this model the dilatation is set to zero after recommendations from Q.N. Trinh (course coordinator for TGB4260 Numerical Analysis for Rock Engineering, NTNU). Disturbance of the rock mass due to blasting is defined by the disturbance factor D . Blasting in the tunnel was not done carefully and therefore D is set to 0.5 according to guidelines presented in appendix J. The disturbed zone is not applied to the weakness zone, since the material already is reduced. It is likely that the stronger material around will take up deformations due to blasting (personal communication with Q.N. Trinh). The rock mass modulus proposed by Hoek et al. (2002) and presented in equation 3.14 and 3.15 are used.

Table 11.1: Input parameters for the numerical analysis. D =disturbed zone.

Input parameters	σ_{ci} [MPa]	ν	E_i [MPa]	GSI	m_i	D	E_{rm} [MPa]
Case 1	24	0.23	-	40	15	0	2754.9
Case 1	24	0.23	-	40	15	0.5	2066.2
Case 2	39	0.23	15120	40	15	0	3511.8
Case 2 D	39	0.23	15120	40	15	0.5	2633.9
Case 3	101	0.23	-	40	15	0	5623.4
Case 3 D	101	0.23	-	40	15	0.5	4217.6
Weakness zone	13	0.23	-	15	8	0	480.8

The residual factors defined in equation 3.10 to 3.13 are applied to the rock mass and weakness zone and listed in table 11.2. Since D is not taken into account in these equations they must be defined differently for the disturbed zone.

Table 11.2: Hoek-Brown and residual parameters for numerical analysis.

Hoek-Brown parameters	Case 1-3	Disturbed zone	Weakness zone
m_b	1.760	0.861	0.384
s	0.0012726	0.0003355	0.0000791
a	0.5114	0.5114	0.5611
Residual parameters			
GSI_r	23	-	12
m_r	0.959	0.469	0.345
s_r	0.0001925	0.0000507	0.0000567
a_r	0.5358	0.5358	0.5747

It is chosen to use the peak/residual ratio for the undisturbed rock mass to decide residual parameters m_r and s_r for the disturbed zone following the approach in the thesis by Flåten, M. (2015). The factor a is independent of the disturbance factor, and will be the same as for undisturbed rock mass.

11.1.4 Support

Since support class IVa was installed according to observations it is used for initial modelling, according to the drawing presented in figure 6.7. After cracks in the shotcrete was discovered, a new 20 cm layer of shotcrete was applied. Properties of the support are listed in table 11.3. The concrete invert is assumed not to have any effect at the time of excavation, and is therefore not implemented in the model.

Table 11.3: Support properties for numerical analysis. References: 1) RS^2 standard value, 2) *Dywidag Systems International (2017)*, 3) *HLC (2010)*.

Bolt properties	Value	Reference
Type	Fully grouted	3
Diameter [mm]	22	3
Length [m]	2/4	3
E-modulus [GPa]	200	1
Tensile Capacity [MN]	0.255	2
Residual tensile capacity	0.1	3
Pre-tensioning	No	-
Spacing [m]	1.5×1.5	3
Shotcrete properties		
Liner type	Standard Beam	1
Young's modulus [MPa]	30000	1
Poisson's ratio	0.2	1
Compressive strength (peak) [MPa]	35	1
Compressive strength (residual) [MPa]	5	1
Tensile strength (peak) [MPa]	5	1
Tensile strength (residual) [MPa]	0	1
Thickness [cm]	8/20	3

RS^2 has several options for liner support. For this model the Standard Beam element with the Timoshenko formula is used. The liner has flexural rigidity and is sufficient for modelling shotcrete (Rocscience, 2017b). The shotcrete can be modelled both as elastic and plastic.

11.2 Modelling Sequences

Several steps are used for the modelling, presented in the following subsections.

11.2.1 Defining rock mass properties

First case 1-3 defined in chapter 10 are analysed with respect to deformations to determine which is more likely. No support is installed and the weakness zone is included at the point of excavation. They are assessed based on deformation in crown, invert and weakness zone. As presented later, case 3 will be used for further analysis.

11.2.2 Weakness zone

To assess the development of shotcrete cracks a model which runs over several stages is used. It is suspected that the quality of the material in the weakness zone has degraded from the point of excavation until shotcrete cracks were discovered. Therefore no weak material is applied in the initial stages. This is also to simulate the stable situation in the tunnel after excavation. Assuming that the rock mass is exposed to a process that reduces the strength, the material properties (UCS and GSI) in the weak zone are gradually reduced by two different approaches. First in subsequent stages with material properties given in table 11.4. The steps are listed in the next points and the support is according to support class IVa.

- Step 1: Intact rock mass
- Step 2: Excavation and application of shotcrete
- Step 3: Installation of bolts
- Step 4: Weakness zone with properties like laboratory results of PK 34+405.
- Step 5: 20 % reduction of intact rock strength.
- Step 6: 40 % reduction of intact rock strength.
- Step 7: 60 % reduction of intact rock strength.
- Step 8: Weakness zone with properties like laboratory results of PK 36+555.
- Step 9: 80 % reduction of intact rock strength.

Table 11.4: Input parameters for reducing the strength of the weakness zone. m_i is set to 8 for all the stages.

Stage	Reduction/strength [%]	UCS	GSI	GSI-r
Stage 4	Lab PK 34+405	39	40	23
Stage 5	20	31	32	21
Stage 6	40	23	24	17
Stage 7	60	16	16	13
Stage 8	Lab PK 36+555	13	15	12
Stage 9	80	8	8	7

Secondly each of the different properties are installed in stage 4, to assess if the modelling method influences on the displacement. The analysis is focused on displacements and yielding of shotcrete in the weakness zone.

11.2.3 Support

The difference between support class IVa and IVc, and the effect of additional shotcrete is assessed. As mentioned it is believed that the support class was IVa with 8 cm shotcrete and 2 m bolts, while the mapping schemes say it is support class IVc. The modelling this far has been with IVa. The following stages are used.

- Stage 1: Intact rock mass
- Stage 2: Excavation and application of 8/12 cm shotcrete.
- Stage 3: Installation of bolts
- Stage 4: Weak zone is introduced + 20 cm additional shotcrete

11.3 Results of Numerical Analysis

11.3.1 Rock mass properties

The most likely input parameters for the analysis are decided by assessing displacements and yielded elements without installed support in the four cases listed in chapter 10. All the elements in the weakness zone is yielded before excavation (no displacement) because of its low strength. The deformations in the crown and invert, in addition to the weakness zone, are presented together with number of yielded elements in table 11.5.

Table 11.5: Displacement in the different cases. Maximum displacement corresponds with the weakness zone in all cases.

Case	Yielded elements	Yielded elements [%]	Max. Disp. [cm]	Disp. crown [cm]	Disp. invert [cm]
LEFT					
Case 1	1701	40	16.2	9.3	9.9
Case 2	1513	35	12.7	4.8	5.5
Case 3	1183	26	10.1	1.5	1.9
RIGHT					
Case 1	1703	38	17.8	8.3	10.3
Case 2	1541	34	16.1	6.0	7.5
Case 3	1289	27	11.7	1.5	2.0

The number of yielded elements and the displacements decrease as the rock mass around the weakness zone gets stronger. From these results it is decided to continue with the input parameters from case 3, as the total strain (excluding the weakness zone) is larger than 1% in case 1 and 2.

11.3.2 Weakness zone

It is possible that the displacements seen for case 3 in table 11.5 are representative of the situation in the tunnel when shotcrete cracks was discovered. To assess the development of instability problems the approach presented in section 11.2.2 has been used. The stress situation leads to a number of 40 yielded liner elements in the crown, as figure 11.3 show. This is before the weakness zone is applied.

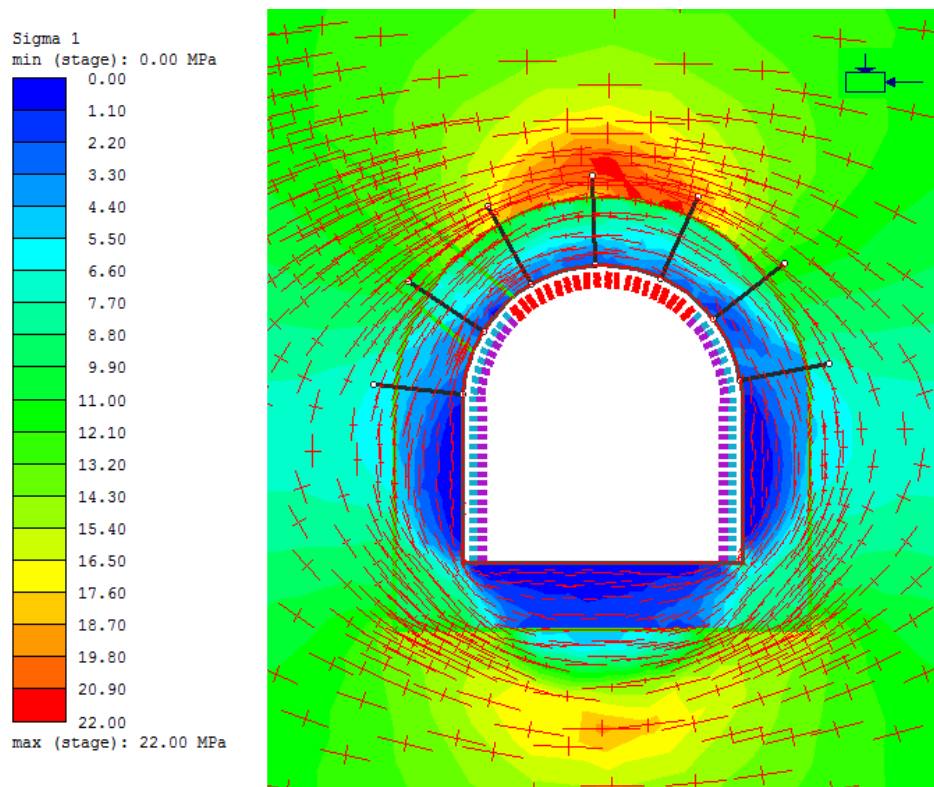


Figure 11.3: Stress situation in stage 3 after excavation, plastic material properties. The weakness zone in the upper left corner.

It is not emphasized further in the analysis, but influences on the high number of yielded liner elements. This is also high because of the double layer of elements in the composite liner. The increased number of stress trajectories in the left corner is caused by the increased number of mesh elements in the area around the weakness zone.

As seen from table 11.6 weakening the material is increasing the displacements and the number of yielded elements in the shotcrete. The increasing number of yielded elements in the left and right side are illustrated in figure 11.4. The background represent percent yielded elements in the mesh. The area with yielded mesh elements are also seen to increase from these figures.

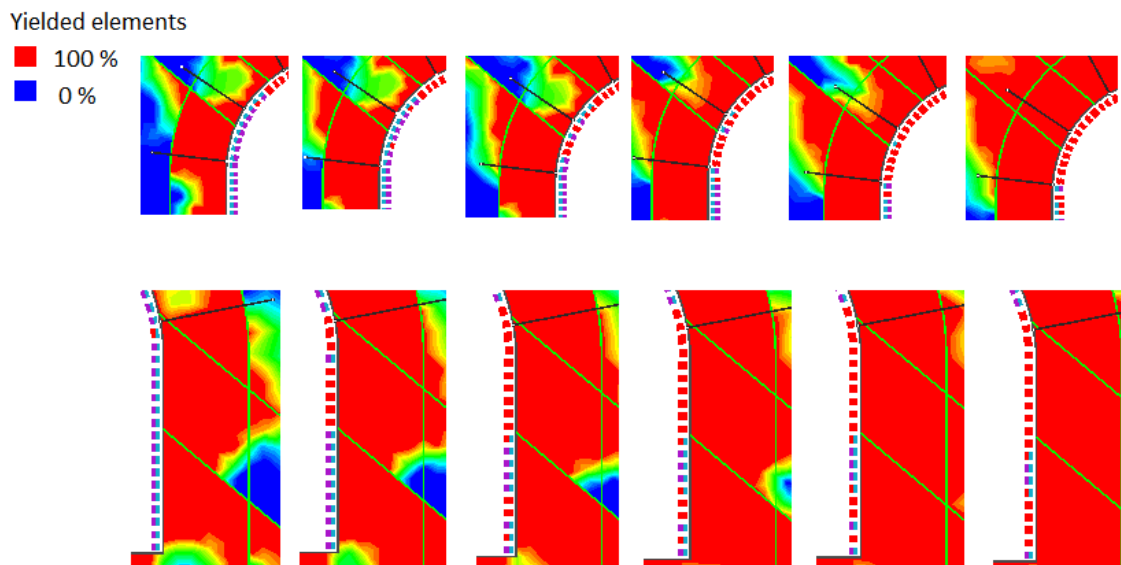


Figure 11.4: Progression of yielded shotcrete elements from stage 4 to 9, in the left side on top and right side on bottom, as properties in the weakness zone are changed.

After the initial analysis where the strength of the material was reduced, a constant load representing swelling pressure is included from stage 4 in the model. It is not applied a higher load than 0.3 MN/m^2 because convergence problems are introduced with this load.

Table 11.6: Displacements after strength reduction and application of swelling pressure from stage 4. Convergence problems are introduced when applied load is 0.3 MN/m^2 . YLE=Yielded liner elements.

Stage	No load		Load 0.1 $\frac{\text{MN}}{\text{m}^2}$		Load 0.2 $\frac{\text{MN}}{\text{m}^2}$		Load 0.3 $\frac{\text{MN}}{\text{m}^2}$	
	Disp.[cm]	YLE	Disp.[cm]	YLE	Disp.[cm]	YLE	Disp.[cm]	YLE
LEFT								
Stage 2	1.8	40	1.8	40	1.8	40	1.8	40
Stage 3	1.9	40	1.9	40	1.9	40	1.9	40
Stage 4	2.4	41	2.5	40	2.8	40	4.1	42
Stage 5	3.6	43	3.8	42	4.3	43	8.5	52
Stage 6	5.8	52	6.3	51	7.4	54	14.5	58
Stage 7	10.3	60	11.4	60	12.9	61	26.0	61
Stage 8	16.2	65	17.9	67	20.1	65	33.7	70
Stage 9	28.2	68	30.8	69	34.7	66	50.3	74
RIGHT								
Stage 2	1.7	40	1.7	40	1.7	40	1.7	40
Stage 3	1.8	40	1.8	40	1.8	40	1.8	40
Stage 4	2.8	41	4.1	52	9.8	63	21.7	67
Stage 5	4.3	56	6.8	58	13.7	70	25.0	70
Stage 6	7.2	66	11.7	62	21.2	72	36.0	73
Stage 7	13.2	68	21.3	68	47.3	77	74.6	75
Stage 8	21.7	69	33.1	71	63.5	78	95.0	77
Stage 9	37.7	73	56.1	77	98.6	79	160.2	78

The application of the uniform load clearly increase displacements on both sides. Stage 8 represents the weakness zone as it was proposed in chapter 10. It is important to note that these displacements are total, not displacement from stage to stage. The results of the second approach where the different weak materials are assessed one by one is given in table 11.7. This is only done for the right side since the largest displacements are seen here.

Table 11.7: Displacement with different strength of the weakness zone, each applied in stage 4 in a single model. YLE = yielded liner elements

Properties	Disp. [cm]	YLE	Comment
PK 34+405	2.8	40	Displacement concentrated to right wall, but no YLE in the wall.
20 % reduced	3.4	53	Yielding in the shotcrete begins.
40 % reduced	4.9	59	Increasing yielding
60 % reduced	8.0	62	Increasing yielding
PK 36+555	11.1	69	Increasing yielding
80 % reduced	20.5	71	Increasing yielding

From these results it is seen that displacements are larger when it is included in the sequence of reduced strength than when it is applied alone (11.1 versus 21.7 cm in the right side). The number of yielded shotcrete elements are the same. Yielding of the shotcrete starts at the same time in both approaches, but the number of elements are larger in the first method until the stage where the weak zone has properties resembling PK 36+555.

11.3.3 Support

To assess the effect of additional support we go back to the first model with material in the weak zone like PK 36+555. Only the right side is considered since the largest displacements are seen here. The stages in section 11.2.3 are used.

Table 11.8: Displacement in weakness zone (UCS=13) MPa with support installed. YLE = yielded liner elements

Support	Displacement [cm]	YLE
IVa	11.1	69
IVc	10.5	57
IVa + 20 cm extra	9.33	69
IVc + 20 cm extra	9.28	64

There is no substantial difference in displacements between the support types, but the number of yielded liner element decreases. Heavier support slightly reduce the displacement as table 11.8 show. It is not possible to assess the effect of the additional 20 cm

with this approach. If added after the weak zone is installed there is no loading on the shotcrete, and it will appear as stable in the model. Yielded bolt elements are seen in weakness zone, but the focus has been on the shotcrete.

11.4 Discussion of Numerical Analysis

A number of approaches have been used to assess the problem. The results show that strength of the material in the weak zone has a large influence on the degree of displacement. However some convergence problems are seen, and modelling of support is complicated. Thus an assessment of the quality of the analysis is given here.

11.4.1 Stress situation

The use of a constant field stress is an idealized situation as the stress will vary with the overburden. Because the input parameters are uncertain it is considered precise enough. Due to the geometry of the valley, it is possible that an inclined stress situation would be more applicable, but since the tunnel is located some distance into the valley side, it was chosen to use the horizontal situation. The stress situation leads to yielding of the shotcrete in the first stages. This may be a sign that the applied stress is too high, but as it is not the focus of the analysis it is neglected. The stress situation is based on measurements some distance away and in another rock unit. It is seen that there is less deformation in the left side. This can possibly be attributed to confinement of the weakness zone due to the stress situation.

11.4.2 Input properties

The rock mass modulus proposed in (Hoek et al., 2002) has been used for the analysis. The difference between the methods that exist is large when the rock mass is weak. In table 11.9 the rock mass modulus calculated with different methods is given. The generalized Hoek-Brown criteria is recommended to use by Rocscience (2017b), but this gives very low values for the weakness zone and deformations from 30-45 cm.

Table 11.9: Different methods for calculating the rock mass modulus [MPa]. ¹Simplified and generalized by (Hoek and Diederichs, 2006) and ² (Hoek et al., 2002). Modulus ratio of 300 is used for weakness zone, case 1 and 3. E_i of 15120 MPa is used for case 2.

Method	Weakness zone	Case 1	Case 2	Case 3
1. E-rm (generalized) ¹	142.2	1149.5	2413.9	4837.5
2. E-rm (simplified) ¹	425.9	3985.6	3985.6	3985.6
3. E-rm ²	480.8	2754.9	3511.8	5623.4

Therefore the modulus proposed by Hoek et al. (2002) was used. The intact modulus is known for case 2, but it was desirable to use the same approach for all the samples.

Method number 2 give the same result for all the cases since it is based on GSI, and is therefore not a good method for the approach used in this analysis. The difference between the methods is decreasing as the rock mass get stronger. However, if method number 1 is more correct, the displacement may be even larger. The width of the weakness zone is larger than in reality, and therefore the displacement found from the model may be to large. A larger zone was applied to be sure that the effect of it was visible, after recommendation from Q.N. Trinh.

The use of both reduced rock mass strength and reduced GSI in the weakness zone might be too pessimistic. Previous work have shown that weathering can reduce the rock strength (Panthi, 2006; Pasamehmetoglu et al., 1981). From the laboratory work it is clear that rock mass which look similar may have quite different behaviour. This support the use of a reduced strength. However, since the rock mass may be decomposing, it is possible that the intact rocks within it will keep its strength. Further testing should be done to assess this.

To not complicate the analysis more, there is no variation in GSI for the surrounding rock mass. The strength of the andesitic tuff in case 3 are also more than twice as large as the results from the laboratory, which may be somewhat optimistic. As the aim of the numerical analysis is to assess deformation in the weakness zone and due to swelling pressure the high UCS chosen for the rock mass can be justified. With a lower UCS the deformation would be high also in the rest of the model.

11.4.3 Model quality

It is observed that there is a large difference between the two different methods used to assess the displacements. This may be attributed to the repeated reloading of the tunnel which is done when new stages are included. Mao (2012) compared the use of Phase² (now *RS²*) and *FLAC^{3D}* for modelling of weakness fault/zones and found that displacements deviated between the two methods. In the two-dimensional model the displacement was higher than in the three-dimensional model. For *RS²* to be applicable the width of the weakness zone should be much wider than the tunnel span and perpendicular to the tunnel alignment, so that it can be considered as a two dimensional problem. It was also found that with lower strength of the material in the weakness zone the deviation increased. The stress situation is often anisotropic in such a zone (Mao, 2012). As the weakness zone in this case is much smaller and not perpendicular, the modelling in *RS²* may be to inaccurate. The application of swelling pressure introduce convergence problems that may imply that the approach is to complex. Trinh and Broch (2008) successfully used a 2D model to model a weakness zone. However this model looked at a cave in that happened during the excavation process. In the thesis it is the situation after excavation is desired to assess.

The applicability of the Hoek Brown criterion can be discussed. It is assumed that the rock mass is overall fractured. As it is a weakness zone that is modelled also the

cohesion and friction angle may provide important information of the rock behaviour. For further modelling it is suggested to use these parameters and the Mohr Coulomb criteria. A further assessment is important to examine if the results of the numerical analysis is valid. When modelling discontinuous rock mass, DEM methods are often preferred. UDEC (Universal Distinct Element Code) is a program which is developed for blocky structures where mechanical discontinuities are important for the deformation behaviour (Nilsen and Palmström, 2000). Since the assessment of additional support gives non-conclusive results, it is suggested that another approach to the problem should be used. This requires additional research.

Chapter 12

Discussion

12.1 Estimation of Rock mass Properties

The factors that are discussed here are mainly related to rock mass behaviour. Factors related to the results of the laboratory investigations have already been discussed and will not be repeated. PK 36+555 reacts strongly in contact with water, proven by the high swelling pressure and low slake durability. Because of these observations, it has been used as a basis for estimating the properties of the weakness zone. However, the sample from the actual weakness zone is decomposed and will likely have lower strength. The slake durability of PK 36+555 makes it easy to imagine that the rock material can degrade to the quality of PK 34+385 after some time in contact with water

With respect to the stability assessment, the most important part of the laboratory analysis was to determine the rock mechanical properties. Initially it was believed that PK 34+405 could be representative of the rock mass around the weak zone. The correlation based on one UCS test and PLI tests was not seen as reliable. A factor of 23 is not in correspondence with the suggestions in Nilsen and Palmström (2000), nor with the results reported by Singh et al. (2012). Based on the deformation seen in the numerical modelling (for case 2) it is suggested that PK 34+405 has degraded from the point of excavation until the sampling/test time, or simply that it represents weaker layers within the rock units. The samples from PK 40+522 to PK40+758 are therefore considered more representative of initial rock strength. That is if the two different PLI tests represent the same type of rock. If rock samples were taken from the same locations in the tunnel repeatedly over years, the development/evolution of strength and deformation properties could be assessed and taken into account for deciding long term stability in similar projects. As both swelling clays and a higher degree of weathering are associated with decreased friction and cohesion (Palmström and Stille, 2010; Pasamehmetoglu et al., 1981; Panthi, 2006), a different approach may be to assess these parameters in stead of GSI and m_i . Panthi (2014) and Mao et al. (2015) both report of reduced friction and cohesion as contributing factors to the rock falls.

12.2 Stability Analysis and Deformations

Both the numerical analysis and the semi-analytical show that substantial deformation can be expected with the initial properties that was estimated for the weakness zone based on laboratory results from PK 36+555. The plot in figure 12.1 is based on the deformation in the right side of the tunnel seen when material properties was reduced in subsiding stages. A swelling pressure of 0.2 MPa increases the deformation by more than 3 times compared to the model without swelling pressure.

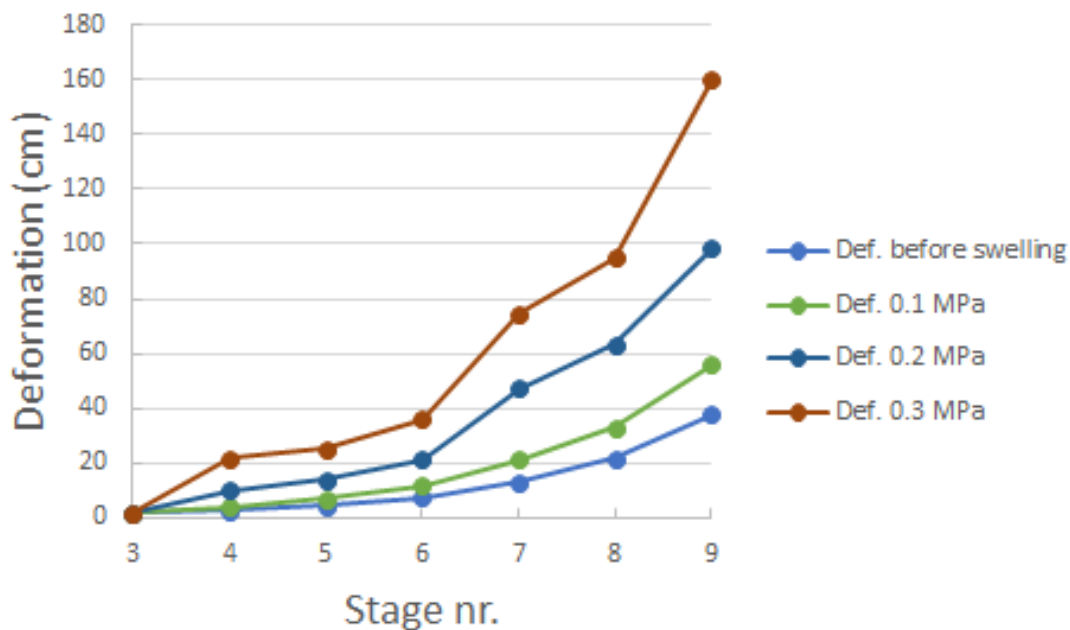


Figure 12.1: Deformation in different stages as strength of material is reduced and swelling pressure added.

The analysis shows that the type of deformation which is seen could be a results of low strength in the weakness zone and/or swelling. If a uniform load representing swelling pressure is added, large deformation is seen already when the properties in the weakness zone correspond with PK 34+405. Without swelling pressure this deformation is first seen when the strength of PK 34+405 is reduced by 60 %.

There seems to be no clear guidelines on how to define the material properties of weakness zones like this. Knowledge or guidelines for this might improve the understanding of the long term process. The displacement from the Hoek & Brown method is much larger than for the numerical approach as it considers the whole tunnel as a weak material. Results from both models are seen in table 12.1.

Table 12.1: Comparison between displacement in weakness zone for analytical and numerical approach (right side). Without support and swelling pressure

Approach	Displacement [cm]
Hoek & Brown	34.22
Numerical case 1	17.8
Numerical case 2	16.1
Numerical case 3	11.7

If the displacement is divided by two (to represent only one wall), it complies better with case 1, which also represent a rock mass with low strength. As both methods have several weaknesses, the reliability can be discussed. The numerical method consider both deformation properties and the horizontal stress and can take several materials into account. However, the result is uncertain because a large number of assumptions must be taken to model the situation.

12.3 Modelling Swelling

In the numerical model the application of higher pressures than 0.3 MPa was not possible. Compared to the results from the laboratory on remoulded samples, this pressure is reasonable as a worst estimate if the extremely high disk pressure of PK 36+555 is excluded. The swelling pressure in the laboratory is not necessarily representative of the pressure in the field. In the Chacabuquito and Los Quilos tunnels, expansion pressures from approximately 0.03 to 0.2 MPa was measured. In the support design process, a load factor of 1.4 was used in addition (Castro et al., 2010). If economically feasible, a conservative approach seems good as the cost of reconstruction is high. The use of both reduced strength and swelling pressure may be to complex in the model. The swelling pressure is not seen as decisive for the development of shotcrete cracks in the numerical modelling. In the modelling of the rock fall at Hanekleiva the greatest amount of yielding were seen related to strength reduction rather than swelling (Mao et al., 2015). The effect of water in the tunnel or ground water is not taken into account directly. Nevertheless is the effect indirectly considered since the swelling process is initiated by water. As the swelling process is complex and may be related to factors such as diffusability of the rock mass a more detailed approach is recommended. A possibly approach suggested by (Carter et al., 2010) is shortly described in chapter 4.

12.4 Rock Support

From the support analysis the following observations are made:

- The initial support in the tunnel was not adequate, as the support had to be rehabilitated after approximately two years.

- With the given Q-values, it is proposed to use 6-9 cm of shotcrete and systematic rock bolting c/c 1.6 m. This is in accordance with the used support
- Based on the support pressure estimations after Hoek (2007a), a 30 cm layer of shotcrete would be able to reduce strain from 34.22 % to 0.12 % if the support is installed in a circular tunnel and no bending moments are induced.

The Q-system is mainly based on cases from hard and fractured rock mass, and there are few cases where the Q-value is less than 1 (NGI, 2015), as is the case for the worst rock mass quality in the Portillo tunnel. This may be one of the reasons why the initial support is not sufficient. SRF in the area is set to 1, a value used for favourable stress conditions. According to the guidelines in the Q-system (NGI, 2015), SRF should be increased to a value between 2.5-10 when crossing weakness zones that can lead to fall-out/loosening of rock mass. In the case of moderately swelling rock mass, the SRF factor should be increased to 5-10. If a SRF of 2.5 had been applied to the chainages in table 10.1 at the time of excavation, the Q-value would be reduced to 1.2, 0.4 and 0.3 respectively. The excavation would then be in the border area between support class 4 and 5. If the conservative approach is chosen, a shotcrete layer of 9-12 cm is recommended. In the numerical model large displacement and yielded liner element is seen with both 8 and 12 cm shotcrete. The improved solution consisted of an additional 20 cm shotcrete. In the support chart for the Q-system, this correspond to category 7 and also includes the use of reinforced ribs of sprayed concrete. As the problems in the section has developed over time, this empirical method does not provide good enough support solutions for the long term stability. The results from mapping is however important for the quality of the analysis and assessment of input parameters.

The support suggested after Hoek (2007a) is based on an idealized situation and the capacity of the support will actually be lower. As it is not the whole cross section that is affected by the zone the calculated deformation may be to pessimistic. The numerical method fails to demonstrate the effect of the additional support, and a deeper assessment will be required to determine if it is adequate. As figure 4.3 show, the swelling pressure is reduced when a certain expansion of the clay is allowed. Support which allows for some of the deformation to happen is recommended in weakness zones, to reduce the pressure on the support. Due to the strike of the zone this type of support would have to be installed over a long section. Effective support solutions should be defined at the point of excavation or before the tunnel is put into operation. More research is necessary to define both economical and efficient long term support. As strength reduction and/or disintegration/degradation of the material behind the shotcrete can happen during the lifetime of the tunnel, also the load of this material must be taken into account when deciding support as Castro et al. (2010) describes was done for the Los Quilos tunnel. Also Carter et al. (2010), states the need for rock support/lining that can withstand the development of swelling and rock deterioration in a long time perspective.

Chapter 13

Conclusions and Further Work

13.1 Conclusions

The long-term stability of water tunnels is of great importance for hydropower projects. Uncertain stability conditions increase the need for inspections, and the risk of expensive rehabilitation. Rock mass with swelling and slaking ability gives especially complicated conditions. Much of the theory is related to weakness zones, and the solutions that exist for small zones are less applicable when larger areas are affected by swelling. The case histories show that problems with rock falls have occurred both in water and road tunnels due to reduced strength and friction. Both 2D and 3D approaches have been used to model weakness zones. Laboratory examinations can contribute to a better understanding of the rock mass and are necessary as input for numerical analysis and stability assessment. Samples from the Portillo tunnel branch have been examined by a variety of tests to assess their mineralogical and rock mechanical properties as well as swelling potential. The main observations of the laboratory results can be listed as follows:

- Normal light microscope and XRD do not provide enough information about the mineralogy. This is a task for an experienced mineralogist.
- Ethylene-glycol treatment is essential to identify smectite in the samples that have been studied.
- A variation in point load strength from low to medium is seen. Sample geometry might have influenced the result.
- The relation found between PLI and UCS for PK 34+405, does not correspond with the recommended correlation factor.
- Visually PK 34+405 and PK 37+060 appear weaker after water saturation for 22 days.
- Only a minor difference was seen between slake durability of PK 34+405 before and after the sample was stored in water for 22 days.

The result has been used to estimate input properties for a stability assessment. Because of some uncertainty in the laboratory result, a variety of input parameters regarding

strength of the rock mass have been modelled. The stability assessment has mainly focused on deformations, and not on stress or structurally related stability problems. The main results from the stability assessment and numerical analysis are summarized below.

- The approach by Hoek's method gives larger deformation than the numerical approach when material properties estimated from PK 36+555 are used. Hoek's method is considered less reliable as it only takes one material into account.
- The deformation in the weakness zone depends on the surrounding rock mass.
- The material properties of the weakness zone have a large impact on the deformations in the tunnel.
- The support proposed by the Q-method is not adequate, and for rock mass with this low Q-value, additional considerations regarding the rock mass quality should be taken.
- The effect of the additional support was not possible to assess with RS^2 in a reliable way. It has not been possible to determine a safety factor with the methods that have been used.
- From the numerical modelling the swelling pressure is not seen as decisive for the development of shotcrete cracks, and thus a further deterioration of the rock mass can lead to more problems.
- It is considered important to continue with regular inspections since further decrease of rock mass quality can affect the support.

It is found that the applied methods have several weaknesses, and the readers must be aware of this. The laboratory results and estimation of input parameters have uncertainties, which also reduce the quality of the analysis. The use of experience, more tests, and research on support systems that can withstand long term deformation in a cost/time effective way are necessary.

13.2 Further Work

For future understanding and efficiency in assessing stability in this type of rock mass, the following recommendations are given for further work:

- Since the thin sections are affected by alteration, and identification of clays with normal light microscope is difficult, a SEM-analysis and further assessment of mineralogy are recommended. This can increase knowledge about mineral chemistry of the clays and give information about the matrix composition.
- It is highly recommended to expand the laboratory investigations and include a sufficient number of samples to assess the rock mass strength. The most appropriate way to assess the development of the rock mass properties will be to collect samples throughout the "lifespan" of the tunnel.

- The complexity of the situation requires in-depth assessment to determine the most efficient, appropriate and reliable way to analyse the problem. A 3D analysis with for example FLAC or UDEC is therefore recommended.
- A study of efficient support methods for this type of rock mass which also take the long term behavior into account. Quick installation and less follow-ups will reduce the costs of the projects.

Bibliography

- Bell, F. (2007). *Engineering Geology*. 2nd ed. Great Britain: Butterworth-Heinemann.
- Bell, F. and Haskins, D. (1997). A geotechnical overview of Katse Dam and Transfer Tunnel, Lesotho, with a note on basalt durability. *Engineering geology*, 46(2):175–198.
- Brattli, B. and Broch, E. (1995). Stability problems in water tunnels caused by expandable minerals. Swelling pressure measurements and mineralogical analysis. *Engineering Geology*, 39(3):151–169.
- Brekke, T. and Howard, T. (1973). *Functional Classification of Gouge Material from Seams and Faults in Relation to Stability Problems in Underground Openings*. California University, Berkeley. Institute of transportation and traffic engineering. Defense Technical Information Center.
- Broch, E. (2013). Underground hydropower projects - lessons learned in home country and from projects worldwide. In *Norwegian Hydropower Tunneling 2 - Publication No. 22*. Norwegian Tunneling Society. pp. 11-19.
- Cai, M., Kaiser, P., Tasaka, Y., and Minami, M. (2007). Determination of residual strength parameters of jointed rock masses using the GSI system. *International Journal of Rock Mechanics and Mining Sciences*, 44(2):247–265.
- Carter, T., Castro, S., Carvalho, J., Hattersley, D., Wood, K., Barone, F., Yuen, D., and Giraldo, C. (2010). Tunnelling Issues of Chilean Tertiary Volcaniclastic Rocks. In *In: Proc. MIR 2010. XIII Ciclo di conferenze di Meccanica ed Ingegneria delle Rocce*. Torino, pp. 215-236.
- Castro, S., Van Sint Jan, M., Gonzalez, R., Lois, P., and Velasco, L. (2010). Dealing With Expansive Rocks In the Los Quilos And Chacabuquito Water Tunnels - Andes Mountains of Central Chile. In *10th ISRM congress – Technology Roadmap for Rock Mechanics*. South African Institute of Mining and Metallurgy, pp. 185-194.
- Dahl, F. (2003). DRI, BWI, CLI standards. *NTNU*.
- Deer, W. A., Howie, R. A., and Zussman, J. (1992). *An Introduction to the Rock-forming Minerals*. 2nd ed. England: Pearson.

- Dhakal, G., Yoneda, T., Kato, M., and Kaneko, K. (2002). Slake durability and mineralogical properties of some pyroclastic and sedimentary rocks. *Engineering Geology*, 65(1):31–45.
- Dinçer, I., Acar, A., Çobanoğlu, I., and Uras, Y. (2004). Correlation between Schmidt hardness, uniaxial compressive strength and Young’s modulus for andesites, basalts and tuffs. *Bulletin of Engineering Geology and the Environment*, 63(2):141–148.
- Dywidag Systems International (2017). *Mechanical Anchors and Rebar Rock Bolts - Dywidag Threadbar*. Available at:https://www.dywidag-systems.com/uploads/media/DSI-ALWAG-Systems_Mechanical-Anchors-and-Rebar-Rock-Bolts_en.pdf.
- Fajnor, V. and Jesenák, K. (1996). Differential thermal analysis of montmorillonite. *Journal of Thermal Analysis and Calorimetry*, 46(2):489–493.
- FCFM (2013). *Rock mechanical tests. Hidroeléctrica La Confluencia*. (Report N0.843.252-C.). Facultad de ciencias físicas y matemáticas universidad de Chile. Unpublished. Provided by Statkraft.
- Flåten, M. (2015). *Stress Induced Stability Assessment of the Underground Caverns for Moglicë Hydropower Project, Albania*. Master Thesis. Norwegian University of Science and Technology, Department of Geology and Mineral Resources Engineering. Trondheim.
- Fossen, H. and Gabrielsen, R. (2005). Spenningsstilstander i litosfæren. In Fossen, H. and Gabrielsen, R., editors, *Strukturgeologi*. Bergen: Fagbokforlaget, pp. 94-103.
- Franklin, J. and Chandra, R. (1972). The slake-durability test. *International Journal of Rock Mechanics and Mining Sciences & Geomechanics Abstracts*, 9(3):325–328.
- Golder Associates (2006). *La Confluencia Hydroelectrical project, Tunnel TC1, TC2 and TC4 Portillo Azufre, geological map and profile*. Appendix 2 in Geological and Geotechnical report: water adduction tunnels for the Confluencia hydroelectrical project.
- Golder Associates (2016). *Geological and Geotechnical report: Water Adduction Tunnels for the Confluencia Hydroelectrical Project*. Golder Associates. Unpublished. Provided by Statkraft.
- Goodman, R. E. (1993). *Engineering geology: Rock in engineering construction*. John Wiley & Sons.
- Google Earth 6.1.0 (2015). *La Confluencia and surroundings, 54°28′56.13″S, 70°15′77″W, elevation 1976 m*. Available at: <https://www.google.com/earth/index.html>.

- Heidbach, O., Rajabi, M., Reiter, K., and Ziegler, M. (2016). *World Stress Map 2016*. GFZ Data Services. Available at: <http://doi.org/10.5880/WSM.2016.002>.
- HLC (2010). *La Confluencia, Tinguiririca and Portillo tunnel, Support drawings*. Hidroeléctrica La Confluencia S.A. Unpublished. Provided by Statkraft.
- HLC (2011). *As-built plane and profile maps of La Confluencia Hydropower Project*. Hidroeléctrica La Confluencia S.A. Unpublished. Provided by Statkraft.
- Hoek, E. (2007a). *Tunnels in weak rock*. Available at: https://www.rocscience.com/documents/hoek/corner/13_Tunnels_in_weak_rock.pdf.
- Hoek, E. (2007b). *When is a rock engineering design acceptable*. Available at: https://www.rocscience.com/documents/hoek/corner/03_When_is_a_rock_engineering_design_acceptable.pdf.
- Hoek, E. (2012). *Blast Damage Factor D*. Available at: <https://www.rocscience.com/documents/pdfs/rocnews/winter2012/Blast-Damage-Factor-D-Hoek.pdf>.
- Hoek, E. and Brown, E. T. (1997). Practical estimates of rock mass strength. *International Journal of Rock Mechanics and Mining Sciences*, 34(8):1165–1186.
- Hoek, E., Carranza-Torres, C., and Corkum, B. (2002). Hoek-Brown failure criterion - 2002 Edition. *Proceedings of the fifth North American rock mechanics symposium, Toronto, Canada* pp. 267-273. Available at: <https://rocscience.com/documents/hoek/references/H2002.pdf>.
- Hoek, E. and Diederichs, M. S. (2006). Empirical estimation of rock mass modulus. *International journal of rock mechanics and mining sciences*, 43(2):203–215.
- Hoek, E. and Marinos, P. (2000). Predicting tunnel squeezing problems in weak heterogeneous rock masses. *Tunnels and tunnelling international*, 32(11):45–51.
- Hoek, E. and Marinos, P. (2007). A brief history of the development of the Hoek-Brown failure criterion. *Brazilian Journal of Soil and Rocks*. Available at: <https://www.rocscience.com/documents/pdfs/uploads/8332.pdf>.
- HTC (2010). *La Confluencia Hydropower project. Control de Geología, excavación y sostenimiento*. Hochtief-Tesca Construction. Mapping schemes. Unpublished. Provided by Statkraft.
- IHA (2016). *2016 Hydropower Status Report*. International Hydropower Association. Available at: <https://www.hydropower.org/2016-hydropower-status-report>.
- ISRM (1978). Suggested methods for the quantitative description of discontinuities in rock masses. *International Journal of Rock Mechanics and Mining Sciences & Geomechanics Abstracts*, 15:319–368.

- ISRM (1979a). Suggested methods for determining the uniaxial compressive strength and deformability of rock materials. *International Journal of Rock Mechanics and Mining Sciences*, 16:138–140.
- ISRM (1979b). Suggested methods for determining water content, porosity, density, absorption and related properties and swelling and slake durability index properties. *International Journal of Rock Mechanics and Mining Sciences*, 16:141–156.
- ISRM (1985). Suggested method for determining point load strength. *International Journal of Rock Mechanics and Mining Sciences*, 22:51–60.
- Itasca (2017). *FLAC3DTM version 6.0. Explicit Continuum Modeling of Non-linear Material Behavior in 3D*. Available at: <http://www.itascacg.com/software/flac3d>.
- Kovári, K. (2009). Design methods with yielding support in squeezing and swelling rocks. *World Tunnel Congress. Budapest, Hungary*.
- Li, C. C. (2017). Rock Mechanics. *Lecture notes-TGB4210 Rock Mechanics*.
- Mao, D. (2012). *Analysis of Rock Support Performance for Tunnelling in Weakness Zones Containing Swelling Clay*. Doctoral thesis. Norwegian University of Science and Technology, Faculty of Engineering Science and Technology, NTNU, Trondheim.
- Mao, D., Nilsen, B., and Dahl, F. (2011a). Laboratory testing of swelling gouge from weakness zone-principle and recent update. In *45th U.S. Rock Mechanics / Geomechanics Symposium, 26-29 June*. San Francisco, California.
- Mao, D., Nilsen, B., Feng, S., Zhao, H., and Lu, M. (2015). A Case Study of Tunnel Instability in Weakness Zone Containing Swelling Clay. In *Shotcrete for Underground Support XII, October 11-13, 2015*. Singapore.
- Mao, D., Nilsen, B., and Lu, M. (2011b). Analysis of loading effects on reinforced shotcrete ribs caused by weakness zone containing swelling clay. *Tunnelling and Underground Space Technology*, 26(3):472–480.
- Marinos, P. and Hoek, E. (2000). GSI: a geologically friendly tool for rock mass strength estimation. In *ISRM International Symposium*. International Society for Rock Mechanics.
- Martin, C., Kaiser, P., and McCreath, D. (1999). Hoek-brown parameters for predicting the depth of brittle failure around tunnels. *Canadian Geotechnical Journal*, 36(1):136–151.
- McKinnon, S. D. and Garrido de la Barra, I. (2003). Stress field analysis at the El Teniente Mine: evidence for N–S compression in the modern Andes. *Journal of Structural Geology*, 25(12):2125–2139.

- MeSy (2008). *Hydraulic tests/hydrofrac tests for stress determination in borehole HTS-02. La Confluencia Hydroelectric Project site, Chile* (Report 14.08). Unpublished. Provided by Statkraft.
- Myrvang, A. (2001). *Bergmekanikk*. Institutt for geologi og bergteknikk. Norges teknisk naturvitenskapelige universitet, Trondheim.
- Nesse, W. D. (2000). *Introduction to mineralogy*. New York: Oxford University Press.
- NGI (2015). *Using the Q-system*. Norwegian Geotechnical Institute.
- Nilsen, B. and Broch, E. (2012). *Ingeniørgeologi-Berg grunnkurskompendium*. Lecture notes. Norges teknisk naturvitenskapelige universitet, Trondheim.
- Nilsen, B. and Palmström, A. (2000). *Engineering Geology and Rock Engineering - Handbook No 2*. Norwegian Group of Rock Mechanics.
- Pacific Hydro (2011). *La Confluencia hydro plant*. Available at:
<http://pacifichydro.com/english/projects/chile/la-confluencia-hydro-plant/?language=en>.
- Palmstrom, A. and Broch, E. (2006). Use and misuse of rock mass classification systems with particular reference to the q-system. *Tunnelling and underground space technology*, 21(6):575–593.
- Palmström, A. and Stille, H. (2010). *Rock engineering*. London: Thomas Telford limited.
- Palmstrøm, A. (1995). *RMi - a rock mass characterization system for rock engineering purposes*. Doctoral thesis, University of Oslo.
- Pankhurst, R. and Hervé, F. (2007). Introduction and overview. In Moreno, T. and Gibbons, W., editors, *The geology of Chile*, pages 1–4. Geological Society of London, London.
- Panthi, K. (2012). Evaluation of rock bursting phenomena in a tunnel in the Himalayas. *Bulletin of Engineering Geology and the Environment*, 71(4):761–769.
- Panthi, K. (2014). Analysis on the dynamics of burst debris flood at the inclined pressure-shaft of svandalsflona hydropower project, norway. *Rock mechanics and rock engineering*, 47(3):923–932.
- Panthi, K. K. (2006). *Analysis of engineering geological uncertainties related to tunnelling in Himalayan rock mass conditions*. Doctoral thesis. Norwegian University of Science and Technology, Faculty of Engineering Science and Technology, NTNU, Trondheim.

- Panthi, K. K. (2017). *Plastic Deformation in Tunnels*. Lecture notes-TGB4212 Rock Mechanics, Advanced Course.
- Pasamehmetoglu, A., Karpuz, C., Irfan, T., et al. (1981). The weathering characteristics of Ankara andesites from the rock mechanics point of view. In *ISRM International Symposium*. International Society for Rock Mechanics.
- Paul, A., Odekerken, C., Meyer, P., Chávez, E., Galera, J., and Müller, M. (2012). The Construction of the Hydroelectrical Project La Confluencia (Andes, Chile). *ITA World Tunnel Congress 2012. Bangkok*.
- Rocscience (2017a). *RS2*. Available at:
<https://www.rocscience.com/rocscience/products/rs2>.
- Rocscience (2017b). *RS2 Webhelp*. Available at:
<https://rocscience.com/help/phase2/webhelp9/phase2.htm>.
- Selmer, R. and Palmstrom, A. (1989). Tunnel collapses in swelling clay zones. *Tunnels & Tunnelling*, 49-58.
- Singh, T., Kainthola, A., and Venkatesh, A. (2012). Correlation between point load index and uniaxial compressive strength for different rock types. *Rock mechanics and rock engineering*, 45(2):259–264.
- Sørlokk, T., Rokoengen, K., and Nilsen, B. (2007). *Geologiske laboratorieundersøkelser*. Trondheim: NTNU.
- Statkraft (2011). *La Confluencia*. Available at:
<http://www.statkraft.com/energy-sources/Power-plants/Chile/La-Confluencia/>.
- TE (2010). *La Confluencia Hydropower project. Registro geotecnico*. Tinguiririca Energia, La Confluencia Hydropower project. Mapping schemes. Unpublished. Provided by Statkraft.
- Trinh, Q. and Broch, E. (2008). Tunnel Cave-in – Convergence Confinement and 2D Analyses. *Australian Centre for Geomechanics, Perth*, 70:106–109.
- Trinh, Q., Broch, E., and Lu, M. (2009). 2D Versus 3D Modelling for Tunnelling at a Weakness Zone. *ISRM Regional Symposium-EUROCK 2009, Croatia*.
- Tu, X., Jian, B., Wang, S., Bian, H., Wang, J., and Li, S. (2005). Swelling behavior induced by alteration in granite and its implications on underground excavation. *Tunnelling and underground space technology*, 20(4):378–389.
- Whittaker, B. N. and Frith, R. C. (1990). *Tunnelling: design, stability and construction*. London: Institution of Mining and Metallurgy.

- Windsor, C., Caviares, P., Villaescusa, E., and Pereira, J. (2006a). Reconciliation of strain, structure and stress in the El Teniente Mine Region, Chile. In *Proceedings of International Symposium on In Situ Rock Stress, Trondheim, Norway*.
- Windsor, C., Cavieres, P., Villaescusa, E., and Pereira, J. (2006b). Rock stress tensor measurements at El Teniente Mine, Chile. In Lu, M., Li, C., Kjørholt, H., and H., D., editors, *In-situ Rock Stress*. Taylor & Francis Group, London, pp.67-72.

Appendix A

Swelling pressure charts

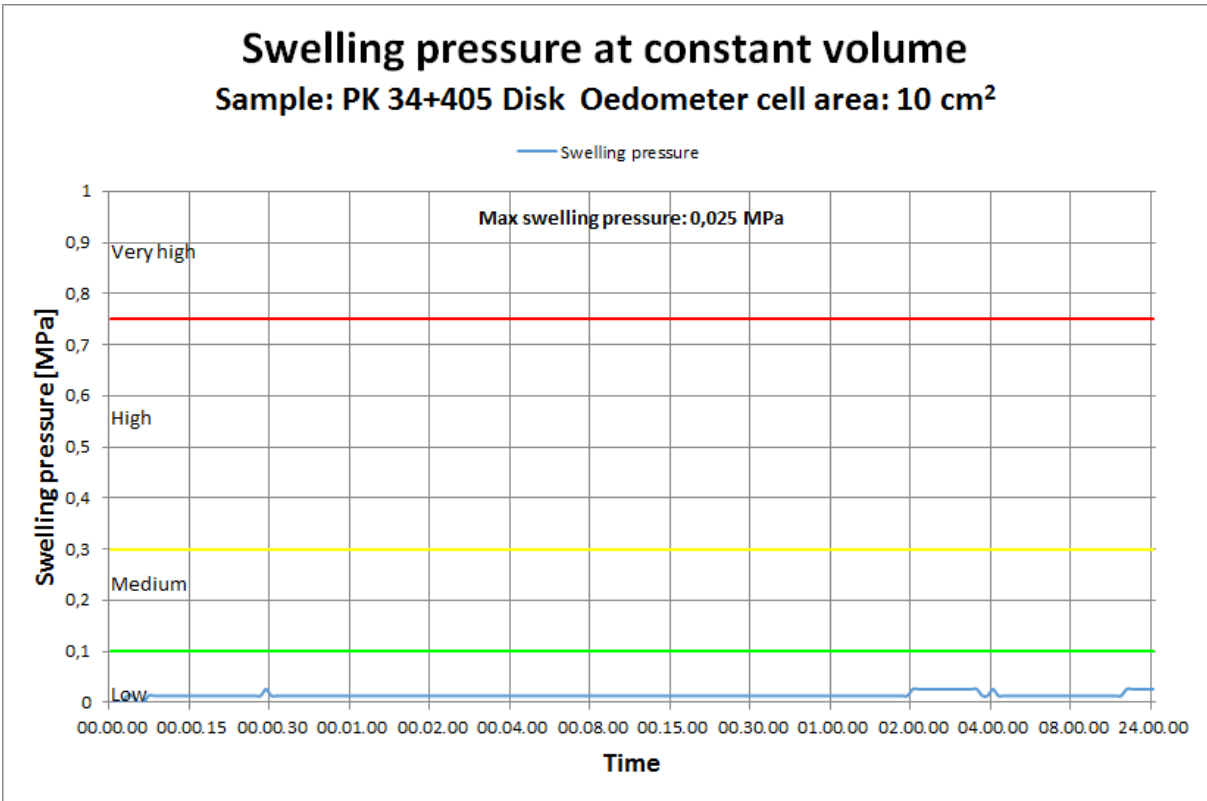


Figure A.1: Swelling pressure chart PK 34+405 Disk

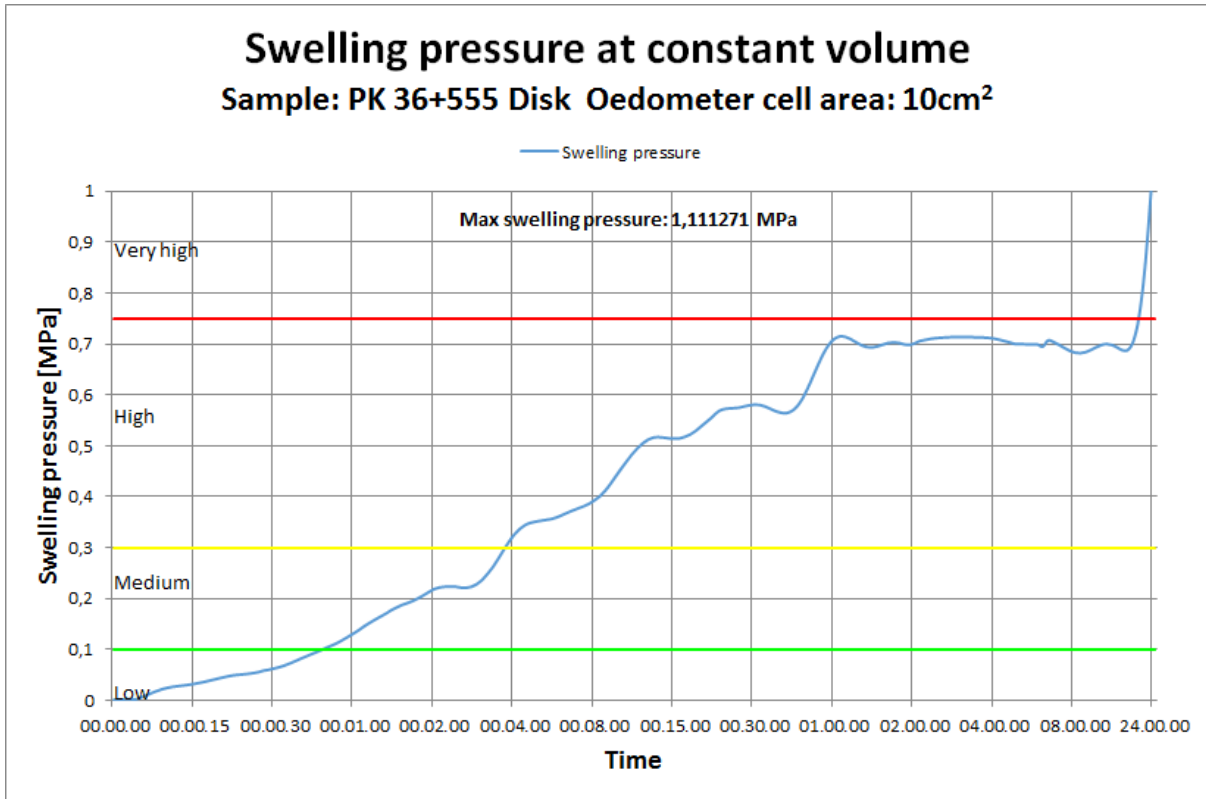


Figure A.2: Swelling pressure chart PK 36+555 Disk

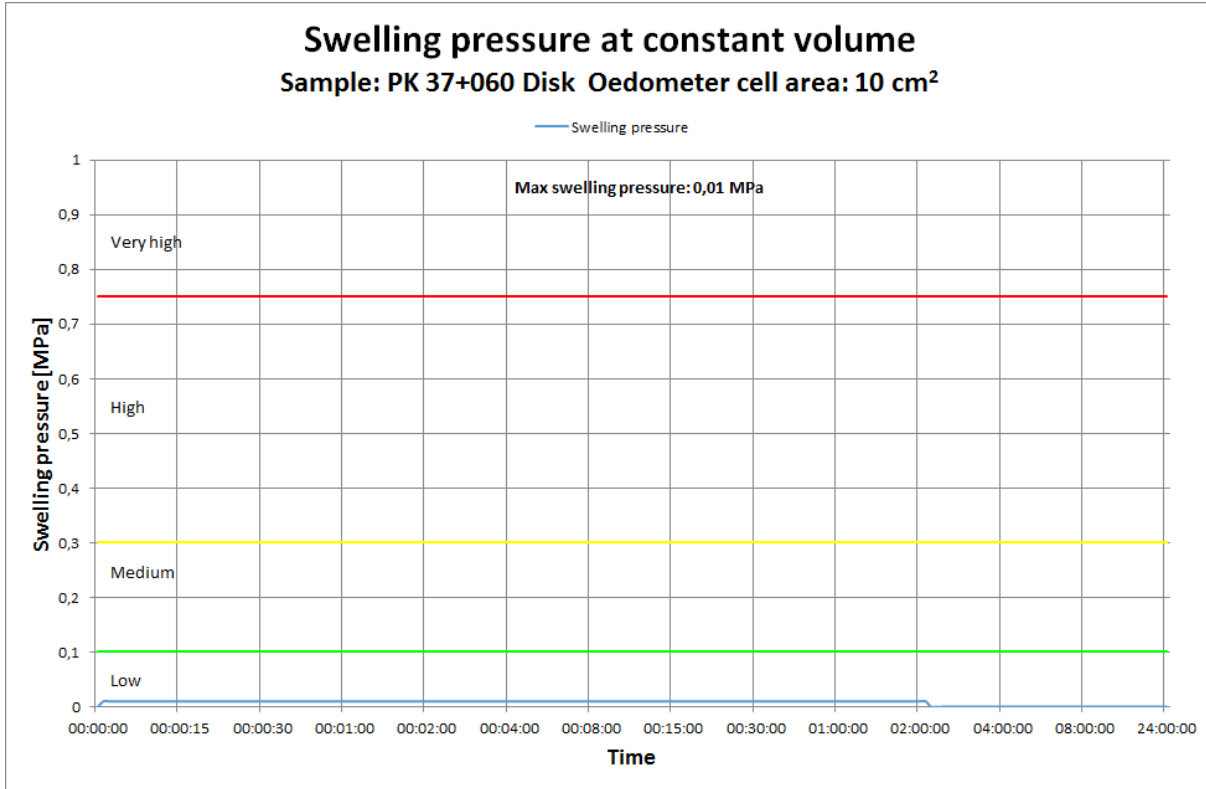


Figure A.3: Swelling pressure chart PK 37+060 Disk

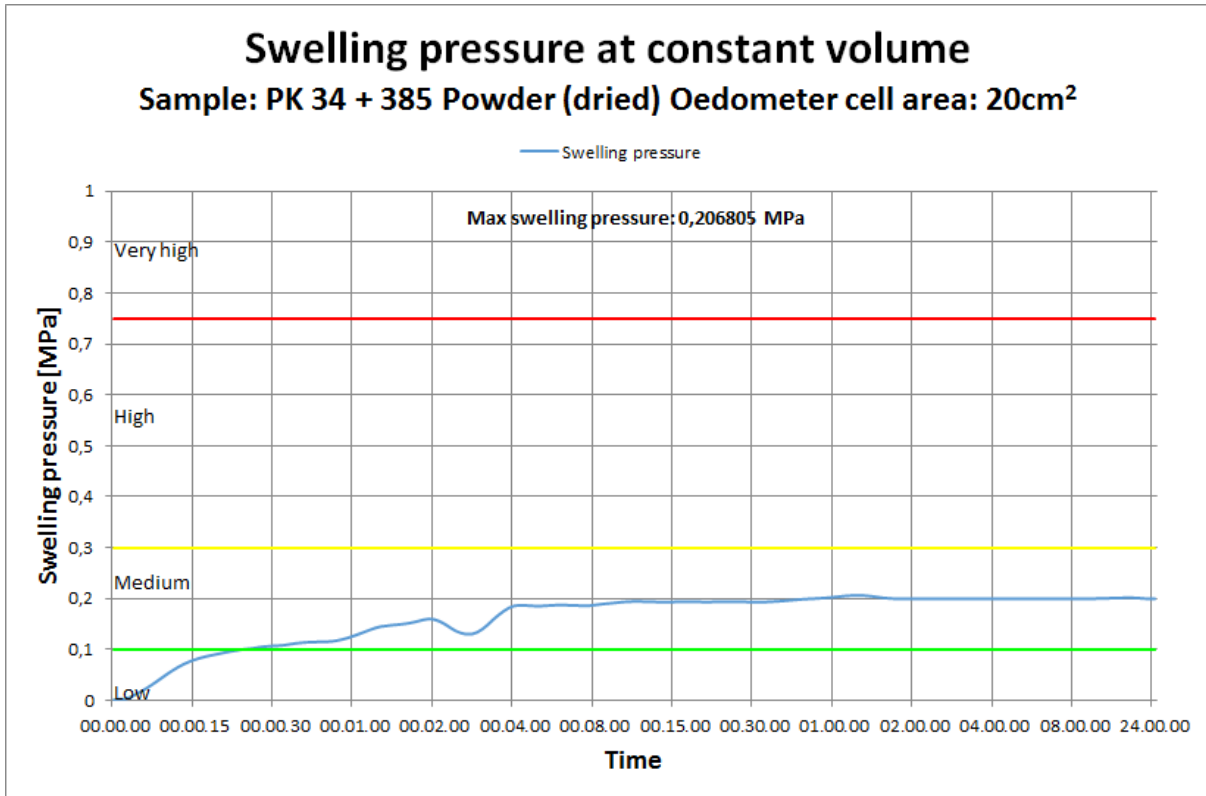


Figure A.4: Swelling pressure chart 34+385 powder (dried)

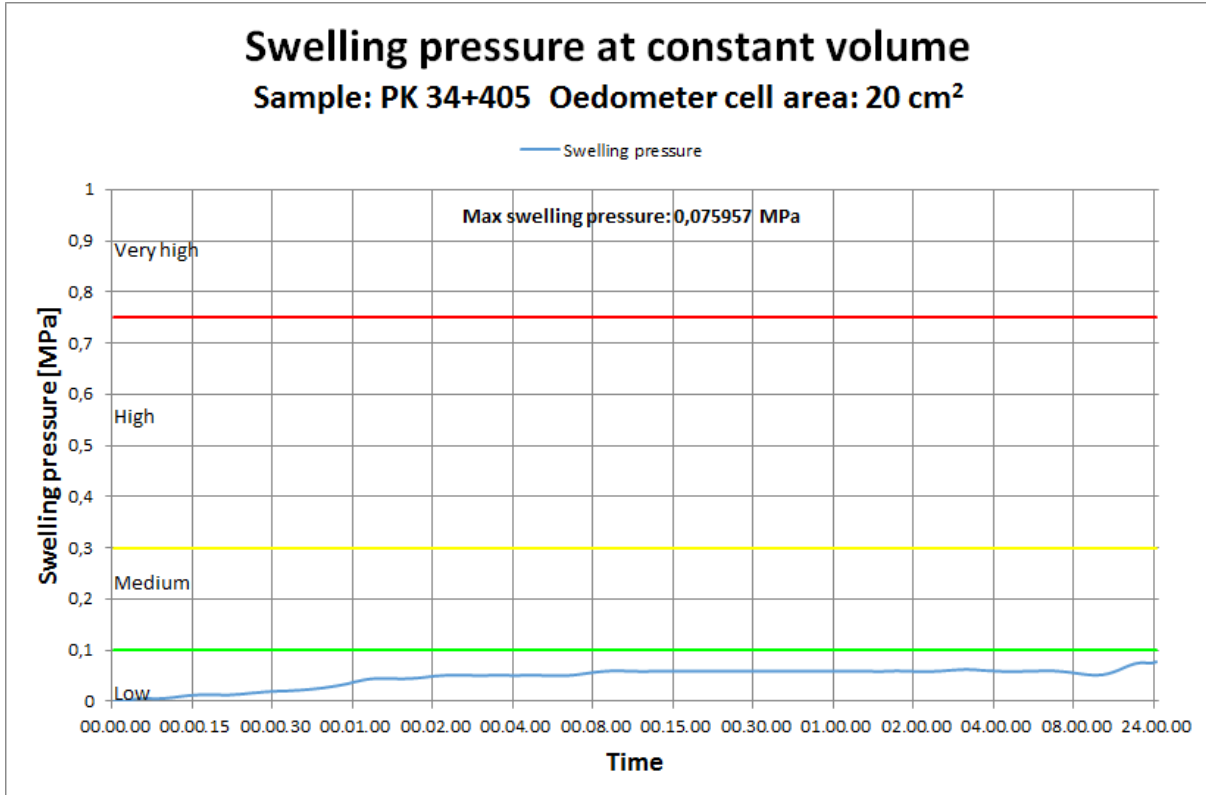


Figure A.5: Swelling pressure chart PK 34+405 powder

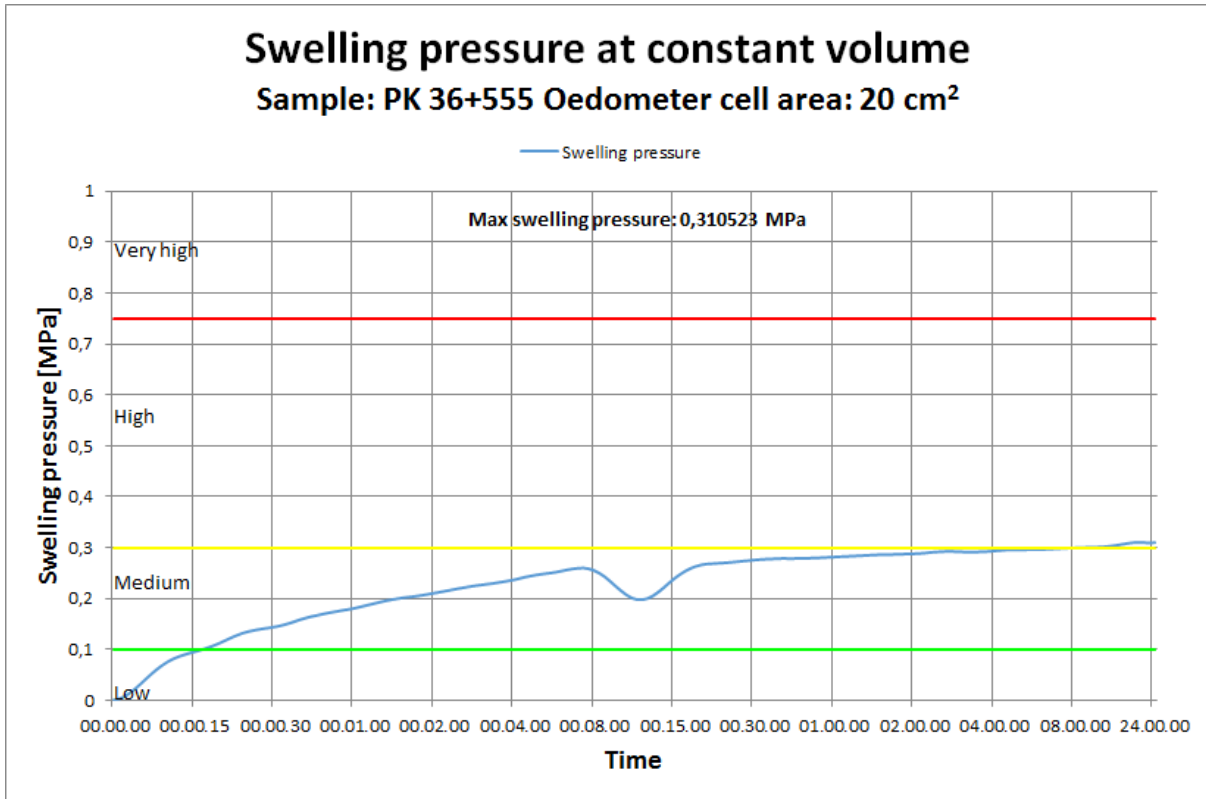


Figure A.6: Swelling pressure chart PK 36+555 powder

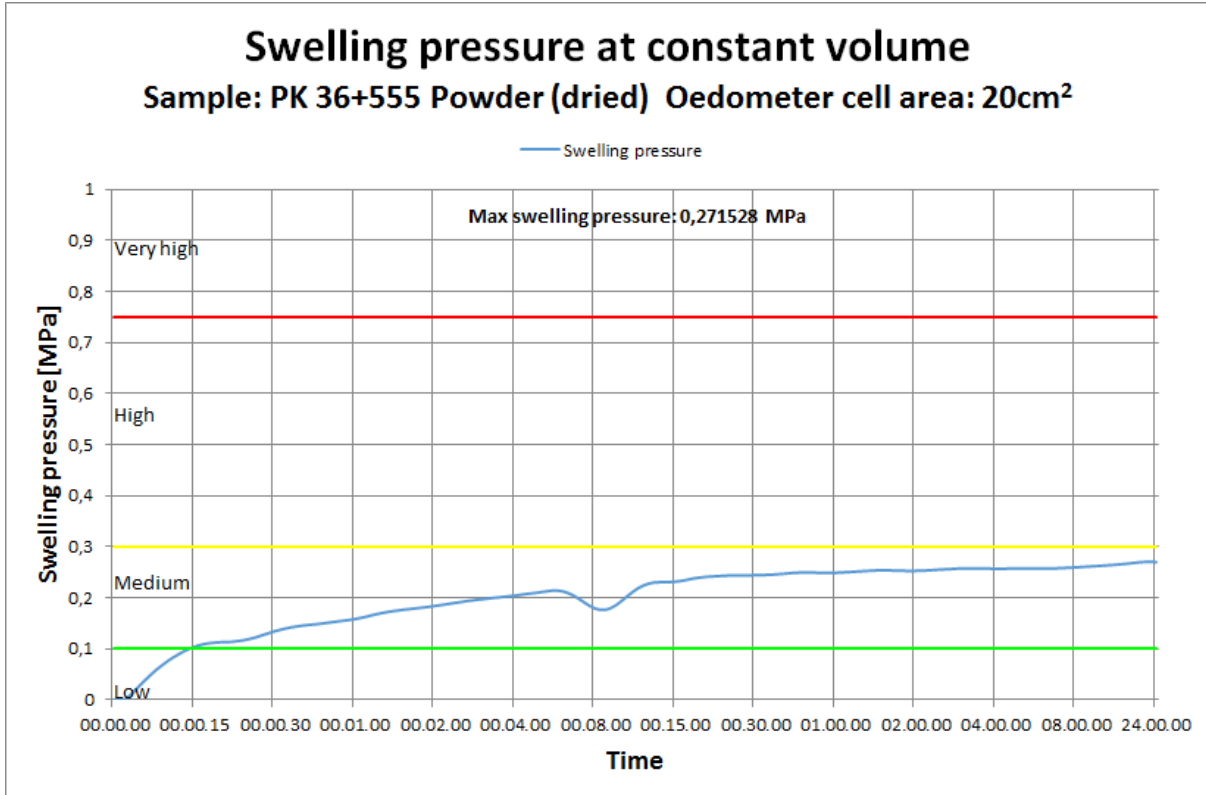


Figure A.7: Swelling pressure chart PK 36+555 powder (dried)

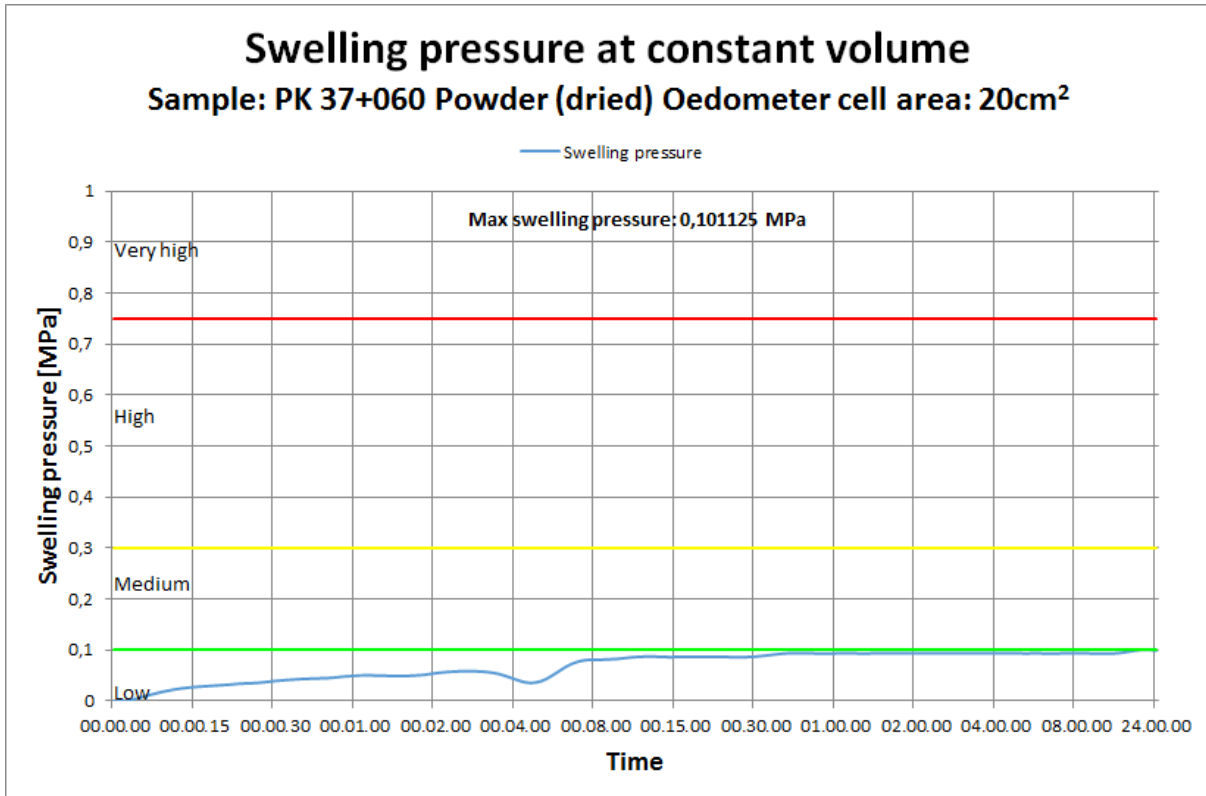


Figure A.8: Swelling pressure chart PK 37+060

Appendix B

X-ray Diffractograms

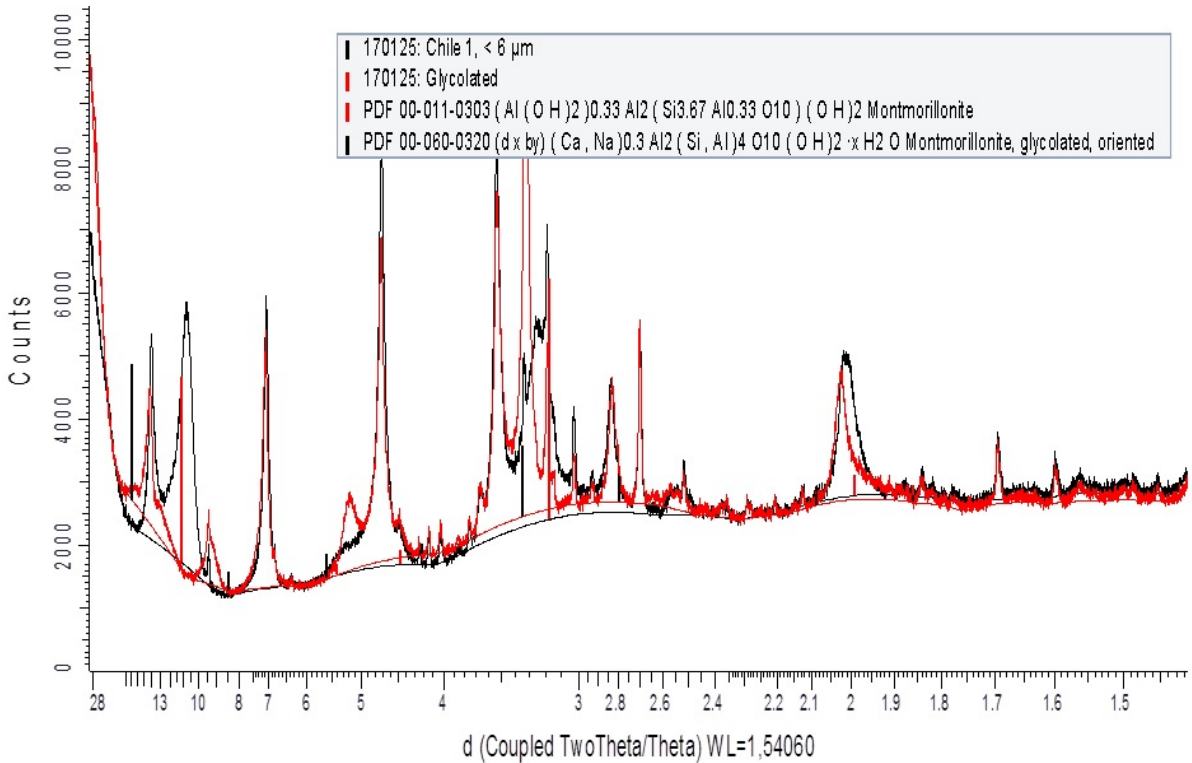


Figure B.1: X-ray diffractogram Glycol-treated PK34+385

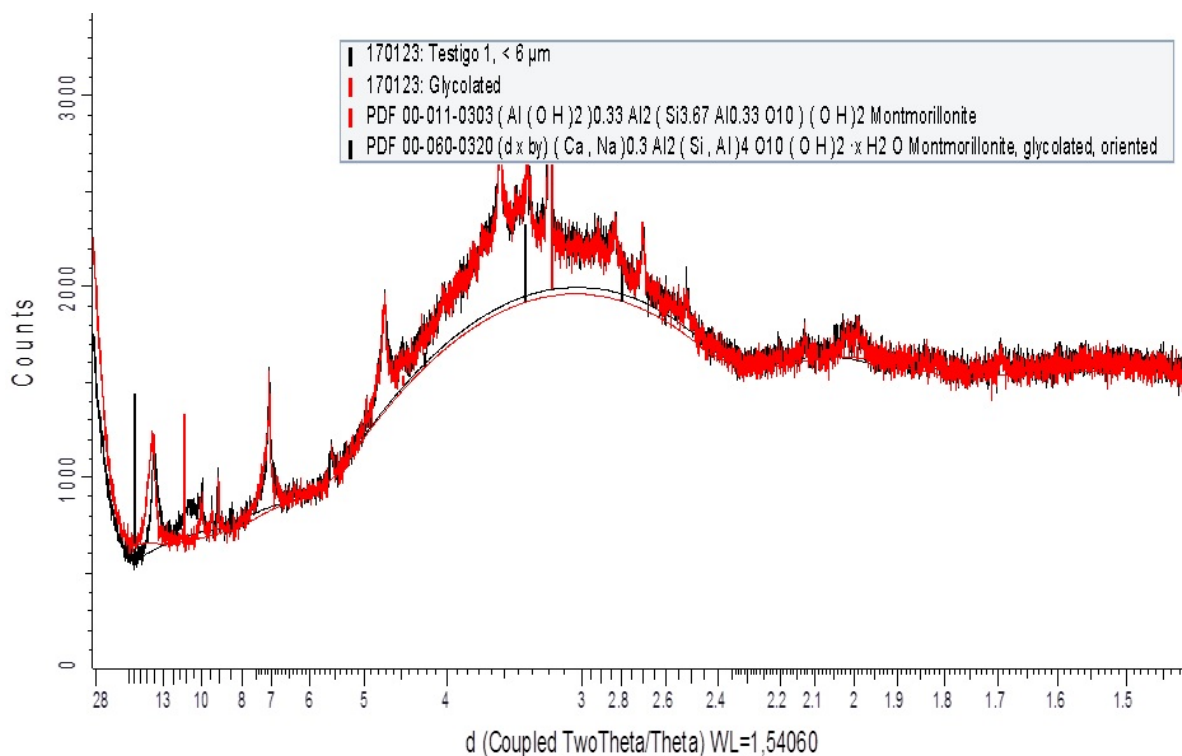


Figure B.2: X-ray diffractogram Glycol-treated PK 34+405

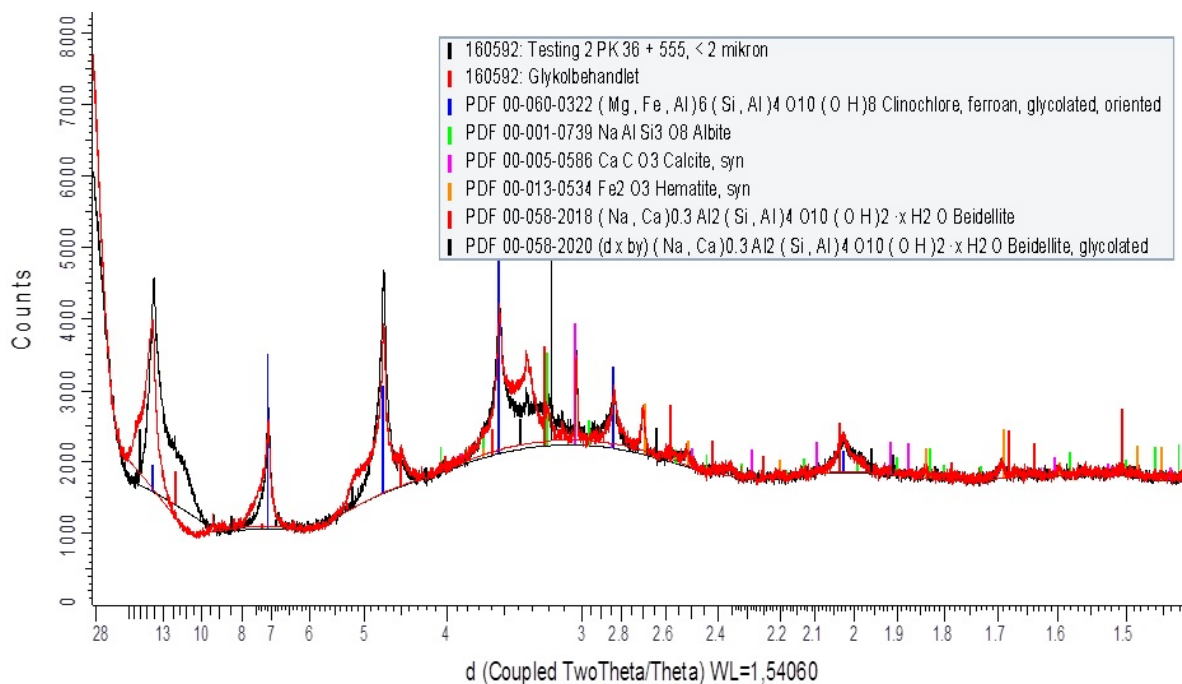


Figure B.3: X-ray diffractogram Glycol-treated PK 36+555

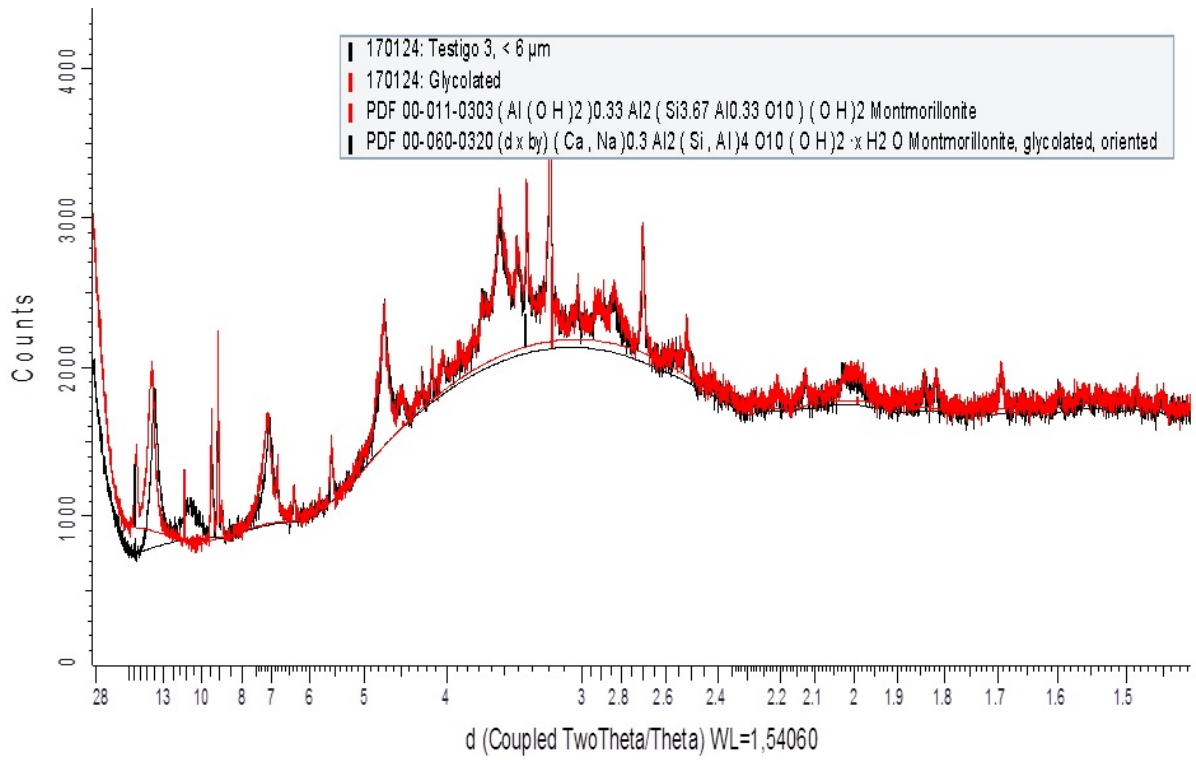


Figure B.4: X-ray diffractogram Glycol-treated PK 37+060

Appendix C

DTA Charts

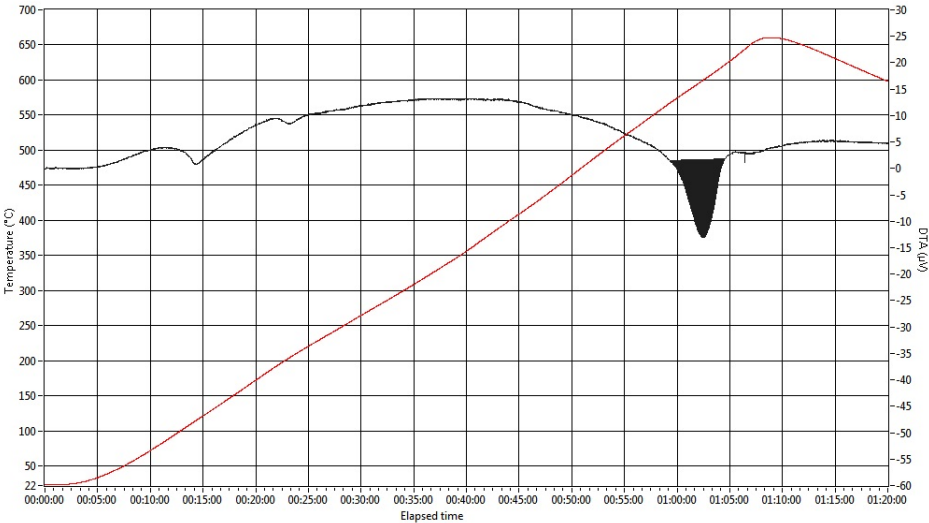


Figure C.1: DTA curve PK 34+385: DTA curve PK 36+555: The red line represents the temperature and the blue line the sample. The red line is peaking downwards as the heating stops at 600 °C. The shaded area shows the peak due to presence of kaolin.

APPENDIX C. DTA CHARTS

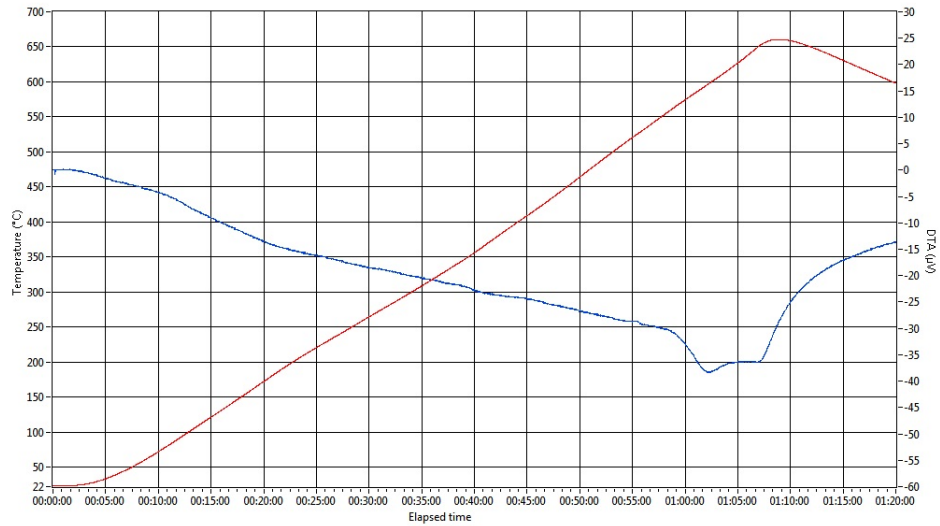


Figure C.2: DTA curve PK 34+405: The red line represents the temperature and the gray line the sample. The red line is peaking downwards as the heating stops at 600 °C. The shaded area shows the peak due to presence of kaolin.

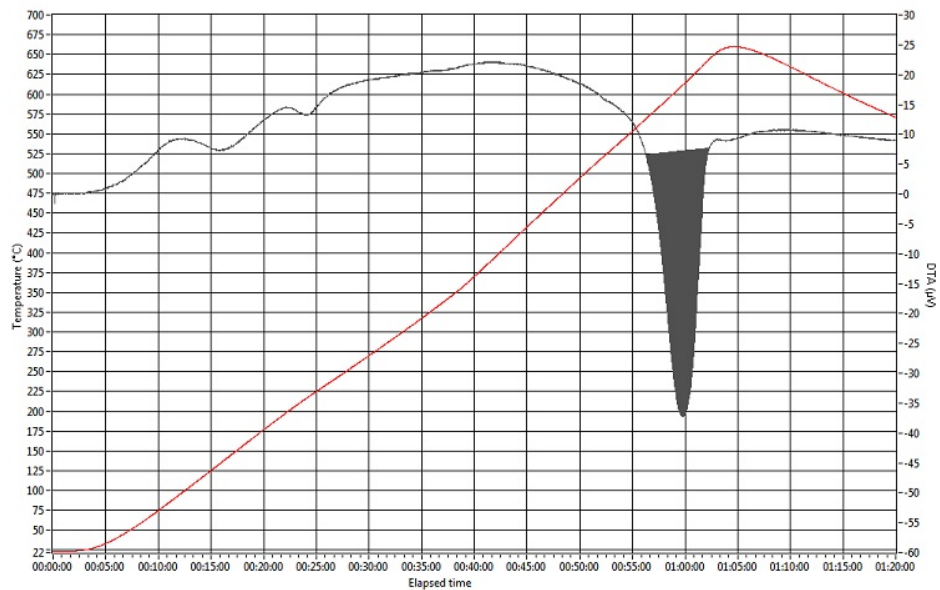


Figure C.3: DTA curve PK 36+555: The red line represents the temperature and the gray line the sample. The red line is peaking downwards as the heating stops at 600 °C. The shaded area shows the peak due to presence of kaolin.

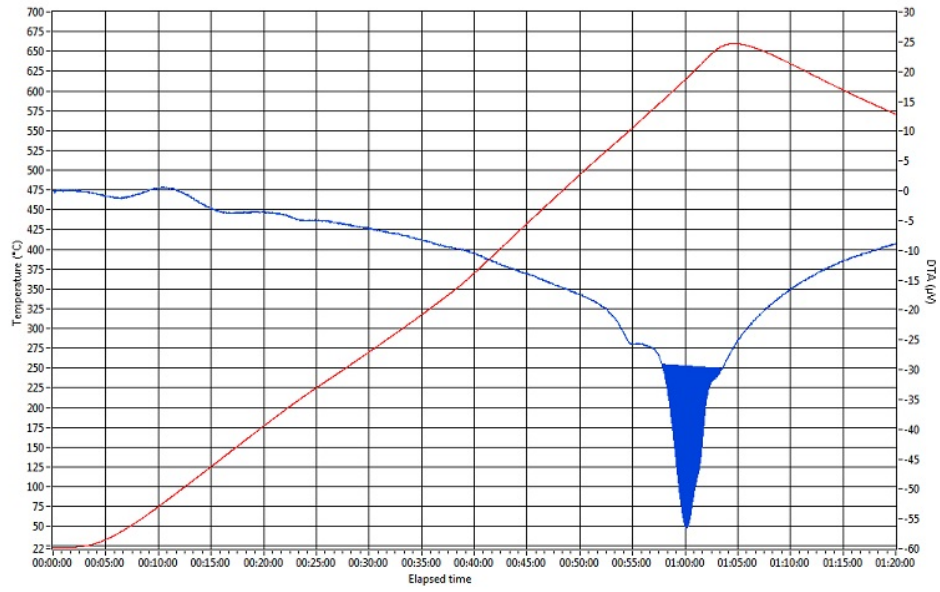


Figure C.4: DTA curve PK 37+060: The red line represents the temperature and the black line the sample. The red line is peaking downwards as the heating stops at 600 °C. The shaded area shows the peak due to presence of kaolin.

Appendix D

Point Load Test Results

Results from point load strength test conducted in the thesis. The two highest and lowest $I_{s(50)}$ was cancelled to obtain the mean value. D is the height between specimen-platen contact points. W_1 and W_2 is the width of the sample measured at top and bottom. D_e is the equivalent core diameter and F the conversion factor used to obtain the size corrected Point Load Strength.

Table D.1: Full dataset from Point Load Index test for PK 34+405.

<i>No.</i>	<i>D</i> [mm]	<i>W</i> ₁ [mm]	<i>W</i> ₂ [mm]	<i>W</i> _{avg} [mm]	<i>De</i> ² [mm ²]	<i>P</i> [N]	<i>I</i> _s [MPa]	<i>F</i>	<i>I</i> _{s(50)} [MPa]
1	27.4	21	46	33.5	1168.7	1370	1.2	0.8	1.0
2	26.7	18.7	46.2	32.5	1103.2	1760	1.6	0.8	1.3
3	29.2	24.3	50.8	37.6	1161.8	3000	2.6	0.8	2.2
4	29.1	23.1	46.3	34.7	1285.7	2380	1.9	0.9	1.6
5	27.9	22	49.3	35.7	1266.4	1870	1.5	0.9	1.3
6	30.7	18.9	46.7	32.8	1282.1	3840	3.0	0.9	2.6
7	30.1	18.7	47.6	33.2	1270.5	2810	2.2	0.9	1.9
8	30.5	18.6	45.8	32.2	1250.4	2690	2.2	0.9	1.8
9	29.4	19	43.5	31.3	1169.8	3030	2.6	0.8	2.2
10	27.5	19.1	48.7	33.9	1187.0	2840	2.4	0.8	2.0
11	28.7	19.1	46	32.6	1189.4	4550	3.8	0.8	3.2
12	28.5	19	44.2	31.6	1146.7	2360	2.1	0.8	1.7
13	28.1	25.1	53.3	39.2	1402.5	2480	1.8	0.9	1.6
14	27.7	19.6	47.8	33.7	1188.6	3120	2.6	0.8	2.2
15	27.6	19.7	47.7	33.7	1184.3	1920	1.6	0.8	1.4
16	26.4	16.8	38.6	27.7	931.1	1680	1.8	0.8	1.4
17	30	24.2	53.8	39.0	1489.7	1070	0.7	0.9	0.6
18	27.4	38	52.1	45.1	1571.6	2070	1.3	0.9	1.2

Table D.3: Full dataset from Point Load Index test for PK 37+060

No.	D [mm]	W_1 [mm]	W_2 [mm]	W_{avg} [mm]	De^2 [mm ²]	P [N]	I_s [MPa]	F	$I_{s(50)}$ [MPa]
1	25.1	31.7	58.5	45.1	1441.3	5000	3.5	0.9	3.1
2	27.1	25.1	46	35.55	1226.6	4230	3.4	0.9	2.9
3	27.5	20	45.5	32.75	1146.7	4420	3.9	0.8	3.2
4	33	17.5	51.4	34.45	1447.5	4420	3.1	0.9	2.7
5	24.6	22	42.9	32.45	1016.4	5660	5.6	0.8	4.5
6	25.1	22.2	41.3	31.75	1014.7	2610	2.6	0.8	2.1
7	26	22.1	46.1	34.1	1128.9	4020	3.6	0.8	3.0
8	28.6	18.4	47.9	33.15	1207.1	3400	2.8	0.8	2.4
9	30.9	19	51.8	35.4	1392.7	1850	1.3	0.9	1.2
10	30.2	19	46	32.5	1249.7	1820	1.5	0.9	1.2
11	27.8	20.5	49.2	34.85	1233.6	2460	2.0	0.9	1.7

Table D.2: Full dataset from Point Load Index test for PK 36+555

No.	D [mm]	W_1 [mm]	W_2 [mm]	W_{avg} [mm]	De^2 [mm ²]	P [N]	I_s [MPa]	F	$I_{s(50)}$ [MPa]
1	39	36.7	65.7	51.2	2542.4	1690.0	0.7	1.0	0.7
2	32.6	42.9	42.9	42.9	1780.7	1330.0	0.7	0.9	0.7
3	23.2	31.5	40.8	36.15	1067.8	1540.0	1.4	0.8	1.2
4	27.3	34.4	40	37.2	1293.1	1580.0	1.2	0.9	1.1
5	23.9	43.3	44.9	44.1	1342.0	1910.0	1.4	0.9	1.2
6	26.9	34	51.5	42.75	1464.2	1130.0	0.8	0.9	0.7
7	26.4	43.4	43.8	43.6	1465.5	2070.0	1.4	0.9	1.3
8	31.5	45.1	52	48.55	1947.2	1300.0	0.7	0.9	0.6
9	26.5	46.2	45.8	46	1552.1	1460.0	0.9	0.9	0.8
10	27.7	45.5	50	47.75	1684.1	1790.0	1.1	0.9	1.0
11	31.7	33	44.7	38.85	1568.1	1290.0	0.8	0.9	0.7
12	21.5	26	50.9	38.45	1052.6	920.0	0.9	0.8	0.7
13	27.6	37.8	41.6	39.7	1395.1	2850.0	2.0	0.9	1.8

Appendix E

Classifications

Classification of free swelling and swelling pressure:

Table E.1: Table modified after Mao et al. (2011a). Classification of free swelling and swelling pressure

Classification	Free swelling [%]	Swelling pressure [MPa]
Low	< 100	< 0.1
Moderate	100 - 140	0.1 - 0.3
High	140 - 200	0.3-0.75
Very high	> 200	> 0.75

Classification of slake-durability::

Table E.2: Classification of slake durability index after (ISRM, 1979b).

Classification	I_d2 [%]
Very high	98-100
High	95-98
Medium high	85-95
Medium	60-85
Low	30-60
Very low	<30

Classification of uniaxial compressive strength:

Table E.3: Classification of uniaxial compressive strength of rocks (ISRM, 1978) in (Nilsen and Palmström, 2000).

Type	Classification	UCS - σ_c [MPa]
Soil	-	<0.25
	Extremely low strength	0.25-1
	Very low strength	1-5
	Low strength	5-25
Rock	Medium strength	25-50
	High strength	50-100
	Very high strength	100-250
	Extremely high strength	>250

Classification of the Point Load Strength:

Table E.4: Classification of the Point Load Strength. Table modified after Biewnaski (1984) and Deere (1966) in (Nilsen and Palmström, 2000).

Classification	I_s [MPa] (Biewnaski, 1984)	I_s [MPa] (Deere, 1966)
Very low strength	< 1	< 1.25
Low strength	1 - 2	1.25 - 2.5
Medium strength	2 - 4	2.5 - 5
High strength	4 - 8	5 - 10
Very high strength	> 8	> 10

Appendix F

PLI and slake durability, PK 40+522 to PK 40+758

Results from PLI and slake durability, PK 40+522 to PK 40+758. Saturated samples have been saturated for 48 hours. Classification according to appendix E.

Table F.1: PLI results, irregular samples, from PK 40+522 to PK 40+758.

Chainage	Water content	$I_{s(50)}$	Classification 1
PK 40+522	0.37	5.24	High
PK 40+522	0.37	6.69	High
PK 40+522	Saturated	6.07	High
PK 40+522	Saturated	8	High
PK 40+540	0.27	5.37	High
PK 40+540	0.27	7.05	High
PK 40+540	Saturated	4.15	High
PK 40+540	Saturated	5.87	High
PK 40+610	0.61	6.19	High
PK 40+610	0.61	6.84	High
PK 40+610	Saturated	6.16	High
PK 40+610	Saturated	7.57	High
PK 40+640	1.91	1.68	Low
PK 40+640	1.91	3.88	Medium
PK 40+640	Saturated	0.66	Very low
PK 40+640	Saturated	2.26	Medium
PK 40+758	1.71	5.09	High
PK 40+758	1.71	5.96	High
PK 40+758	Saturated	6.15	High
PK 40+758	Saturated	6.58	High

Table F.2: Slake durability results from PK 40+522 to PK 40+758. Test conducted by FCFM (2013) according to ASTM standard D464408.

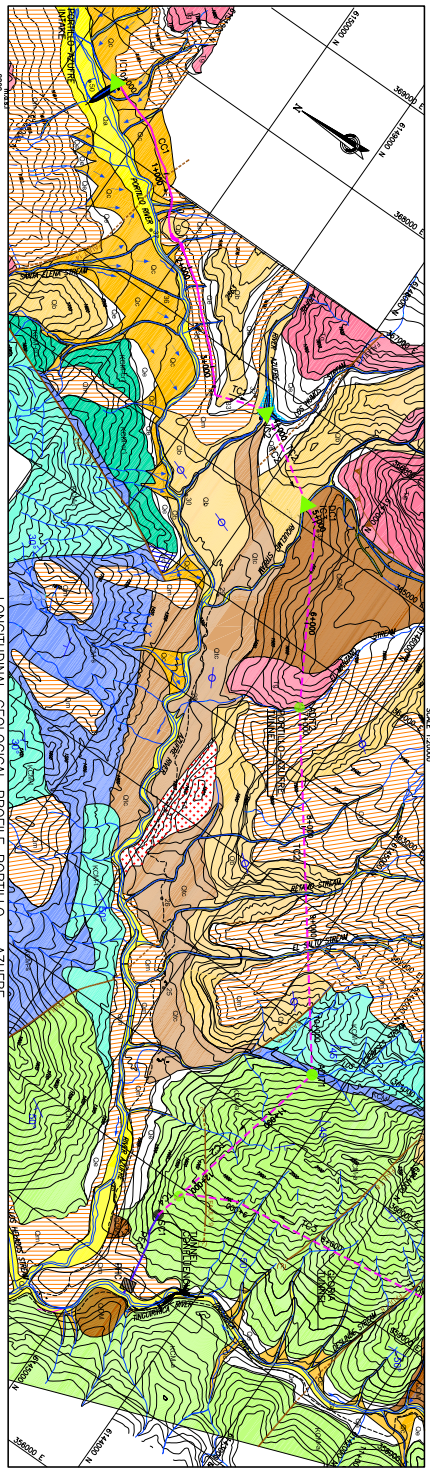
Chainage	Water content [%]	Slake-dur	Classification 1
PK 40+540	0.27	98.53	Extremely high
PK 40+540	Saturated	99.47	Extremely high
PK 40+640	1.91	96.05	High
PK 40+640	Saturated	92.65	Medium high

Appendix G

Geological map

Geological maps, plan and profile by Golder Associates (2006).

PORTILLO - AZUFRE GEOLOGICAL PLAN



LONGITUDINAL GEOLOGICAL PROFILE PORTILLO - AZUFRE

SCALE 1:20,000

STATION	ELEVATION (m)	DESCRIPTION
0+00	1500.00	GROUND WATER
0+50	1460.00	DRY
1+000	1460.00	DRY
1+400	1470.00	DRY
1+500	1471.11	DRY
1+515.28	1475.28	DRY
1+516.00	1450.00	DRY
1+520	1450.00	DRY
2+000	1515.52	DRY
2+500	1666.43	DRY
3+000	1574.72	DRY
3+500	1867.71	DRY
4+000	2000.00	DRY
4+500	1807.17	DRY
5+000	1600.00	DRY
5+500	1563.17	DRY
6+000	1400.00	DRY
6+500	1372.02	DRY
7+000	1250.00	DRY
7+549.97	1249.97	DRY

UNCONRODATE DEPOSITS

LEGEND

QUATERNARY

- Q3a: Alluvial deposits
- Q3a: Colluvial deposits
- Q3b: Deposited cones
- Q3b: Depositional deposits
- Q4: TINGARRICA VOLCANICS-SOROLO LLOCAUS UNIT
- Q4: IGNEOUS
- Q4: Metasedimentary
- Q4: Metavolcanic

TRICONGLOMERATE DEPOSITS

- T1: Conglomerate with light to medium siltstone, claystone, shaly siltstone
- T2: Conglomerate with medium to coarse siltstone, claystone, shaly siltstone
- T3: Conglomerate with coarse siltstone, claystone, shaly siltstone
- T4: Conglomerate with fine to medium siltstone, claystone, shaly siltstone

INTRUSIVE UNITS

- I1: Andesite
- I2: Andesite
- I3: Andesite
- I4: Andesite
- I5: Andesite
- I6: Andesite
- I7: Andesite

CRETACEOUS

- C1: Andesite
- C2: Andesite
- C3: Andesite
- C4: Andesite
- C5: Andesite
- C6: Andesite
- C7: Andesite
- C8: Andesite
- C9: Andesite
- C10: Andesite

COYA MACHAL FORMATION

- CM1: Andesite
- CM2: Andesite
- CM3: Andesite
- CM4: Andesite
- CM5: Andesite
- CM6: Andesite
- CM7: Andesite
- CM8: Andesite
- CM9: Andesite
- CM10: Andesite
- CM11: Andesite
- CM12: Andesite
- CM13: Andesite
- CM14: Andesite
- CM15: Andesite
- CM16: Andesite
- CM17: Andesite
- CM18: Andesite
- CM19: Andesite
- CM20: Andesite

SMITHOLOGY

GEOTECHNICAL ROCK CLASSES

ROCK CLASS	GROUP	UNIT	STRATIGRAPHIC POSITION	DESCRIPTION	COMPOSITION	TEXTURE	STRUCTURE	ALTERATION	WEATHERING						
K1	M1	C1	T1	T1	Siltstone	Medium	Vertical	Andesite	Slight						
										2.0	100	100	100	100	100
										2.5	100	100	100	100	100
										3.0	100	100	100	100	100
										3.5	100	100	100	100	100
										4.0	100	100	100	100	100
										4.5	100	100	100	100	100
										5.0	100	100	100	100	100
										5.5	100	100	100	100	100
										6.0	100	100	100	100	100
K2	M2	C2	T2	T2	Siltstone	Medium	Vertical	Andesite	Slight						
										2.0	100	100	100	100	100
										2.5	100	100	100	100	100
										3.0	100	100	100	100	100
										3.5	100	100	100	100	100
										4.0	100	100	100	100	100
										4.5	100	100	100	100	100
										5.0	100	100	100	100	100
										5.5	100	100	100	100	100
										6.0	100	100	100	100	100

NOTES

1. This geological map is based on "Geological Reconnaissance and Geology of the Portillo - Azufre Area" prepared by the author and published by the author.

2. The author is not responsible for any errors or omissions in this map.

SCALE 1:20,000

PROJECT LA CONCRETION TUNNEL TCA AZUFRE

DRAWING PORTILLO - AZUFRE

DATE 2024

DRAWN BY [Name]

CHECKED BY [Name]

SCALE 1:20,000

PROJECT LA CONCRETION TUNNEL TCA AZUFRE

DRAWING PORTILLO - AZUFRE

DATE 2024

DRAWN BY [Name]

CHECKED BY [Name]

Appendix H

Strike and dip measurements

Table H.1: Strike and dip measurements, outcrop around PK 34+750.

Strike	Dip
N115°E	77°S
N85°E	88°S
N110°E	74°S
N98°E	76°S
N90°E	76°S
N168°E	78°SE
N10°E	50°E

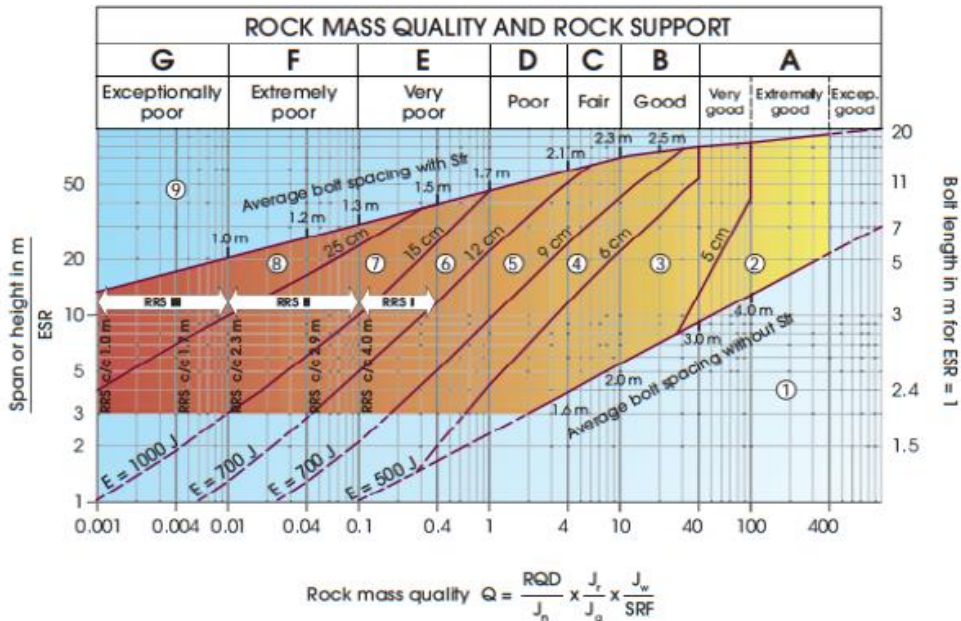
Appendix I

The Q-system and modified q-system

Geotechnical Rock Classes Index "Q"	Name	Geotechnical Categorization	Geotechnical Description	Rock Mass Stand Up Time
> 40	Class 1 = Very good	Very good to Extremely good	Massive rock to weakly fractured (≤ 4 fractures per linear meter), sound and very strong. Closed fractures planes, showing almost no infilling materials.	Undefined
10 - 40	Class 2 = Good	Good	Weakly to moderately fractured (2-7 fractures per linear meter) rock; it is a weakly disturbed, sound and strong rock. Planes of fractures in some cases show thin coats of infilling materials.	Many years.
4 - 10	Class 3 = Regular	Regular	Moderate to strongly fractured rock (5-15 fractures per linear meter), weakly to moderately decomposed or weathered, relatively strong and dense. All the fracture planes have sometimes argillaceous mineral and iron oxide as infilling materials.	Several months, up to 1 year
1 - 4	Class 4 = Poor	Poor	Strong to intensely fractured rock ($\geq 14-17$ fractures per linear meter), moderate to strongly decomposed or weathered, presenting the occurrence of fault zones, which include disintegrated rock. Most of the fractures planes show iron oxide and clays as infilling materials.	Several hours and up to 1 week
0,1 - 1	Class 5a = Very poor rock	Very poor rock	Strong to intensely decomposed or weathered rock, relatively soft and moderately dense, presenting a strong alteration to argillaceous minerals. Occurrence of important fault zones and/or disintegrated argillaceous rock, generally breakable by hand.	Several hours
0,1 - 0,01	Class 5b = Extremely Poor	Extremely Poor	Completely decomposed or weathered rock, soft and moderately dense, presenting a total alteration to argillaceous minerals. Occurrence of important fault zones and/or disintegrated argillaceous rock, breakable by hand.	Less than 1 hour

Figure I.1: Geotechnical Categorization by the Modified "Q" Index method by Grimstad and Barton (1993) in (Golder Associates, 2016).

The Q-system (NGI, 2015)



Support categories

- ① Unsupported or spot bolting
- ② Spot bolting, **SB**
- ③ Systematic bolting, fibre reinforced sprayed concrete, 5-6 cm, **B+Sfr**
- ④ Fibre reinforced sprayed concrete and bolting, 6-9 cm, **Sfr (E500)+B**
- ⑤ Fibre reinforced sprayed concrete and bolting, 9-12 cm, **Sfr (E700)+B**
- ⑥ Fibre reinforced sprayed concrete and bolting, 12-15 cm + reinforced ribs of sprayed concrete and bolting, **Sfr (E700)+RRS I+B**
- ⑦ Fibre reinforced sprayed concrete >15 cm + reinforced ribs of sprayed concrete and bolting, **Sfr (E1000)+RRS II+B**
- ⑧ Cast concrete lining, **CCA** or **Sfr (E1000)+RRS III+B**
- ⑨ Special evaluation

Bolts spacing is mainly based on Ø20 mm

E = Energy absorption in fibre reinforced sprayed concrete

ESR = Excavation Support Ratio

Areas with dashed lines have no empirical data

RRS - spacing related to Q-value

- I** **Si30/6 Ø16 - Ø20 (span 10m)**
D40/6+2 Ø16-20 (span 20m)
- II** **D45/6+2 Ø16-20 (span 10m)**
D55/6+4 Ø20 (span 20m)
- III** **D40/6+4 Ø16-20 (span 5m)**
D55/6+4 Ø20 (span 10 m)
D70/6+6 Ø20 (span 20 m)

Si30/6 = Single layer of 6 rebars, 30 cm thickness of sprayed concrete

D = Double layer of rebars

Ø16 = Rebar diameter is 16 mm

c/c = RSS spacing, centre - centre

Table 7 ESR - values

Type of Excavation	ESR
A Temporary mine openings etc.	ca. 3-5
B Vertical shafts, j) circular sections k) rectangular/square section * Dependent of purpose. May be lower than given values.	ca. 2.5 ca. 2.0
C Permanent mine openings, water tunnels for hydro power (exclude high pressure periods), water supply tunnels, pilot tunnels, drifts and headings for large openings.	1.6
D Minor road and railway tunnels, surge chambers, access tunnels, sewage tunnels, etc.	1.3
E Power houses, storage rooms, water treatment plants, major road and railway tunnels, civil defence chambers, ports, intersections, etc.	1.0
F Underground nuclear power stations, railway stations, sports and public facilities, factories, etc.	0.8
G Very important covers and tunnels with a long lifetime, > 100 years, or without access for maintenance.	0.5

For the types of excavation B, C and D, it is recommended to use ESR = 1.0 when Q ≤ 0.1. The reason for that is that the stability problems may be severe with such low Q-values, perhaps with risk for cover-in. ESR together with the span (or wall height) gives the Equivalent dimension in the following way:

$$\frac{\text{Span or height in m}}{\text{ESR}} = \text{Equivalent dimension}$$

Table 8 Conversion from actual Q-values to adjusted Q-values for design of wall support

In rock masses of good quality	Q > 10	The actual Q-value is multiplied by 5
For rock masses of intermediate quality	0.1 < Q < 10	The actual Q-value is multiplied by 2.5 (in cases of high stresses the actual Q-value is used)
For rock masses of poor quality	Q < 0.1	The actual Q-value is used

$$Q = \frac{RQD}{J_n} \times \frac{J_r}{J_a} \times \frac{J_w}{SRF}$$

1 RQD (Rock Quality Designation)		RQD
A	Very poor (> 27 joints per m ³)	0-25
B	Poor (20-27 joints per m ³)	25-50
C	Fair (13-19 joints per m ³)	50-75
D	Good (8-12 joints per m ³)	75-90
E	Excellent (0-7 joints per m ³)	90-100

Note: 1) Where RQD is reported or measured as ≤ 10 (including 0) the value 10 is used to evaluate the Q-value

2) RQD values of 5, i.e. 100, 95, 90, etc., are arbitrarily accurate

2 Joint set number		J _s
A	Massive, no or few joints	0.5-1.0
B	One joint set	2
C	One joint set plus random joints	3
D	Two joint sets	4
E	Two joint sets plus random joints	6
F	Three joint sets	9
G	Three joint sets plus random joints	12
H	Four or more joint sets, random heavily jointed "sugar-cube", etc	15
J	Crushed rock, earth like	20

Note: 1) For tunnel investigations, use 3 \leq J_s

2) For joints, use 2 \leq J_s

3 Joint Roughness Number		J _r
a) Rock-wall contact, and		
b) Rock-wall contact below 10 cm of shear movement		
A	Discontinuous joints	4
B	Rough or irregular, undulating	3
C	Smooth, undulating	2
D	Stepped, undulating	1.5
E	Rough, irregular, planar	1.2
F	Smooth, planar	1
G	Slackened, jointed	0.5

Note: 1) Description refers to small scale features and intermediate scale features, in that order

c) No rock-wall contact when sheared

H Zone containing clay mineral thick enough to prevent rock-wall contact when sheared

Note: 3) Add 1 if the mean spacing of the relevant joint set is greater than 3 m

(dependent on the size of the underground opening)

4) J_r = 0.5 can be used for planar slackened joints having the features provided the features are oriented in the estimated sliding direction

4 Joint Alteration Number		J _a
a) Rock-wall contact (no mineral fillings, only coatings)		
A	Highly altered, heavy mineralizing, replacement zone, i.e., quartz or epidote	U/2
B	Unaltered joint walls, surfaces staining only	25-35 ^a
C	Slightly altered joint walls, non-staining mineral coatings, sandy particles, clay-like disintegrated rock, etc.	25-30 ^a
D	Silty or sandy clay coatings, small clay floccion (non-staining)	20-25 ^a
E	Soltering or low friction clay mineral coatings, i.e., muscovite or mica. Also chromite, talc, gypsum, graphite, etc., and small quantities of swelling clays.	8-16 ^a

b) Rock-wall contact below 10 cm shear (thin mineral fillings)		
F	Sandy particles, clay-free disintegrated rock, etc.	25-30 ^a
G	Silt/clay over-consolidated, non-staining, clay mineral fillings (continuous, but < 2mm thickness)	16-24 ^a
H	Medium or low over-consolidation, softening, clay mineral fillings (continuous, but < 2mm thickness)	12-16 ^a
J	Swelling-clay fillings, i.e., montmorillonite (continuous, but < 2mm thickness). Value of J _a depends on percent of swelling clay-size particles.	6-12 ^a

c) No rock-wall contact when sheared (thick mineral fillings)		
K	Zones of bands of disintegrated or crushed rock. Strongly over-consolidated	16-24 ^a
L	Zones of bands of clay, disintegrated or crushed rock. Medium or low over-consolidation or softening fillings.	12-16 ^a
M	Zones of bands of clay, disintegrated or crushed rock. Swelling clay. J _a depends on percent of swelling clay-size particles.	6-12 ^a
N	Thick continuous zones or bands of clay. Strongly over-consolidated	16-24 ^a
O	Thick, continuous zones or bands of clay. Medium to low over-consolidation.	12-16 ^a
P	Thick, continuous zones or bands with clay. Swelling clay. J _a depends on percent of swelling clay-size particles.	6-12 ^a

Note: 1) Factors C to O are crude estimates. Increase J_a if the rock is drilled or grouting is carried out

2) Special problems caused by ice formation are not considered

6 Stress Reduction Factor		SRF
a) Weak zones intersecting the underground opening, which may cause loosening of rock mass		
A	Multiple occurrences of weak zones within a short section containing clay or organically altered, very loose surrounding rock (any depth), or bond sections with incompetent (weak) rock (any depth). For squeezing, see B, C and D.	10
B	Multiple shear zones within a short section in competent clay-free rock with loose surrounding rock (any depth)	7.5
C	Single weak zones with or without clay or chemical disintegrated rock (depth \leq 50m)	5
D	Loose, open joints, heavily jointed or "sugar-cube", etc. (any depth)	5
E	Single weak zones with or without clay or chemical disintegrated rock (depth $>$ 50m)	2.5

Note: 1) Reduce these values of SRF by 25-50% if the weak zones only influence but do not intersect the underground opening

b) Competent, mainly massive rock, stress problems				
F	Low stress, near surface, open joints	$\sigma_1/\sigma_3 < 200$	$\sigma_1/\sigma_3 < 10$	SRF 2.5
G	Medium stress, favourable stress condition	200-10	0.01-0.3	1
H	High stress, very tight structure, usually favourable to stability. May also be unfavourable to stability (dependent on the orientation of stresses compared to jointing/weakness planes)	10-5	0.3-0.4	0.5-2
J	Moderate spalling and/or slabbing after $>$ 1 hour in massive rock	5-3	0.5-0.65	5-30
K	Spalling of rock burst after a few minutes in massive rock	3-2	0.65-1	50-200
L	Heavy rock burst and immediate dynamic deformation in massive rock	$<$ 2	$>$ 1	200-400

Note: 1) For strongly anisotropic virgin stress field (if measured) when $\xi \leq \sigma_1/\sigma_3 \leq 10$, reduce σ_1/σ_3 to 0.75 σ_1/σ_3 . When $\sigma_1/\sigma_3 >$ 10, reduce σ_1/σ_3 to 0.5 σ_1/σ_3 , where ξ = unconfined compression strength, σ_1 and σ_3 are the major and minor principal stresses, and σ_2 = maximum tangential stress (determined from elastic theory)

2) When the depth of the crown below the surface has (from the spurt suggest SRF increase from 2.5 to 5 for such cases (see F))

c) Squeezing rock, plastic deformation in incompetent rock under the influence of high pressure				
M	Mild squeezing rock pressure	σ_1/σ_3 1.5	σ_1/σ_3 5-10	SRF 10-20
N	Heavy squeezing rock pressure	$>$ 5	$>$ 10	10-20

Note: 1) Determination of squeezing rock conditions must be done according to relevant literature (e.g. Singh et al., 1992 and Brown and Gerlach, 1995)

d) Swelling rock: chemical swelling activity depending on the presence of water				
O	Mild swelling rock pressure			SRF 5-10
P	Heavy swelling rock pressure			10-15

Note:






The values for J and J_a should be chosen based on the orientation and shear strength, τ (where $\tau = \sigma \tan(\phi + \lambda)$) of the joint or discontinuity that gives the most unfavourable stability for the rock mass, and along which failure most likely will occur.

Appendix J

Guidelines for the Disturbance factor

Guidelines for the Disturbance factor (Hoek, 2012).

Table 1: Guidelines for estimating disturbance factor D

Appearance of rock mass	Description of rock mass	Suggested value of D
	<p>Excellent quality controlled blasting or excavation by Tunnel Boring Machine results in minimal disturbance to the confined rock mass surrounding a tunnel.</p>	<p>$D = 0$</p>
	<p>Mechanical or hand excavation in poor quality rock masses (no blasting) results in minimal disturbance to the surrounding rock mass.</p> <p>Where squeezing problems result in significant floor heave, disturbance can be severe unless a temporary invert, as shown in the photograph, is placed.</p>	<p>$D = 0$</p> <p>$D = 0.5$ No invert</p>
	<p>Very poor quality blasting in a hard rock tunnel results in severe local damage, extending 2 or 3 m, in the surrounding rock mass.</p>	<p>$D = 0.8$</p>
	<p>Small scale blasting in civil engineering slopes results in modest rock mass damage, particularly if controlled blasting is used as shown on the left hand side of the photograph. However, stress relief results in some disturbance.</p>	<p>$D = 0.7$ Good blasting</p> <p>$D = 1.0$ Poor blasting</p>
	<p>Very large open pit mine slopes suffer significant disturbance due to heavy production blasting and also due to stress relief from overburden removal.</p> <p>In some softer rocks excavation can be carried out by ripping and dozing and the degree of damage to the slopes is less.</p>	<p>$D = 1.0$ Production blasting</p> <p>$D = 0.7$ Mechanical excavation</p>

